COPPE
Instituto Alberto Luiz Coimbra de
Pós-Graduação e Pesquisa de Engenharia
UFRJ

AN INDIRECT ADAPTIVE CONTROL APPROACH TO IMAGE BASED VISUAL SERVOING FOR TRANSLATIONAL TRAJECTORY TRACKING

Jonathan Fried

Dissertação de Mestrado apresentada ao Programa de Pós-graduação em Engenharia Elétrica, COPPE, da Universidade Federal do Rio de Janeiro, como parte dos requisitos necessários à obtenção do título de Mestre em Engenharia Elétrica.

Orientador: Fernando Cesar Lizarralde

Rio de Janeiro
Agosto de 2019

AN INDIRECT ADAPTIVE CONTROL APPROACH TO IMAGE BASED VISUAL SERVOING FOR TRANSLATIONAL TRAJECTORY TRACKING

Jonathan Fried

DISSERTAÇÃO SUBMETIDA AO CORPO DOCENTE DO INSTITUTO ALBERTO LUIZ COIMBRA DE PÓS-GRADUAÇÃO E PESQUISA DE ENGENHARIA (COPPE) DA UNIVERSIDADE FEDERAL DO RIO DE JANEIRO COMO PARTE DOS REQUISITOS NECESSÁRIOS PARA A OBTENÇÃO DO GRAU DE MESTRE EM CIÊNCIAS EM ENGENHARIA ELÉTRICA.

Examinada por:

Prof. Fernando Cesar Lizarralde, D.Sc.

Prof. Geraldo Figueiredo da Silveira Filho, D.Sc.

Prof. Liu Hsu, Dr. d'État

RIO DE JANEIRO, RJ – BRASIL
AGOSTO DE 2019

Fried, Jonathan

An indirect adaptive control approach to Image Based Visual Servoing for translational trajectory tracking/Jonathan Fried. – Rio de Janeiro: UFRJ/COPPE, 2019.

XIII, 95 p.: il.; 29, 7cm.

Orientador: Fernando Cesar Lizarralde

Dissertação (mestrado) – UFRJ/COPPE/Programa de Engenharia Elétrica, 2019.

Referências Bibliográficas: p. 87 – 95.

1. Visual Servoing. 2. Adaptive Control. 3. Cascade Control. I. Lizarralde, Fernando Cesar. II. Universidade Federal do Rio de Janeiro, COPPE, Programa de Engenharia Elétrica. III. Título.

A meu pai, Charles, que não pode ver em vida o final desta jornada.

Agradecimentos

Gostaria de agradecer a meu pai, Charles, que me incentivou a iniciar este mestrado com alegria e que certamente celebra de onde estiver. A minha mãe, Rosangela, pelo apoio e incentivo em momentos de pressão e nervosismo.

Agradeço a meu orientador Fernando Lizarralde, paciente e instigador, que me ajudou a ir além e concluir este trabalho. A meus amigos e colegas de laboratório, Alex, João, Ricardo, Rafael, Fernando, entre muitos outros, pelo ambiente de trabalho agradável e pelos momentos descontraídos. Não menos importante, agradeço também a tantos amigos e parentes, presentes ou distantes, que me acompanharam por momentos muito difíceis durante esta jornada.

Gostaria de agradecer também ao CNPq/Brasil pelo auxílio financeiro durante dois anos de trabalho. O presente trabalho foi realizado com apoio da Coordenação de Aperfeiçoamento de Pessoal de Nível Superior - Brasil (CAPES) - Código de Financiamento 001.

Resumo da Dissertação apresentada à COPPE/UFRJ como parte dos requisitos necessários para a obtenção do grau de Mestre em Ciências (M.Sc.)

SERVOVISÃO BASEADA EM IMAGEM POR MÉTODO DE ADAPTAÇÃO INDIRETO PARA SEGUIMENTO DE TRAJETÓRIA TRANSLACIONAL

Jonathan Fried

Agosto/2019

Orientador: Fernando Cesar Lizarralde

Programa: Engenharia Elétrica

No presente trabalho, consideramos o problema de servovisão no espaço da imagem de um manipulador robótico incerto observado por uma câmera monocular fixa, com parâmetros incertos, para o propósito de rastrear trajetórias translacionais de um alvo esférico. Para um caso inicial, onde apenas a cinemática do robô é considerada, propomos um controlador adaptativo por método indireto, onde a estimação de profundidade da câmera em relação ao alvo é realizada através de conhecimento prévio de propriedades geométricas, porém com alguns parâmetros geométricos relacionados sendo considerados incertos. Para aplicar métodos de adaptação indiretos em servovisão, é parametrizado o Jacobiano de imagem do sistema, os parâmetros estimados são continuamente atualizados, construindo uma estimativa do Jacobiano em questão e fazendo uso da inversa dessa estimativa para o cálculo da lei de controle do sistema. Em seguida, estende-se então, baseado em uma estrutura de controlador em cascata, o controlador adaptativo por servovisão proposto para o caso mais geral que considera tanto a cinemática quanto a dinâmica do manipulador robótico, combinando o controlador anterior com um controlador dinâmico adaptativo também indireto. A análise da estabilidade do sistema é feita através do método de Lyapunov, e simulações e experimentos apresentados ao final ilustram e realçam a performance e viabilidade do controlador proposto.

Abstract of Dissertation presented to COPPE/UFRJ as a partial fulfillment of the requirements for the degree of Master of Science (M.Sc.)

Jonathan Fried

August/2019

Advisor: Fernando Cesar Lizarralde

Department: Electrical Engineering

In this work, we consider an image based visual servoing control problem, for uncertain robot manipulators. Visual feedback is provided by a fixed monocular camera with uncertain parameters, for the purpose of tracking translational trajectories of a spherical target. First, only the manipulator kinematic is considered, we propose an indirect adaptive control, with depth measurement done by prior knowledge of a few geometric properties, albeit with some uncertain geometric parameters. This method relies on parameterizing the image Jacobian, continuously updating an estimate of the parameters, using these parameters to construct an estimative image Jacobian matrix and using its inverse to calculate control laws. Based on a cascade structure, the proposed adaptive visual servoing is combined with an adaptive motion control strategy, extending the controller to a case that considers not only the nonlinear kinematics but also the dynamics of the robot arm. The stability and passivity properties are analyzed with Lyapunov method. Simulations and experimental results illustrate and highlight performance and feasibility of the controller proposed.

Contents

List of Figures

List of Tables

Chapter 1

Introduction

The field of robotics has been developing very fast in the latest years, however there is still an essential need to even faster and more precise robots, be it for the repetitive tasks that the industry requires, for activities in inhospitable or hazardous environments, or even for tasks that might be detrimental for a human operator. Aside from the industry, benefits from robotics development have been increasingly spreading to further fields of science and service, with potential to spread into everyday activities. Robotics is the field studying machines that can replace human beings in the execution and decision-making of a task (SICILIANO *et al.*, 2011).

In this context, it is not surprising to see robotics advancing on a large variety of fields, a few of which we can contextualize, for example,

- medicine, with minimally invasive surgery, increasing precision and length of operation, lessening the burden on both patients and operators (LI *et al.*, 2015) (KARTHIKEYAN and NITHYA, 2017);
- deep sea exploration and mapping, using autonomous underwater vehicles, useful in search operations. (LEE *et al.*, 2017) (VIDAL *et al.*, 2018);
- space operations, the feasibility of humanoid robots being used as astronauts, removing human operators of such environments (TANAKA *et al.*, 2017), or the use and control of robots in free-floating environments (WANG *et al.*, 2017);
- agriculture, where it is possible to obtain normally time consuming soil measurements with unmanned ground vehicles (TOKEKAR *et al.*, 2016), and automatic detection of certain crops for harvest (SA *et al.*, 2017);
- entertainment, by introducing unmanned aerial vehicles to cinematography, for target tracking, dynamic scenes that optimizes for visibility when under occlusions (NÄGELI *et al.*, 2017) (ZACHARIADIS *et al.*, 2017).

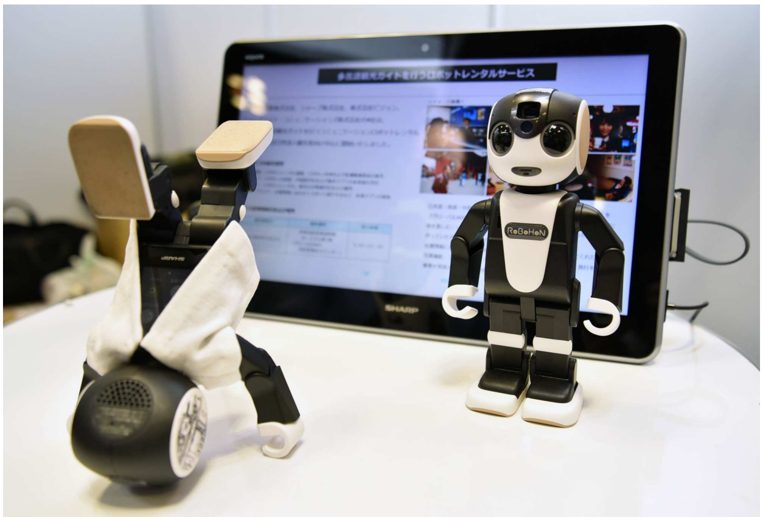

Figure 1.1: Sharp Corp.'s humanoid robot, RoBoHon (The Japan Times, September 2018)

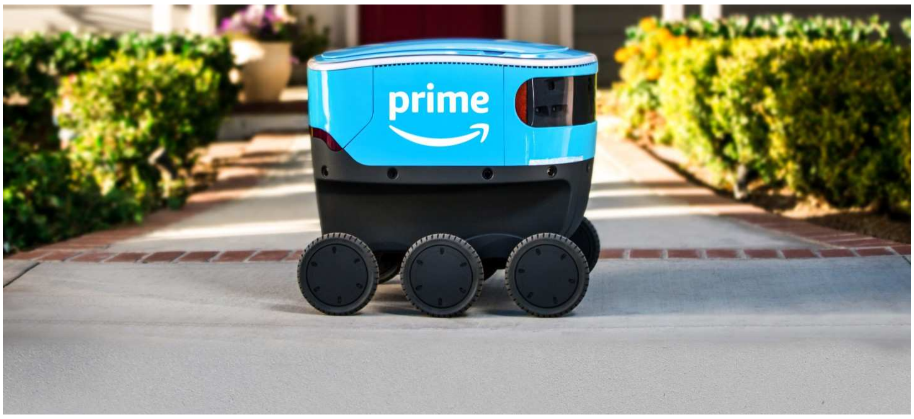

Figure 1.2: Amazon delivery robot, Scout (Amazon, January 2019)

- access to dangerous arousal, including but not restricted to bomb defusing, tracking wildfires and under-rubble searching (PATIC *et al.*, 2017) (PHAM *et al.*, 2017) (BOZKURT *et al.*, 2016).
- maintenance of seabed pipelines, detecting and repairing defects caused by the environment, such as corrosion and cracks, in order to prevent possible hazardous environmental disasters (WANG and CHEN, 2018)

In Kyoto, Japan, from September 2018 until March 2019, a small humanoid robot *RoBoHon* (Figure 1.1), built by Sharp Corp., accompanies tourists in taxis to provide service as sightseeing guides, in a joint project between the aforementioned company, the taxi operator MK Co. and the travel agency JTB Corp. In January 2018, Amazon.com, Inc. experiments with its new delivery robots, *Scout*(Figure 1.2), initially accompanied by their employees for testing purposes. *BattleBots* is a running competition of robot combat, for the sole purpose of entertainment, broadcast in over 150 countries (Figure 1.3). LuxAI, a company that spun-off from

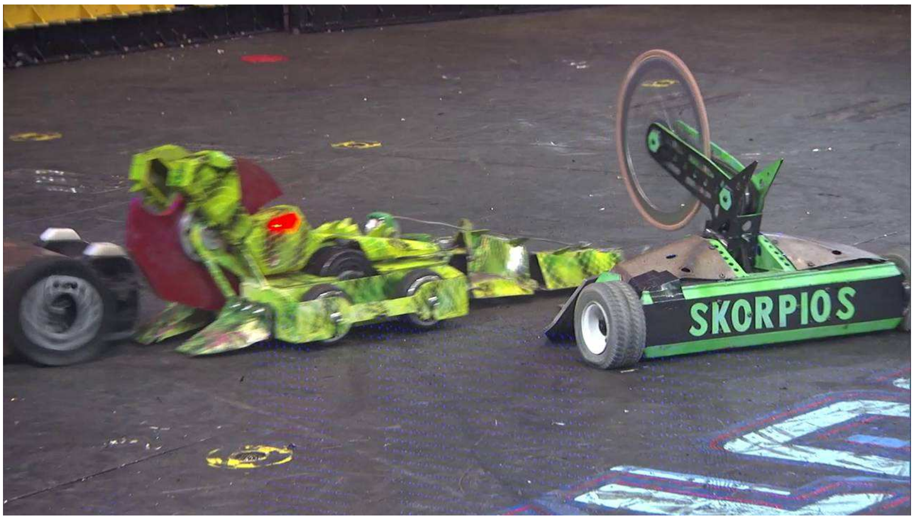

Figure 1.3: Skorpios, Death Roll and Bucktooth Burl (Battlebots Season 2, 2016)

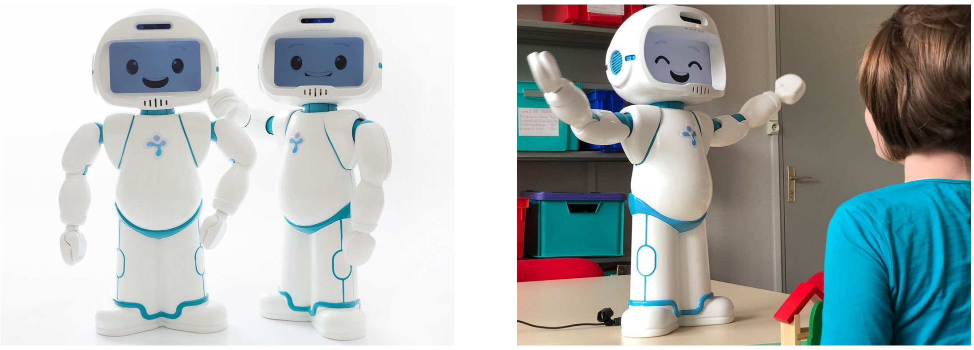

Figure 1.4: LuxAI's QTrobot (LuxAI, 2017)

the University of Luxembourg, has develop the *QTrobot* (Figure 1.4), an expressive humanoid social robot, to help therapists teach human interactions to children with autism. The Waymo One, a commercial self-driving taxi service developed by Waymo LLC, previously known Google self-driving car project, was launched in Phoenix (Arizona, USA) in December 2018 (Figure 1.5). Robots are spreading far and wide, with a wide range of fields finding use to them.

1.1 Motivation and Related Work

Vision is a useful robotic sensor, since it mimics human vision and allows for non-contact measurement of the environment (HUTCHINSON *et al.*, 1996). One of the earliest works in the area, (SHIRAI and INOUE, 1973), describes how visual feedback can be used to correct the position of a robot and increase accuracy. Visual servoing, closed loop position and rotation control of the end-effector of a manipulator through vision, is a term first coined by 1979, (HILL and PARK, 1979), to differentiate that in this case, visual information is used to control the pose of a

Figure 1.5: Self-driving Car Waymo One (Waymo LLC, 2018)

robot, with respect to a target, or set of target features. In this section, we follow a bit of the development of visual servoing through the years, starting from 1985, before presenting some of the newest developments in the field.

In (WEISS *et al.*, 1985), a model reference adaptive controller is used to control an image based visual servoing applicated to a manipulator with non-negligible, coupled and non-linear dynamics. In image-space visual servoing, instead of using the image features to obtain the robot pose, a desired task is planned in image space and error is given as the comparison between measured and desired features. In (WALLACE *et al.*, 1986), an idea is proposed for mobile robots capable of operating in unstructured environments, using a monocular TV camera on a six-wheeled robot to apply a image-based visual servoing strategy, but assumes that the terrain is locally planar. In (WEISS *et al.*, 1987), an adaptive Image Based Visual Servoing system is proposed, with performance analysis through simulation for systems with up to three degrees-of-freedom.

In (KOIVO and HOUSHANGI, 1991), visual information obtained from a camera is used in an adaptive control system to control a robotic manipulator to grasp a moving object. At this time, however, image processing inputed a significant delay to the system, and motion of the target was predicted in real time, for an on-line planning of the manipulator trajectory, a self-tuner controlling the end-effector. A Jacobian matrix estimator is proposed in (HOSODA and ASADA, 1994) to ensure the convergence of the visual servoing system, using a feedforward term, for both continuous and discrete-time domain.

Eye-to-hand Image Based Visual Servoing control of planar manipulators modeled by Lagrangian dynamics is addressed in (KELLY, 1996),the proposed strategy is robust to camera lens radial distortion, uncertainty in its orientation and other camera parameters are considered to be unknown. In (CORKE and GOOD, 1996), non-negligible dynamics are studied on a visual servoing context, along a number of problems generated by hardware at the time, significant latency, low sample rates and coarse quantization. A Cartesian position-based visual servoing control is studied in (WILSON *et al.*, 1996), for robots with a single eye-in-hand camera. It requires a number of known features on the target object, and uses an extended Kalman filter to obtain recursive solutions and eliminate redundancy from the multiple measurements. Position-based visual servoing reconstructs the robot pose using the features extracted from an image, and the task is planned in Cartesian space. In (JAGERSAND *et al.*, 1997), an evaluation of the visual servoing performance is presented, adaptive and non-adaptive, and comparing it to traditional joint feedback control. The main results there presented is that: the positioning of a 6 axis PUMA 762 arm is up to 5 times more precise under visual control, rather than joint control, positioning of a UTAH/MIT dextrous hand (16 DoFs) visual control is better by a factor of 2.

In (WHAITE and FERRIE, 1997), a theory is presented over autonomous exploration, a robot to seek and collect information about its environment, using visual data feedback to adapt to model uncertainty. By decoupling translation and rotation, an optimal motion control is planned for image-based visual servoing, to guide a eye-in-hand camera to a desired goal image (DEGUCHI, 1998). For planar objects, it proposes and makes use of the relation between current and goal image through homography, and for general 3D objects, it uses epipolar conditions to make the decoupling. An hybrid between position and image-based approaches is proposed in (KELLY, 1999), with particular tasks defined in different workspace. In (MA *et al.*, 1999), image-based visual control for a nonholonomic mobile robot is presented for tracking an arbitrarily shaped continuous ground curve. This problem is formulated as controlling the shape of the ground curve in the image plane.

In (WINTERS *et al.*, 2000) and (GASPAR *et al.*, 2000), an omni-directional camera is used in mobile robot navigation, both for position based control, requiring knowledge of the robot global position, and vision based control, requiring only a set of landmarks to be followed.

In (CORKE and HUTCHINSON, 2001), by decoupling of z-axis rotational and translational components of the control, seemingly desirable trajectories in the image-based approach also translates into a smooth trajectory in the Cartesian space, but still requires that the z-axis of the camera to be aligned with the workspace. A model that guarantees an occlusion-free condition is proposed in (COWAN *et al.*, 2002), making a change of coordinates from image-space to this proposed model-space.

An application of visual servoing is seen in (KRUPA *et al.*, 2003), for 3D positioning of surgical instruments in robotized laparoscopic surgery (Figure 1.6). Several laser pointers are projected in the endoscopic image, so the surgeon precisely knows where instrument is located. Visual servoing is used both to bring the instrument

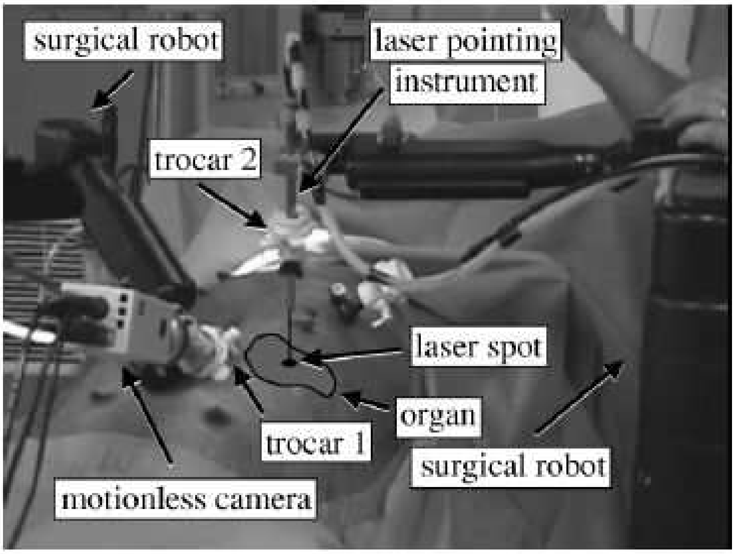

Figure 1.6: Configuration of the surgical system (KRUPA *et al.*, 2003)

to the center of the image as well as to regulate its position to any setpoint in the image given by the surgeon. In (MALIS, 2004), an algorithm robust to changes in intrinsic camera parameters is developed, meaning that the reference image for the visual servoing goal could have been taken with any camera, not necessarily the one being used in the task itself. Regulation of both position and orientation of a mobile robot is done in (FANG *et al.*, 2005), by exploiting homography-based control strategies, comparing features of multiple landmarks from a reference image to the currently captured one, image-based geometric relationships are used to construct a homography matrix. A Model-Reference Adaptive control for use in MIMO cases for plants with relative degree of two is seen in (HSU *et al.*, 2006), with applications to a visual servoing problem.

A review of the most common and known concepts and techniques related visual servoing studied over the years is seen in (CHAUMETTE and HUTCHINSON, 2006) and (CHAUMETTE and HUTCHINSON, 2007). Visual servoing control is directly related to the development of both image capturing technology and computer vision techniques, and interest in the field has been continuously growing during recent years. IBVS for regulation of an unmanned aerial vehicle is developed in (GUENARD *et al.*, 2008), a set of stationary and disjoint landmarks in a plane, an eye-in-hand setup, with an inertial measurement unit and an explicit complimentary filter combined with visual data is used to estimate the translational velocity. Instead of the classical geometric features, using luminance of image pixels for visual servoing is proposed in (COLLEWET and MARCHAND, 2011), named photometric visual servoing, to control the robot motion. A sliding-mode control law for mobile robots in (BECERRA *et al.*, 2011) avoids precise camera calibration and singularities, while making use of three different views to attain depth regulation. In (CHEN, 2012), a review of many variations of the Kalman filter is presented, and its applications in robot vision.

A 3D visual servoing technique is proposed in (SILVEIRA, 2014), with the goals based on the intensity of pixels in the image, rather than relying on feature extraction and matching. This approach shows to be effective even in the case of incorrect camera parameters being used in the controller scheme, and three different intensity-based 3D visual servoing algorithms are presented to illustrate it. A position-based visual servoing controller scheme is proposed in (WANG *et al.*, 2014), for nonholonomic mobile robots. An adaptive algorithm for estimating position of a robot using natural image features is developed, based on a nominal image error linearly parameterized by the unknown position of the robot and features. In (PUTRA *et al.*, 2017), a prototype for an autonomous line following robot is presented. Visual information only is used to develop an image-based line follower.

In (KAUFMANN *et al.*, 2018), in order to improve control for robust autonomous flying, a new approach introduced estimative for maneuvering around waypoints, a predefined set of landmarks subject to uncertainties, without a precise map or extensive data collection. The coarse set of waypoints information are incorporated to the control through an extended Kalman filter, followed by the use of a model predictive control. A system comprised of three parts, it takes an image from a forward-facing eye-in-hand camera, estimating the relative pose of the next waypoint and an uncertainty related to it, then, using that information and the state estimate of the UAV, filtered estimates are produced and finally the controller uses those to generate feasible tracks using these landmarks and follow those trajectories simultaneously.

A vision-based approach to achieve tracking for kinematic car-like mobile robots is provided in (ZHOU *et al.*, 2018), taking in consideration wheel skidding and slippage. A visual-inertial estimator provides the main states of the robot, position, velocity, skidding and slipping. These online estimations are then fed to a control system based on backstepping, for an unknown and unstructured environment.

In (CUEVAS-VELASQUEZ *et al.*, 2018), a case of an hybrid, eye-to-hand and eye-in-hand approach is studied. The global, eye-to-hand, cameras are used in the initial stages of the manipulator alignment, when the distance between it and desired pose are above a certain setpoint, while the arm-mounted, eye-in-hand, camera is used to fine tune the result when under said setpoint. If the target goes out of the arm-mounted camera field of view, the system switches back to the global cameras. The information provided by this is used in two forms, for target-tracking and for position-based control of the manipulator.

In (LAMPARIELLO *et al.*, 2018), visual servoing is used for grasping a partially cooperative tumbling satellite with a free-floating robot. A reference trajectory is

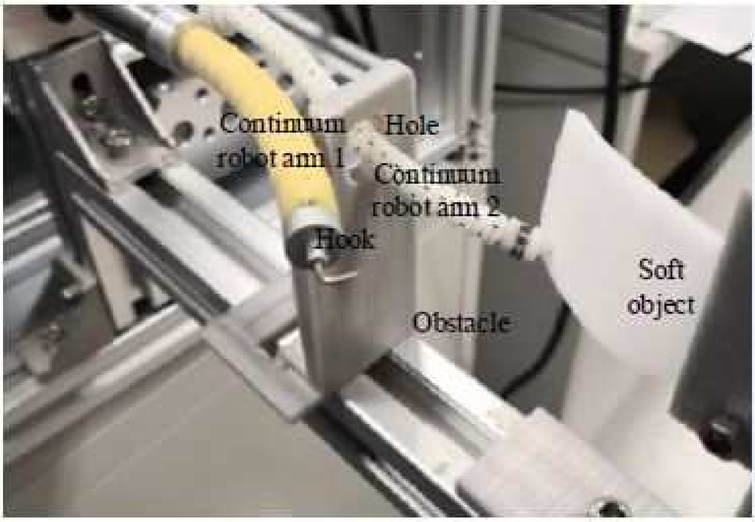

Figure 1.7: Prototype of a continuum robot system for deformation of soft objects (OUYANG *et al.*, 2018)

tracked through position-based visual servoing for approach, and then a joint-space controller for rigidization. Unexpecrted impacts with the target are answered with an impedance control, while for the latter phase, the desired trajectory is adapted online due to the uncertainties generated by the former. An extended Kalman filter is used to obtain rough estimates of the target pose and velocity, and those are used both for feedback and feedforward.

A study case for flexible continuum robots performing deformation control of a soft object in the presence of obstacles is seen in (OUYANG *et al.*, 2018), meaning the robot shape varies with the contact force (Figure 1.7). Using a frame-fixed, eye-to-hand, camera to obtain external data, a Geman-McClure estimator is used to obtain an on-line estimation of the Jacobian matrix, which slowly changes over time, following a linear approximation model mapping the actuation space of the robot to the deformation space of the soft target object. A Geman-McClure estimator is a non-convex type of M-estimator, the class of estimators to which the non-linear least square estimator belongs, is used to eliminate the influence of disturbances and model uncertainties from the estimated Jacobian. With this information, a model predictive control is used to converge the soft object to a desired shape.

In (CHERUBINI *et al.*, 2018), a visual servoing control is proposed for a dual-arm robot to manipulate flexible cables on a 2D-plane. The shape of the flexible cable is parameterized by a Fourier series, and a local deformation model of the cable is estimated on-line with the shape parameters. This model is used to design a velocity control law for the kinematic robot arms, with information regarding shape of the cable being captured by a fixed camera, perpendicular to the workspace.

In (ZHENG *et al.*, 2018), an image-based visual servoing control for a quadrotor unmanned aerial vehicle is proposed. The novelty of this proposal is directly plan-

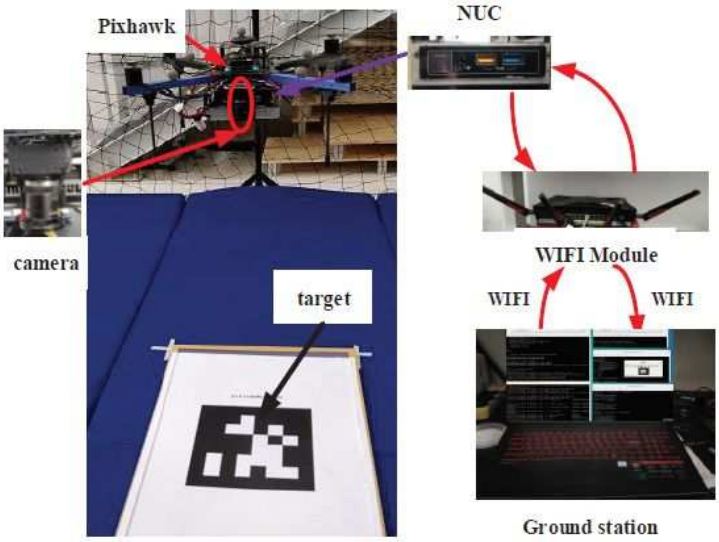

Figure 1.8: System configuration for visual servoing control of a quadrotor (ZHANG *et al.*, 2019)

ning of the trajectory of image features, by combining a virtual camera approach and the image moment features, and using said planning to make mild trajectories that do not exponentially reduce the error to zero, but better account for visibility and occlusion. In (YANG *et al.*, 2019), an optimized image-based visual servoing scheme is presented for similarly tracking a ground target, by using fixed-wing unmanned aerial vehicles, instead of quadrotors. Using least squares, an optimized control law is proposed without solving the pseudo-inverse of the image Jacobian, its stability properties analyzed by Lyapunov method.

A nonlinear geometric hierarchical visual servoing approach to drive a quadrotor is proposed in (ZHANG *et al.*, 2019). It extends a position-based nonlinear hierarchical control to an image-based control, making use of the cascade properties of the system to integrate the geometrical control with it (Figure 1.8). In (BECHLIOULIS *et al.*, 2019), a visual servoing scheme that imposes predefined performance specifications is proposed. It satisfies visibility constraints from a camera limited field of view in a image based scheme, and has the novelty of guaranteeing a predefined transient error, in the presence of camera calibration and depth measurement errors.

In (FERRO *et al.*, 2019), a reactive vision-based navigation scheme for omnidirectional robots is proposed, exploiting kinematic redundancy and keeping clear of obstacles by moving in the direction of their camera gaze, with an image-based visual servoing scheme. It has a restriction, in which the control assumes that the robot actual velocity is fed back into the control loop. A position-based visual servoing is developed in (YAHYA and ARSHAD, 2016), for docking of an autonomous underwater vehicle, contrasting with the usual image-based approach for the task.

1.2 Objective

In this work, we consider the translational trajectory tracking, for position and depth, control problem for the positioning of a spherical objeted mounted on the robot manipulator end-effector viewed by a fixed camera. The extracted image feature for the task are the centroid coordinates and target area, with references given in the camera image frame and considering uncertain camera and manipulator parameters, both kinematic and dynamic.

A recent work (LEITE and LIZARRALDE, 2016) proposes a passivity-based direct adaptive image based visual servoing with depth control, without camera calibrations, for uncertain manipulators and free of image velocity measurement. To perform 3D motions in the Cartesian space, at least three degrees of freedom have to be controlled by the visual servoing system. To solve the depth tracking problem, a standard model reference adaptive control is employed, while the SDU factorization method (COSTA *et al.*, 2003) is applied to the planar tracking problem, solving both tasks for a Cartesian control. An indirect/direct adaptive control method is used to solve the parametric uncertain problem of the robots kinematics and dynamics, by means of a cascade control strategy seen in (GUENTHER and HSU, 1993). By cascading the manipulator and camera passive subsystems, the stability of the overall closed-loop system is demonstrated via Lyapunov method.

Remark 1. *It is worth of note that the use of the SDU factorization only guarantees stability of the visual servoing scheme as the sign of the leading minors of the camera calibration matrix K_p is known, typically by assuming the camera misalignment angle is known to be restricted in a $\left(-\frac{\pi}{2}, \frac{\pi}{2}\right)$ interval.(COSTA* et al.*, 2003)*

Remark 2. *Four parameterizations are used in (LEITE and LIZARRALDE, 2016): The robot manipulator dynamic and kinematic parameters use a hybrid direct/indirect adaptation method, with a parameter vector for each kinematic and dynamic subsystem. The camera calibration planar and depth parameters both use direct methods of adaptation, with the former using the SDU factorization.*

Remark 3. *(LEITE and LIZARRALDE, 2016) To avoid measuring the image velocity, a first-order low-pass filter is used, so the filtered velocity depends only on the position and a suitable filter time-constant.*

Another approach to a similar problem is presented in (WANG *et al.*, 2018), for the task of tracking a trajectory in the camera image space, with unmeasured depth, a fixed uncertain camera, and uncertainties in the robot manipulator parameter. The controller proposed achieves separation of kinematic and dynamic loops, with visual servoing applied on the kinematic loop. The visual servoing loop is solved by an inverse-Jacobian-like control with nonlinear feedback, while an indirect adaptive method is used to solve estimate uncertain parameters in the image Jacobian. Whereas the dynamic loop is solved by the Slotine-Li adaptive scheme (SLOTINE *et al.*, 1991).

Remark 4. *The number of degrees of freedom of the manipulator and that of the feature points are subjected to the constraint that* $n \geq 2m$ *and* $m \leq 3$*, and in the case* $m = 3$*, the three feature points are non-collinear.*

Remark 5. *Three parameterizations are used in (WANG* et al.*, 2018): The depth-independent parameters, the depth-dependent parameters and the manipulator dynamic parameters. However, six regressor matrices need to be calculated, as they differ for the manipulator differential kinematics and the proposed observer.*

Remark 6. *Though an indirect adaptation scheme avoids the usual camera misalignment angle constraint, it is necessary to guarantee that the estimated image Jacobian is nonsingular due to its inversion in the control scheme. A common approach to this problem is the use of projections on the adaptation update laws (CHEAH* et al.*, 2010).*

Remark 7. *To avoid measuring the image velocity, a passive nonlinear observer is chosen, so the observed position and velocity are used in the control schemes instead. The observer also guarantees the passivity property of the complete closed-loop system.*

Here, we propose an adaptive image-based visual servoing controller using of indirect methods of adaptation. Through image processing, the visual system needs to be able to pinpoint the centroid position and area of the target as seen in (LEITE and LIZARRALDE, 2016), to track a position and depth trajectories. The controller proposed should adapt through all the system uncertainties and guarantee a correct tracking of a given trajectory in the image frame, with good performance. A passivity based controller scheme is proposed, separating the kinematic visual servoing and dynamics loop, based on the cascade control strategy seen in (GUENTHER and HSU, 1993). The visual servoing loop is solved with an inverse-Jacobian control as in (WANG *et al.*, 2018), extended to a case that considers depth control, with parameterizations simplified to require calculation of less regression matrices. The known Slotine-Li adaptive scheme is used to solve the dynamics loop. An observer is adopted to avoid the use of centroid velocities, however, in this work, the area variation is considered measurable. Furthermore, two projection algorithms are considered in the adaptive update laws, one to guarantee the inverse of the estimated Jacobian matrix, and another to reduce the effects from parameter drift during the transient response. These features are compared to previous controller schemes, in Table 1.1.

Table 1.1: Controller Scheme Features

	(LEITE et al, 2016)	(WANG et al., 2018)	This work
VS scheme	IBVS	IBVS	IBVS
Tracking Task	Position and Depth	Position	Position and Depth
VS. Control	MRAC/SDU	Indirect	Indirect
Dynamic Control	Slotine-Li	Slotine-Li	Slotine-Li
Camera Misalignment	$(-\frac{\pi}{2}, \frac{\pi}{2})$	Any	Any
Projection Algorithm.	0	1	2
# of parameter vectors	4	3	3
# of regressor matrices	4	6	3

Remark 8. *While the Slotine-Li adaptive scheme is used in this work, another passive strategy could be used to solve the dynamic loop due to the nature of the cascade strategy employed. One such possibility is a robust control, as seen in (SLOTINE* et al.*, 1991), (ZACHI, 2007).*

The overall performance of the proposed method is primarily illustrated by simulations and experimental results.

1.3 Methodology

In this work, the task of controlling a robotic manipulator end effector to track position and depth through a image-based trajectory, with information captured by a fixed camera is considered. An adaptive visual servoing control strategy is proposed for the task, in the presence of unknown intrinsic camera and manipulator parameters. Depth measurement is made by prior knowledge of the target feature geometry, but the parameters related to this are also unknown, making the depth measurement also uncertain (LEITE and LIZARRALDE, 2016). While it is possible to control a robot manipulator orientation using visual servoing, as seen in (SILVEIRA, 2014), (YAHYA and ARSHAD, 2017) and (YAHYA and ARSHAD, 2016), by making use of multiple target features or position based controllers for example, in this work are only interested in controlling the position of the manipulator end-effector.

A controller is proposed for position and depth trajectory tracking, in the image space, taking in consideration all the previously mentioned uncertainties. Parameterizing the image Jacobian, an indirect adaptive method is considered for this problem, providing a control law that makes use of the inverse of a estimative image Jacobian. Compared to the direct adaptive approach, the indirect method does not need any prior knowledge over the direction which the camera is facing, assuming that the target still is in its field of view. As a trade-off, care should be taken so the inverse of the estimative Jacobian exists, usually done by assuming a minimum magnitude the unknown parameters can assume and projecting the parameter vector out of this minimum, which is a reasonable assumption for physical systems.

Furthermore, through a cascade approach, we extend the aforementioned controller from kinematics to a case with non-negligible dynamics, combining the initially proposed adaptive visual servoing to dynamic control strategies. This strategy, however, would initially require the measurement of image velocity, which is known to be noisy. To avoid using it, the control scheme makes use of an observer, taking the observer velocity instead, as seen in (WANG *et al.*, 2018).

The feasibility of the proposed indirect adaptive image based visual servoing control method is verified through simulation, using Matlab and Simulink. A three degrees-of-freedom manipulator, with revolute joints, is considered for the simulation, for both the kinematic and dynamic cases.

1.4 Text Organization

This work is organized as follows:

- Chapter 2 - In this chapter, we present kinematic and dynamic models for a robot manipulator, followed by control schemes for each model. Adaptive control strategies are used for uncertainties in the kinematic and dynamic parameters. Lastly, a control strategy is introduced to separate the kinematic and dynamic control design.

- Chapter 3 - In this chapter, we introduce the concepts and models for visual servoing schemes. Then, we develop an adaptive control scheme for a robot manipulator with non negligible dynamics with a fixed camera setup, tracking trajectories for position and depth. We develop equations and discuss use of a cascade controller scheme, followed by a brief discussion on how to avoid using image-plane velocity and the proposal of an observer. Lyapunov functions are proposed to guarantee validity of the controller.

- Chapter 4 - Simulations are presented to show feasibility of the control laws proposed in chapter 3, followed by initial simplified experimental setups for the planar case.

- Chapter 5 - Summarizes the final conclusions about this work and proposal for future works.

Chapter 2

Robot Manipulator System

In this chapter, we consider the position control problem for a robot manipulator with non-negligible dynamics. The kinematic and dynamic models of the manipulator are introduced and the properties relevant to this work are analyzed. The ideas, definitions and techniques presented here are based on the contents of (SICILIANO *et al.*, 2011), (MURRAY *et al.*, 1994), (MAREELS and POLDERMAN, 2012) and are restated here to make this work as self-contained as possible. The problem with uncertainties on its kinematic and dynamic models is solved through an adaptive control scheme, as seen in (SLOTINE *et al.*, 1991), and a cascade controller strategy as seen in (GUENTHER and HSU, 1993). Similarly, the relevant definitions and techniques presented on those works are restated here for convenience.

2.1 Robot Manipulator

The mechanical structure of a serial robot manipulator consists of a sequence of rigid bodies, *links*, interconnected by means of articulations, *joints*; a manipulator is characterized by an arm that ensures mobility, a wrist that confers dexterity and an end-effector that performs the task required of the robot (SICILIANO *et al.*, 2011). Each joint moves a link, and the composition of those displacements cause the final movement of the end-effector in the workspace. Figure 2.1 below illustrates such a manipulator.

For the goal of motion control, an analysis of the robotic system is desired, that means an analysis of its kinematics and dynamics. Kinematics refer to the geometric relation between the robot movement in the joint space and its end-effector movement in the Cartesian space. The dynamics describe a relation between the generalized forces actuating on the robot manipulator and its resulting motion, as dictated by the acceleration, velocities and positions of its joints (SICILIANO *et al.*, 2011).

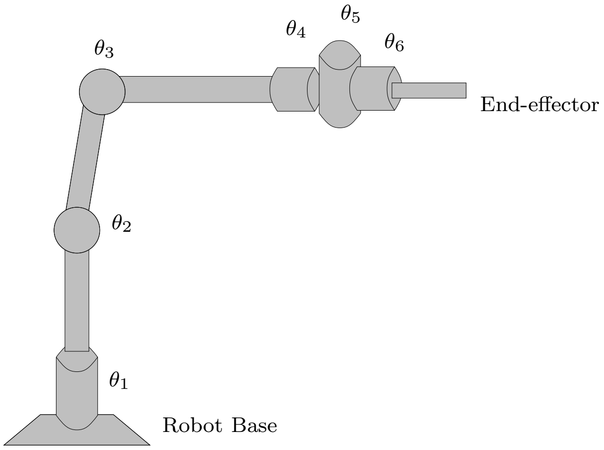

Figure 2.1: A robot manipulator with six revolute joints

2.2 Kinematic Model

The kinematic analysis of a manipulator structure considers the description of robot motion with respect to a fixed Cartesian coordinates system, neglecting forces and moments that cause movements to. In this context, it is important to distinguish between the robot kinematics and differential kinematics. The former describes the analytical relation between position of manipulator joints and position and orientation of its end-effector. Differential kinematics, however, is the analytical description of a relation between the joints and end-effector motions, as defined by their velocities, as given by the manipulator Jacobian (MURRAY *et al.*, 1994).

The kinematics formulation allows a study of two fundamental problems in robotics: the forward and inverse kinematics. The former refers to the determination of a general and systematic method to describe position of a robot manipulator as a function of the position of its joints, through linear algebra. The second refers to the opposite problem, and its solution is important to transform the desired end-effector motion, naturally given in Cartesian coordinates, into joint-space motion.

2.2.1 Forward Kinematics

The structure of a manipulator is characterized by a number of degrees of mobility which determine its unique configuration. Each degree of mobility is typically associated with a joint articulation and composes a joint variable (angle or displacement). The objective of forward kinematics is to compute pose of the end-effector as a function of the manipulator joint variables with respect to a Cartesian coordinate system. The inverse kinematics, likewise, consists of computing the joint variables as a function of the end-effector pose.

Now, consider a robotic manipulator as a combination of $n + 1$ rigid bodies connected by n joints, where, typically, the first link is chained to a base or fixed

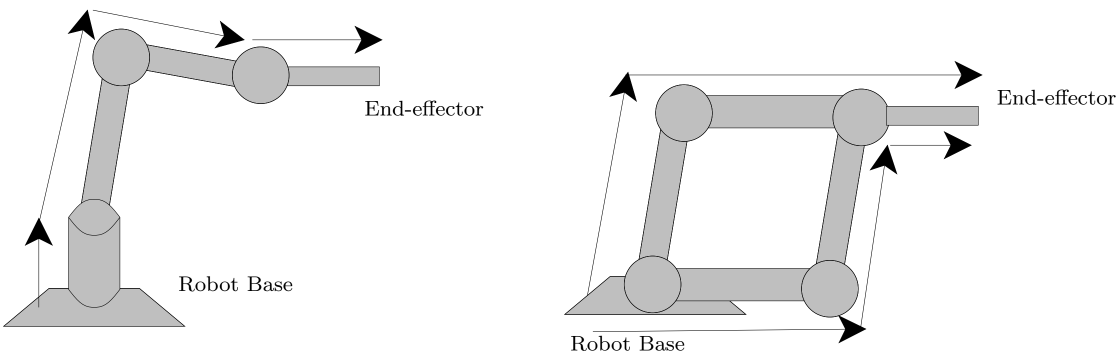

Figure 2.2: Manipulators with an open chain and a closed chain, respectively

frame, and the last one ends in the end-effector. The whole structure is what we call a kinematic chain. The goal of a kinematics analysis is describing the movement of the end-effector based on the joint variables of this chain, while disregarding the forces and torques causing them.

A kinematic chain can be classified as open or closed chain. An open chain contains one possible sequence of links between the base and an end-effector of the manipulator. Likewise, a closed chain contains a loop on its links, therefore resulting in more than one possible sequence of links between the base and end-effector (Figure 2.2).

For a simple manipulator, kinematics could be found by making an analysis of its structure geometry, directly obtaining a function that maps from the base frame to the end-effector as a function of its joints variables (angles if a revolute joint, displacement if prismatic). As the complexity of the manipulator increases, however, it becomes harder to directly infer this function through geometry alone. As such, certain procedures were adopted to facilitate this computation like the *Denavit-Hartenberg* convention (SICILIANO *et al.*, 2011). Another approach to this problem is the product of exponentials, which is, at most times, more intuitive than the Denavit-Hartenberg convention, facilitating a geometrical approach, link by link, by associating the motion of each joint as generated by a twist along the joint axis (MURRAY *et al.*, 1994).

Attaching a coordinate frame to each base, each of the links and end-effector, we can say that the homogeneous transformation between the first and last link T_{be} is given by post-multiplications of the consecutive link-to-link homogeneous transformation $T_{(i-1)i}$, so

$$T_{be}(\theta) = T_{b0}T_{01}(\theta_1)T_{12}(\theta_2).....T_{(n-1)i}(\theta_n)T_{ie} \tag{2.1}$$

where

$$T_{i-1,i}(\theta_i) = \begin{bmatrix} R_{i-1,i} & (p_{i-1,i})_{i-1} \\ 0^{1\times 3} & 1 \end{bmatrix}, \tag{2.2}$$

$\theta = [\theta_1\ \theta_2 .....\ \theta_n]^T$ is the vector containing each joint displacement, $\theta_i \in \mathbb{R}$, $R_{(i-1)i} \in SO(3)$ is the rotation matrix of frame i with respect to frame $i-1$ and $(p_{(i-1)i})_{i-1}$ is the distance between frames $i-1$ and i, in frame $i-1$ coordinates (SICILIANO *et al.*, 2011). For a revolute joint $R_{i-1,i}$ is a function of θ_i and $(p_{i-1,i})_{i-1}$ is constant, while for a prismatic joint $R_{i-1,i}$ is constant and $(p_{i-1,i})_{i-1}$ is a function of θ_i.

Finally, we can say that the final homogeneous transformation base to end-effector is

$$T_{be}(\theta) = \begin{bmatrix} R_{be} & p_{be} \\ 0 & 1 \end{bmatrix}, \tag{2.3}$$

where $R_{be} \in SO(3)$ represents the rotation matrix from the base frame to the end-effector with respect to the base frame and $p_{be} \in \mathbb{R}^3$ represents its position.

In this work, we are interested in controlling the end-effector position p_{be}, which can also be obtained through directly mapping the forward kinematics as

$$p_{be} = k(\theta) \tag{2.4}$$

where $k(\cdot)$ is a function, generally non-linear, which calculates the position variables in the Cartesian space by using the joint variables in the joint space.

2.2.2 Differential Kinematics

Similar to how forward kinematics establish the relation between end-effector position and joints displacement, differential kinematics maps relation from joint velocities to the end-effector linear and angular velocities. This mapping is given by means of a matrix, called *Jacobian*, a tool that has a vast number of applications, allowing to analyze redundancy, finding kinematic singularities, link operational and joint spaces, find its manipulability, map forces applied on the end effector to torque at joints and to design controls in operational space as seen in (MURRAY *et al.*, 1994) and (SICILIANO *et al.*, 2011).

In differential kinematics, it is desired to express and map the linear velocity $\dot{p}$ as a function of the joint velocities $\dot{\theta}$. First, consider the forward kinematics mapping, given by

$$p = k(\theta), \tag{2.5}$$

where $p \in \mathbb{R}^3$ is manipulator end-effector position in the Cartesian space. It is possible to differentiate this forward kinematics equation to obtain a Jacobian matrix.

As such, by calculating the time derivative $\dot{p}$

$$\dot{p} = \frac{\partial k}{\partial \theta}\dot{\theta} = J(\theta)\dot{\theta} \tag{2.6}$$

where $J \in \mathbb{R}^{3\times n}$ is called the position Jacobian.

Remark 9. *It is possible to find different Jacobian matrix, by different means. By analyzing the geometry of the manipulator, it is possible to calculate the Geometric Jacobian, dependent on its configuration. However, if it is possible to express the end-effector pose in a minimal representation in the operational space, it is also possible to obtain another Jacobian matrix by differentiating this expression, resulting in the so called Analytical Jacobian. Generally, these two different computations do lead into different Jacobian matrices, particularly with respect to the manipulator orientation. In this work, as we only take in consideration the position Jacobian, there is no difference between the two.*

A property of the Jacobian that is important to control design is given as follows:

- $(P1)$ The product of the Jacobian $J(\theta)$ with any measurable vector $\phi(t)$ can be linearly parameterized as

  $$Y_k(\theta, \phi)a_k = J(\theta)\phi, \tag{2.7}$$

  where $Y_k(\phi, \theta)$ is the kinematic regressor matrix, which contains measurable elements ϕ and θ, a_k is a vector of constant kinematic parameters of the Jacobian matrix. The lower and upper bound $a_{k_{min}}$ and $a_{k_{max}}$, respectively, are assumed known for the kinematics parameters and satisfy

  $$||a_{k_{min}}|| \leq ||a_k|| \leq ||a_{k_{max}}|| \tag{2.8}$$

Example 1. *Consider a 2R planar manipulator, as seen in Figure 2.3. The end-effector position is mapped to joint variables as follows:*

$$p = \begin{bmatrix} l_1\cos(\theta_1) + l_2\cos(\theta_1+\theta_2) \\ l_1\sin(\theta_1) + l_2\sin(\theta_1+\theta_2) \end{bmatrix} \tag{2.9}$$

where p is the position of the end effector, l_1 and l_2 are the lengths of links 1 and 2, respectively, $\theta = [\theta_1\ \theta_2]^T$ are the joint variables.

Then, the differential kinematics can be obtained by obtaining the time derivative of p

$$\dot{p} = \begin{bmatrix} -l_1\sin(\theta_1) - l_2\sin(\theta_1+\theta_2) & -l_2\sin(\theta_1+\theta_2) \\ l_1\cos(\theta_1) + l_2\cos(\theta_1+\theta_2) & l_2\cos(\theta_1+\theta_2) \end{bmatrix}\dot{\theta} = J(\theta)\dot{\theta} \tag{2.10}$$

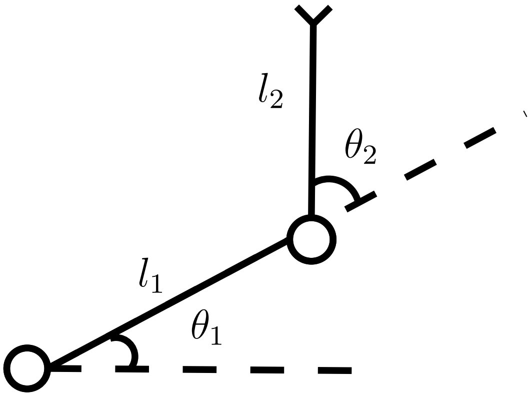

Figure 2.3: A simple 2R planar manipulator

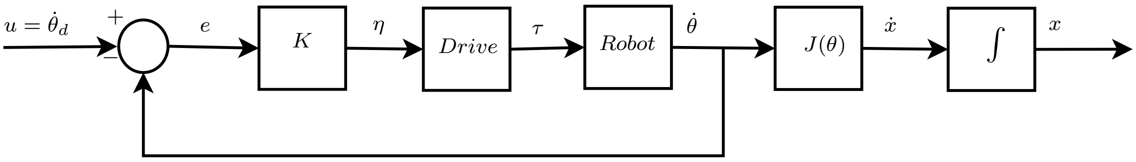

Figure 2.4: Block Diagram for a manipulator inner control loop

Furthermore, the linear parameterization of $J(\theta)\dot{\theta}$

$$\dot{p} = \begin{bmatrix} -\sin(\theta_1)\dot{\theta}_1 & -\sin(\theta_1+\theta_2)(\dot{\theta}_1+\dot{\theta}_2) \\ \cos(\theta_1)\dot{\theta}_1 & \cos(\theta_1+\theta_2)(\dot{\theta}_1+\dot{\theta}_2) \end{bmatrix} \begin{bmatrix} l_1 \\ l_2 \end{bmatrix} = Y_k(\theta,\dot{\theta})a_k \qquad (2.11)$$

where $Y_k(\theta,\dot{\theta})$ is the regressor matrix and a_k is the kinematic parameter vector.

2.3 Kinematic Position Control

In this section, we consider the kinematic control problem for a robot manipulator. Hereby, the following assumption is made:

- $(A1)$ The effects of the robot manipulator dynamics are negligible.

This assumption is applicable to most industrial robots, with high reduction gear ratio, or when the velocities involved in the task are relatively slow. In this context, many of these industrial robot manipulators have an inner joint velocity control loop. Figure 2.4 illustrates a velocity control loop scheme, where x represents the position of a robot $\dot{x}$ represents its velocity and τ is the torque vector applied to the robots joints.

The *Drive* block gives the necessary power to activate the robot actuators with a control signal η as input. The control signal η is generated with a proportional controller with gain K that amplifies the error signal e between a reference sinal $\dot{\theta})_d$

and the joint velocity $\dot{\theta}$. So, for a signal input $u = \dot{\theta}_d$ and a high gain control loop, we have that $e \to 0$ and, consequently $u \to \dot{\theta}$.

2.3.1 Kinematic Control Strategy

Considering the kinematic control assumption, the robot manipulator motion can be simply described by:

$$\dot{\theta}_i = u_i, \quad i = 1, ..., n, \tag{2.12}$$

where θ_i and $\dot{\theta}_i$ are the angular position and velocity of the joint i, respectively, and u_i is the velocity control signal applied to motor joint drive i. In this manner, considering $\dot{\theta}_i$ as the input signal u_i and the equation (2.6), we obtain the following control system

$$\dot{p} = J(\theta)u \tag{2.13}$$

A Cartesian control signal v can be transformed as a joint-space control signal by using the inverse of the Jacobian matrix

$$u = J^{-1}(\theta)v \tag{2.14}$$

if v does not take the robot manipulator to singular configurations. This is an important condition, still studied at large by the academic community. In this work, we assume that the robot motions stay away from singular configurations.

Now, if $p_t(t)$ is a tracking goal in the Cartesian space,

$$e_p = p - p_t(t) \to 0, \qquad t \to \infty \tag{2.15}$$

where $e_p \in \mathbb{R}^3$ is the end-effector position error. Calculating the time derivative of the error e_p, we obtain:

$$\dot{e}_p = \dot{p} - \dot{p}_t \tag{2.16}$$

however, since that $\dot{p} = J(\theta)J^{-1}(\theta)v = v$, and considering the following position-based control law, with feedforward and proportional feedback.

$$v = \dot{p}_t - K_k e_p \tag{2.17}$$

where K_k is a positive gain matrix. With simple algebraic formulation, the error dynamic equation is given by

$$\dot{e}_p + K_p e_p = 0 \tag{2.18}$$

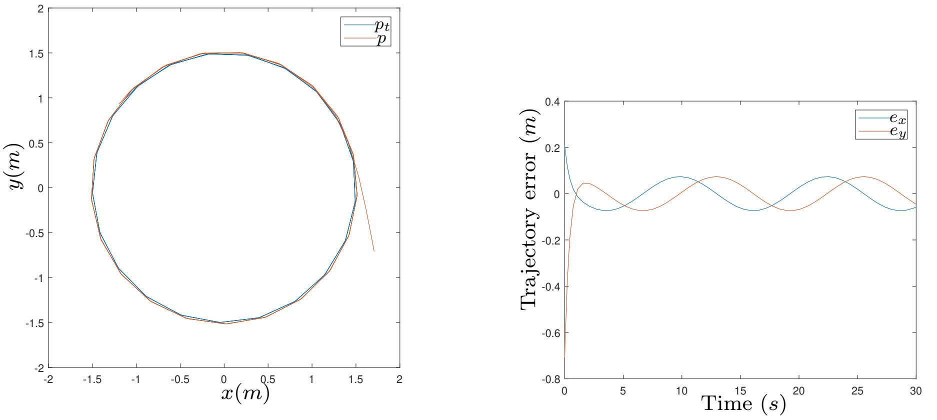

Figure 2.5: (a) Manipulator trajectory in XY plane. (b)Trajectory error

which means the system is exponentially stable in closed-loop, and consequently $\lim_{t\to\infty} e_p(t) = 0$.

2.3.2 Adaptive Kinematic Control

An adaptive control system is able to tune its control parameters, in face of unknown or changing operating conditions, to guarantee a satisfactory performance (MAREELS and POLDERMAN, 2012). It is evident that presence of uncertainties in the robotic kinematics and dynamics are a relevant issue, commonly addressed as two separate problems. The following example illustrates the significance of adaptive control, by simulating the previous kinematic control strategy on a robot with uncertainties on its kinematic parameters.

Example 2. *Consider the 2R robot manipulator given in Example 1, with differential kinematic model given by (2.10) and control law given by (2.14) and (2.17). Consider as well that $l_1 = l_2 = 1m$. However, assume that known values for this manipulator kinematic parameters are $\hat{l}_1 = \hat{l}_2 = 0.8m$, which will be used in the control law.*

The tracking goal p_t is given by

$$p_t = \begin{bmatrix} 1.5\cos(0.5t) \\ 1.5\sin(0.5t) \end{bmatrix} \tag{2.19}$$

Considering the controller gain $K_k = 2I_{2\times 2}$ and $\theta(0) = [-\frac{\pi}{4} \quad \frac{pi}{4}]^T$, we obtain the following results by simulation. As Figure 2.5 shows, in the presence of parameter uncertainties, the tracking error does not go to zero with the inverse Jacobian kinematic control.

In this section, we treat the uncertainties of a kinematic robot manipulator and assume these to be limited to uncertain geometric and physical parameters.

It is important to note that adaptation of these uncertain parameters needs to happen on-line, while the system is running. The controller collects information in real time, and uses those to achieve a better performance. In conventional model reference adaptive control schemes, the adaptation laws extract information about the parameters to be calculated from the output tracking error. Here, to illustrate this strategy, we present an adaptive scheme as seen in (LEITE, 2011).

Tracking-error based adaptation

Considering the presence of uncertainties in the robot kinematics, the inverse Jacobian control law (2.14), can be de rewritten as

$$u = \hat{J}^{-1}(\theta)v \tag{2.20}$$

where $\hat{J}(\theta) \in \mathbb{R}^{3\times n}$ is an estimative of the Jacobian matrix and $v \in \mathbb{R}^3$ is a position-based control signal. Rewriting the kinematic control system in term of $\hat{J}$ and its parameterization, one has:

$$\dot{p} = J(\theta)u = Y_k(\theta,u)a_k = Y_k(\theta,u)(\hat{a}_k - \tilde{a}_k) = \hat{J}(\theta)u - Y_k(\theta,u)\tilde{a}_k \tag{2.21}$$

The error dynamic is given by

$$\dot{e}_p = \hat{J}(\theta)u - Y_k(\theta,u)\tilde{a}_k - \dot{p}_t \tag{2.22}$$

and by using the proposed control law (2.20), with position-based control signal v given by (2.17)

$$\dot{e}_p + K_k e_p = -Y_k(\theta,u)\tilde{a}_k \tag{2.23}$$

which is similar to the error dynamic equation in the case with no uncertainties, except for a term depending on the parameter error. Finally, to update the parameter vector $\hat{a}_k$, we can choose a gradient-type adaptation law

$$\hat{a}_k = \Gamma_k Y_k^T e_p \tag{2.24}$$

where Γ_k is a positive gain matrix. The following theorem establishes the stability analysis of the closed loop system.

Theorem 1. *Consider the kinematic model given in equation (2.21), with control law (2.20), (2.17) and kinematic adaptation law (2.24). Assume that $Y_k(\theta,u)$ is measured from system signals. Thus, the following properties hold:*

- *All signals of the closed loop system are uniformly bounded and*
- $\lim_{t\to\infty} e(t) = 0$

Proof. Consider the following Lyapunov function candidate

$$2V = e_p^T e_p + \tilde{a}_k^T \Gamma_k^{-1} \tilde{a}_k \tag{2.25}$$

The derivative with respect to time of the candidate V is given by

$$\dot{V} = -e_p^T \dot{e}_p + \tilde{a}_k^T \Gamma_k^{-1} \dot{\hat{a}}_k \tag{2.26}$$

By using the dynamic error equation given by (2.23) and the kinematic adaptation law (2.24), we obtain

$$\dot{V} = -e_p^T K_k e_p - e_p^T Y_k(\theta, u)\tilde{a}_k + \tilde{a}_k^T Y_k(\theta, u)^T e_p \tag{2.27}$$

$$\dot{V} = -e_p^T K_k e_p \tag{2.28}$$

$$\dot{V} \leq 0 \tag{2.29}$$

This implies, by Lyapunov theory, that e_p, $\tilde{a}_k \in \mathcal{L}_\infty$[1] and thus, the equilibrium state is uniformly stable. As e_p and $\tilde{a}_k$ are limited, the derivative with respect to time $\ddot{V}_k = -2e_p^T K_k \dot{e}_p$ is uniformly limited. So, by using the Barbalat's Lemma, we can conclude that $lim_{t\to\infty} e_p(t) \to 0$.

□

Estimation-error based adaptation

First, consider the presence of uncertainty in the robot kinematic model (2.13), and the parameterization given by equation (2.13). The estimated end effector velocity, denoted by $\dot{\hat{p}}$ can be expressed as

$$\dot{\hat{p}} = \hat{J}(\theta)u = Y_k(\theta, u)\hat{a}_k \tag{2.30}$$

where $\hat{J}(\theta) \in \mathbb{R}^{3\times n}$ is the approximate Jacobian and $\hat{a}_k \in \mathbb{R}^k$ denotes a set of k estimated kinematic parameters. Provided that $\dot{p}$ and Y_k are measurable, the linearly parameterized model can be used for online estimation, as the kinematic regressor matrix Y_k depends only on joint position, assumed measurable, and the control signal u. However, to avoid the need of measuring the end effector velocity $\dot{p}$, it is possible to employ a differential equation, representing a first-order low-pass filter, such as

[1] (KHALIL, 2002) The definition of $\mathcal{L}_\infty$ stability is a bounded-input-bounded-output stability; namely, if a system H is $\mathcal{L}_\infty$ stable, then for every bounded input $u(t)$, the output $Hu(t)$ is bounded.

$$\dot{p}_f + \lambda_f p_f = \lambda_f \dot{p}, \qquad p_f(0) = 0, \tag{2.31}$$

where $p_f \in \mathbb{R}^3$ is the filtered output of the end effector velocity $\dot{p}$ and $\lambda_f > 0$ is the cutoff frequency in radians per second. From the combination of differential kinematics and the differential equation for the low pass filter, we have

$$p_f = \lambda_f p - \frac{\lambda_f^2}{s + \lambda_f} p = Y_{k_f} a_k \tag{2.32}$$

with

$$Y_{kf}(t) = \frac{\lambda_f}{s + \lambda_f} Y_k(\theta, u). \tag{2.33}$$

Notice that the filter output p_f can be calculated by measuring only the end effector position p and choosing a suitable filter time-constraint $\tau_f = (1/\lambda_f)$.

Now, consider $\epsilon \in \mathbb{R}^3$ to be the prediction error obtained from the difference between the estimated and measured values of the filter output, that is

$$\epsilon = \hat{p}_f - p_f \tag{2.34}$$

The prediction error can be related to the parameter estimation error $\tilde{a}_k = \hat{a}_k - a_k$ as follows

$$\epsilon = Y_{kf}(t)\hat{a}_k - p_f = Y_{kf}(t)\tilde{a}_k. \tag{2.35}$$

Note that p_f and Y_{kf} are required to be measured from system signals, thus the only uncertain variable is the estimated parameter vector $\hat{a}_k$. From equations (2.32) and (2.33), observe that the first term depends on p and the second depends on Y_k assumed to be measurable.

Consider an estimation algorithm based on gradient method to estimate the robot kinematic parameters. The key idea is to update the estimated parameter vector $\hat{a}_k$ so that the prediction error ϵ can be minimized. Thus, the kinematic adaptive law for updating a_k is given by

$$\dot{\hat{a}}_k = \Gamma_k Y_{kf}^T \epsilon, \qquad \Gamma_k = \Gamma_k^T > 0, \tag{2.36}$$

where Γ_k is an adaptive gain matrix for the kinematic parameters. The following theorem can be stated:

Theorem 2. *(LEITE and LIZARRALDE, 2016) Consider the linear parameterization given in equation (2.32) with prediction error (2.35) and kinematic adaptation law (2.36). Assume that $p(\theta)$ and $Y_k(\theta, u)$ are measured from system signals. Thus, the following properties hold:*

- *All signals of the closed loop system are uniformly bounded and*

- $\lim_{t\to\infty} \epsilon(t) = 0$

Proof. Consider the following Lyapunov function candidate

$$V_k(\tilde{a}_k) = \tilde{a}_k^T \Gamma_k^{-1} \tilde{a}_k \tag{2.37}$$

The time derivative of V_k, along the solutions of equation (2.36) is given by

$$\dot{V}_k(\tilde{a}_k) = -\tilde{a}_k^T Y_k^T Y_k \tilde{a}_k = -\epsilon^T \epsilon \tag{2.38}$$

So, in result

$$\dot{V}_k(\tilde{a}_k) \leq 0 \tag{2.39}$$

Since V_k is positive definite with a non-positive time-derivative, we have that $V_k \in \mathcal{L}_\infty$, which implies that $\hat{a}_k \in \mathcal{L}_\infty$ and the equilibrium state is uniformly stable and $\lim_{t\to\infty} V_k(\hat{a}_k) = V_\infty$ exists. From the time derivative of V_k, we have $\int_0^\infty -\dot{V}_k(t')dt' = V_0 - V_\infty \geq 0$, where $V_0 = V(\hat{a}_k(0))$, implying that $\epsilon \in \mathcal{L}_2$. Considering θ, u are bounded, then Y_k, Y_{kf} are also bounded. Thus, equations (2.33) and (2.35) imply that $\dot{\epsilon} \in \mathcal{L}_\infty$. Therefore, we can conclude that $\ddot{V}_k = -\epsilon\dot{\epsilon}$ is bounded, and from Barbalat's Lemma, because $\epsilon \in \mathcal{L}_2, \dot{\epsilon} \in \mathcal{L}_\infty$ we can imply that $\lim_{t\to\infty} \epsilon(t) = 0$, demonstrating stability and convergence of the estimation algorithm. □

2.4 Dynamic Model

In contexts where the robot manipulator joints may move at high speeds, the intrinsic dynamic properties of the manipulator cannot be disregarded, torques and forces should be considered and the kinematics equations alone are not sufficient to properly model the system. Here, we derive the equations of motions for a general open-chain manipulator considering an Euler-Lagrange system, as shown in (MURRAY *et al.*, 1994) and (SICILIANO *et al.*, 2011), determined by the following second order model, in the absence of friction and external disturbances.

$$M(\theta)\ddot{\theta} + C(\theta, \dot{\theta})\dot{\theta} + G(\theta) = \tau \tag{2.40}$$

where $M \in \mathbb{R}^{n\times n}$ is the inertia matrix, $C \in \mathbb{R}^{n\times n}$ is the Coriolis matrix, $G \in \mathbb{R}^n$ is a vector of gravitational torques and $\tau \in \mathbb{R}^n$ is the joint torque vector. It is important to note that the choice of C is not unique. A particular choice however, known as *Christoffel* symbols, present useful algebraic qualities. This model, classified as an Euler-Lagrange system, has the following properties (MURRAY *et al.*, 1994):

- $(P1)$ $M(\theta)$ is symmetric, positive-definite, differentiable and limited for all θ, exists c_0, c_1 so that $c_0 \leq M(\theta) \leq c_1$ and $M(\theta) = M(\theta)^T > 0$.
- $(P2)$ If $C(\theta, \dot{\theta})$ is chosen using *Christoffel* symbols, then matrix $\dot{M}(\theta) - 2C(\theta, \dot{\theta})$ is anti-symmetric, meaning:

$$\eta^T [\dot{M}(\theta) - 2C(\theta, \dot{\theta})]\eta = 0, \ \forall \eta \in \mathbb{R}^n \tag{2.41}$$

- $(P3)$The Euler-lagrangian model is linear with respect to a constant parameter vector a_d and a matrix of signals $Y(\theta, \dot{\theta}, \ddot{\theta})$, so that:

$$M(\theta)\ddot{\theta} + C(\theta, \dot{\theta})\dot{\theta} + G(\theta) = Y_d(\theta, \dot{\theta}, \ddot{\theta})a_d \tag{2.42}$$

  where $Y_d(\theta, \dot{\theta}, \ddot{\theta}) \in \mathbb{R}^{n \times d}$ is the dynamic regressor matrix, which contain measurable elements in function of $\theta, \dot{\theta}, \ddot{\theta}$, $a_d \in \mathbb{R}^d$ is the vector of d dynamic parameters. The lower and upper bounds are given by a_{d_min}, $a_{d_max} \in \mathbb{R}^d$, respectively, are assumed known and satisfy

$$||a_{d_{min}}|| \leq ||a_d|| \leq ||a_{d_max}|| \tag{2.43}$$

- $(P4)$ The system is passive from $\tau \rightarrow \dot{\theta}$, that is,

$$\int_0^C \dot{\theta}^T \tau \ dt \geq -c_3, \ \forall C \tag{2.44}$$

  for some $c_3 > 0$.

Among the various dynamic control schemes developed in the joint-space, we can mention: PD control with gravity compensation, computed torque, robust control and adaptive control. In these schemes, it is assumed that the desired trajectory is defined as acceleration, velocities and position of the joint angles, and as such, the errors should be expressed in the joint-space. However, it is more intuitive to express the desired trajectory in the Cartesian workspace, so inverse kinematics could be used to transform the references from one workspace to another. This process has a high computational load, since the inverse kinematics of both forward and differential kinematics are necessary. For this reason, the current control system of industrial robots calculate the joint angles through inverse kinematics and then use a numerical differentiation to compute velocities and accelerations.

A different approach consists in considering control schemes directly in the Cartesian workspace, where tasks and restrictions imposed by the environment are more naturally described. If the robot motion is specified in the Cartesian space, the variables in the joint-space can be transformed directly into Cartesian space equivalents through the following differential kinematics functions:

$$\dot{\theta} = J^{-1}(\theta)\dot{p}, \qquad \ddot{\theta} = \dot{J}^{-1}(\theta)\dot{p} + J^{-1}(\theta)\ddot{p}. \tag{2.45}$$

So, we can rewrite equation (2.40) expressed in Cartesian coordinates, as

$$M_c(\theta)\ddot{p} + C_c(\theta,\dot{\theta})\dot{p} + G_c(\theta) = \tau_c \tag{2.46}$$

where M_c, C_c and G_c are defined as

$$M_c(\theta) = J^{-T}(\theta)M(\theta)J^{-1}(\theta) \tag{2.47}$$

$$C_c(\theta,\dot{\theta}) = J^{-T}(\theta)[C(\theta,\dot{\theta})J^{-1}(\theta) + M(\theta)\dot{J}^{-1}(\theta)] \tag{2.48}$$

$$G_c(\theta) = J^{-T}(\theta)G(\theta) \tag{2.49}$$

and $\tau_c = J^{-T}(\theta)\tau$. Note that the matrices M_c and C_c are similar to their joint-space correspondents, and as such satisfy the same properties. However, it is important to note that in the Cartesian space, it is necessary to avoid Jacobian singularities, and the control strategies should be designed inside the robot workspace.

2.5 Adaptive Dynamic Control

Now, we consider parametric uncertainties in the robot dynamics described by equation (2.40). In this context, we present here the Slotine-Li adaptive scheme (SLOTINE *et al.*, 1991), to solve the problem of following a desired trajectory $\theta_d(t)$, given in the joint-space. First, assume that there exists a control law $\tau = F(\theta, \dot{\theta}, \theta_d, \dot{\theta}_d, \ddot{\theta}_d)$ which guarantees a goal is reached, i.e.,

$$e(t) = \theta - \theta_d \to 0, \qquad t \to \infty \tag{2.50}$$

where $\theta_d \in \mathbb{R}^n$ denotes the desired trajectory, assigned to the joint space and assumed uniformly bounded, and e is the joint position error vector. Now, consider the following signals, similarly defined in the joint space as:

$$\dot{\theta}_r = \dot{\theta}_d - \lambda_d e \tag{2.51}$$

$$\sigma = \dot{\theta} - \dot{\theta}_r = \dot{e} + \lambda_d e \tag{2.52}$$

where $\dot{\theta}_r \in \mathbb{R}^n$ is a velocity reference signal, $\sigma \in \mathbb{R}^n$ is a measure of tracking accuracy and $\lambda_d > 0$ is a constant parameter. Now, consider the following linear parameterization, assumed to exist due to the properties of an Euler-Lagrangian model (2.42):

$$M(\theta)\dot{\eta} + C(\theta, \dot{\theta})\eta + G(\theta) = Y_d(\theta, \dot{\theta}, \eta, \dot{\eta})a_d, \tag{2.53}$$

where $\eta \in \mathbb{R}^n$ is an arbitrary vector, $Y_d(\theta, \dot{\theta}, \eta, \dot{\eta})$ is the dynamics regressor matrix and a_d is a vector that has all constant parameters of model (2.40). Considering that signals θ and $\dot{\theta}$ are measurable, that is, it is possible to calculate the regressor matrix Y_d, the adaptive controller proposed in (SLOTINE *et al.*, 1991) can be used in the system, given by:

$$\tau = Y_d(\theta, \dot{\theta}, \dot{\theta}_r, \ddot{\theta}_r)\hat{a}_d - K_D\sigma + \omega_2, \tag{2.54}$$

where K_d is positive definite gain matrix, $\omega_2 \in \mathbb{R}^n$ is a fictitious external input and $\hat{a}_d$ is a vector of estimated dynamic parameters, which are updated by the following adaptation law

$$\dot{\hat{a}}_d = -\Gamma_d Y_d^T \sigma, \quad \Gamma_d = \Gamma_d^T > 0 \tag{2.55}$$

where Γ_d is a positive definite gain matrix.

Now, defining the parametrization error $\tilde{a}_d = \hat{a}_d - a_d$, from the robot dynamic model (2.53) and the dynamic control law (2.54), the closed-loop error dynamics

$$M(\theta)\ddot{\theta} + C(\theta, \dot{\theta})\dot{\theta} + G(\theta) = Y_d(\theta, \dot{\theta}, \dot{\theta}_r, \ddot{\theta}_r)\tilde{a}_d + Y_d(\theta, \dot{\theta}, \dot{\theta}_r, \ddot{\theta}_r)a_d - K_D\sigma + \omega_2 \tag{2.56}$$

can be re-written as

$$M(\theta)\dot{\sigma} + (C(\theta, \dot{\theta}) + K_D)\sigma = Y_d(\theta, \dot{\theta}, \dot{\theta}_r, \ddot{\theta}_r)\tilde{a}_d + \omega_2 \tag{2.57}$$

We present the algorithm for the adaptive dynamic controller in Table (2.1), and its block diagram in (Figure 2.6). The following theorem establishes the passivity properties and stability analysis of the closed-loop system.

Remark 10. *It is worth of note that*

(i) *Considering the vectors θ and $\dot{\theta}$ measurable, all signals necessary to compute the regressor matrix Y_d are available, and*

(ii) *the convergence of the estimated parameters $\hat{a}_d$ to the real values depends on the level of excitation of the regressor matrix Y_d.*

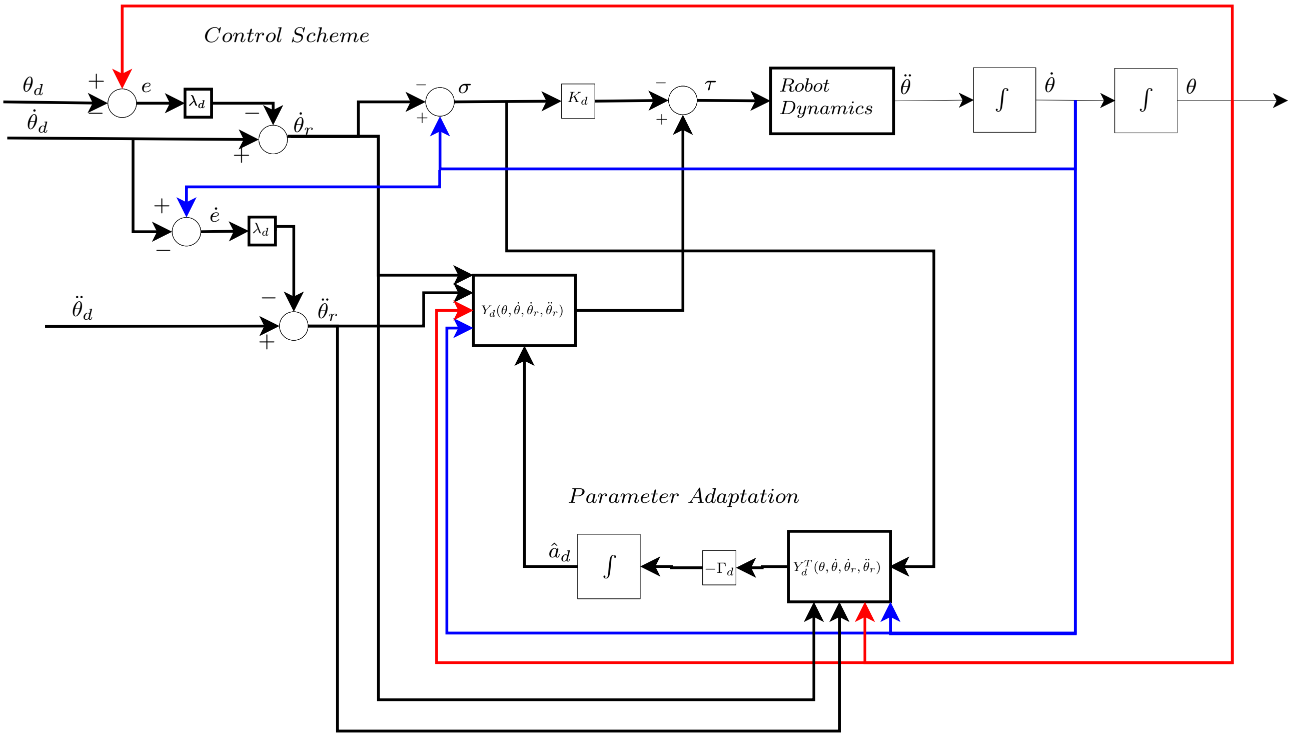

Figure 2.6: Block Diagram for the Slotine-Li Adaptive Controller

Table 2.1: Algorithm for Adaptive Dynamic Control

Robot Dynamic Model	$M(\theta)\ddot{\theta} + C(\theta,\dot{\theta})\dot{\theta} + G(\theta) = \tau$
Dynamic Control Law	$\tau = Y_d(\theta,\dot{\theta},\dot{\theta}_r,\ddot{\theta}_r)\hat{a}_d - K_D\sigma + \omega_2$
Parameterization	$M(\theta)\dot{\eta} + C(\theta,\dot{\theta})\eta + G(\theta) = Y_d(\theta,\dot{\theta},\eta,\dot{\eta})a_d$
Dynamic Adaptation Law	$\dot{\hat{a}}_d = -\Gamma_d Y_d^T \sigma$
Model Errors	$\sigma = \dot{\theta} - \dot{\theta}_r = \dot{e} + \lambda_d e \qquad \tilde{a}_d = \hat{a}_d - a_d$ $e = \theta - \theta_d \qquad \dot{\theta}_r = \dot{\theta}_d - \lambda_d e$
Closed-loop Equation	$M(\theta)\dot{\sigma} + (C(\theta,\dot{\theta}) + K_D)\sigma = Y_d(\theta,\dot{\theta},\dot{\theta}_r,\ddot{\theta}_r)\tilde{a}_d + \omega_2$

Theorem 3. *(LEITE and LIZARRALDE, 2016) Consider the uncertain robot manipulator dynamic model given by equation (2.40), the control law given by (2.54), the parameterization given by (2.53) and the parameter adaptation law given by (2.55). Assume that θ and $\dot{\theta}$ are measured system signals, so that regressor matrix Y_d can be calculated. Then, the map $\omega_2 \to \sigma$ is output strictly passive with positive definite storage function*

$$2V_d(\sigma,\tilde{a}_d) = \sigma^T M(\theta)\sigma + \tilde{a}_d^T \Gamma_d^{-1} \tilde{a}_d \tag{2.58}$$

Moreover, for $\omega_2 = 0$, the following properties hold:

- *(i) All system signals are uniformly bounded;*
- *(ii) $lim_{t\to\infty}\sigma(t) = 0$*

- *(iii)* $lim_{t\to\infty}\dot{e}(t) = 0$ *and* $lim_{t\to\infty}e(t) = 0$

6

Proof. The derivative with respect to time of the storage function V_d (2.58) is given by:

$$\dot{V}_d(\sigma, \tilde{a}_d) = \sigma^T M(\theta)\dot{\sigma} + \frac{1}{2}\sigma^T \dot{M}\sigma + \tilde{a}_d^T \Gamma_d^{-1}\dot{\tilde{a}}_d \tag{2.59}$$

Using the closed-loop error dynamics given by equation (2.58), we obtain:

$$\dot{V}_d(\sigma, \tilde{a}_d) = \sigma^T Y_d(\theta, \dot{\theta}, \dot{\theta}_r, \ddot{\theta}_r)\tilde{a}_d + \sigma^T\omega_2 - \sigma^T C(\theta, \dot{\theta})\sigma - \sigma^T K_D\sigma + \frac{1}{2}\sigma^T \dot{M}\sigma + \tilde{a}_d^T \Gamma_d^{-1}\dot{\tilde{a}}_d \tag{2.60}$$

By using the anti-symmetry properties of Euler-Lagrangian systems (2.41)

$$\dot{V}_d(\sigma, \tilde{a}_d) = \sigma^T Y_d(\theta, \dot{\theta}, \dot{\theta}_r, \ddot{\theta}_r)\tilde{a}_d + \sigma^T\omega_2 - \sigma^T K_D\sigma + \tilde{a}_d^T \Gamma_d^{-1}\dot{\tilde{a}}_d \tag{2.61}$$

Finally, using the adaptation law (2.55), we obtain the following result:

$$\dot{V}_d(\sigma, \tilde{a}_d) = +\sigma^T\omega_2 - \sigma^T K_D\sigma \tag{2.62}$$

which defines an output strictly passive map[2], from $\omega_2 \to \sigma$. Thus, with $\omega_2 = 0$, $\dot{V}_d \leq 0$, which implies, by Lyapunov theory, that σ, $\tilde{a} \in \mathcal{L}_\infty$ and thus, the equilibrium state is uniformly stable. Since $V_d > 0$ and $\dot{V}_d \leq 0$, then $lim_{t\to\infty}V_d(\sigma, \tilde{a}_d) = V_\infty \geq 0$ exists. Therefore, $\int_0^\infty -\dot{V}_d(t')dt' = V_0 - V_\infty \geq 0$ where $V_0 = V_d(\sigma(0), \hat{a}_d(0))$, which implies that $\sigma \in \mathcal{L}_2$. Since θ_d and its derivative are assumed uniformly bounded, we can conclude that $e, \dot{e} \in \mathcal{L}_\infty$, which implicates that $\theta, \dot{\theta}, \dot{\theta}_r, \ddot{\theta}_r$ and $Y_d(\theta, \dot{\theta}, \dot{\theta}_r, \ddot{\theta}_r) \in \mathcal{L}_\infty$ as well. Therefore, $\dot{\hat{a}}_d \in \mathcal{L}_\infty \cap \mathcal{L}_2$ and so $\dot{\sigma} \in \mathcal{L}_\infty$. As σ and $\tilde{a}$ are limited, the derivative with respect to time $\ddot{V}_d = -2\sigma^T K_D\dot{\sigma}$ is uniformly limited. So, by applying the Barbalat's Lemma, we can conclude that $lim_{t\to\infty}\sigma(t) \to 0$ and consequently $lim_{t\to\infty}\dot{e}(t) \to 0$, $lim_{t\to\infty}e(t) \to 0$, proving the global stability of the closed loop system. □

2.6 Cascade Controller Strategy

A dynamic control scheme can be developed in the Cartesian workspace (2.46) or in the joint workspace (2.40). It is known, that control schemes in the joint workspace is more suitable for robot manipulators with no restrictions (SICILIANO *et al.*, 2011).

[2] A system is output strictly passive if $u^T y \geq \dot{V} + y^T\rho(y)$ for some function ρ where $y^T\rho(y) > 0$, $\forall y \neq 0$, where $V(x)$ is a positive semi-definite function

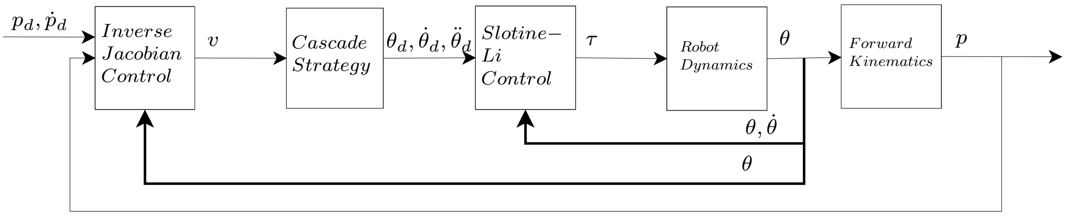

Figure 2.7: Block diagram of a cascade structure for a Cartesian control

The Slotine-Li adaptive scheme previously proposed is general enough to solve most problems dealing with uncertainties in the manipulator dynamics. However, if there are uncertainties on the joint actuators torques τ (e.g. electric direct-drive motors, visual servoing) it can't be directly used. Taking the Cartesian workspace model as an example:

$$M_c(\theta)\ddot{p} + C_c(\theta, \dot{\theta})\dot{p} + G_c(\theta) = Y_c(\theta, \dot{\theta}, \dot{p}, \ddot{p})a_c = J^{-T}\tau \tag{2.63}$$

In the case of an uncertain a_c and J^{-T}, the Slotine-Li adaptive scheme cannot be directly applied, and this problem has been solved by adapting a_d and J^{-T} separately, in a standard adaptive solution (IOANNOU and SUN, 1995). Here, however, we propose a cascade control strategy as seen in (GUENTHER and HSU, 1993), separating the problem into kinematic and dynamic schemes. To gain some intuition on how this separation is done, Figure 2.7 illustrates this strategy which is useful in the following chapters, where a adaptive visual servoing scheme will be applied on the control loop and connected to the dynamic loop through this cascade strategy.

The general strategy is proposed as follows. First, we assume that there exists a control law $\tau = F(\theta, \dot{\theta}, \theta_d, \dot{\theta}_d, \ddot{\theta}_d)$ which guarantees a goal θ_d is reached, i.e.,

$$e(t) = \theta - \theta_d \to 0, \qquad t \to \infty \tag{2.64}$$

where $\theta_d \in \mathbb{R}^3$ denotes the desired trajectory for the dynamic control, assigned to the joint space and assumed uniformly bounded, and e is the joint position error vector.

Now, let us suppose it is possible to define the following signals in joint space θ_d and its time derivatives $\dot{\theta}_d$ and $\ddot{\theta}_d$ in terms of a control signal v so that we have $\dot{p} \to v$ except for a vanishing term, as follows.

$$\dot{p} = v + J(\theta)L(s)e, \tag{2.65}$$

where $L(.)$ denotes a linear operator, possibly noncausal, with s being the differential operator. Therefore we can conclude that it is possible to project a control law for the kinematic model given by equation (2.13), extend it to the dynamic model

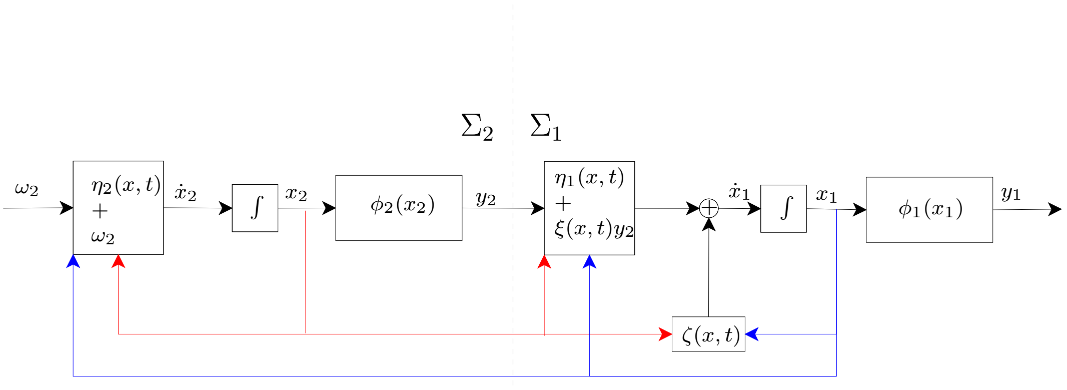

Figure 2.8: Interconnected system in cascade

given by equation (2.40) and the stability property of the closed loop system still remains.

To carry out a stability analysis for cascade strategy proposed, we make use of the passivity property of the system. As seen in (LEITE and LIZARRALDE, 2016), (ZACHI, 2007) and (LIZARRALDE *et al.*, 2013) the visual servoing kinematic control approach has passivity properties, which allows us, in later chapters, to ensure the closed-loop stability when it is connected in a cascade with a dynamic control scene with similar passivity properties. For passive interconnected systems with external disturbances, the following general result can be stated:

Theorem 4. *(HSU* et al.*, 2007) Consider the following interconnected systems, where Σ_1 is the driven system and Σ_2 is the driving system, described by:*

$$\Sigma_1: \quad \dot{x}_1 = \eta_1(x,t) + \xi(x,t)y_2 + \zeta(x,t), \qquad y_1 = \phi_1(x_1), \tag{2.66}$$

$$\Sigma_2: \quad \dot{x}_2 = \eta_2(x,t) + \omega_2, \qquad y_2 = \phi_1(x_2), \tag{2.67}$$

as seen in (Figure 2.8), where $x = [x_1\ x_2]^T$, η_1, η_2 are piecewise continuous functions in time t and locally Lipschitz in x for all $t > 0$;. $x \in \mathcal{D}$, where $\mathcal{D} \subset \mathbb{R}_n$ is a domain that contains the origin $x = 0$; ϕ_1, ϕ_2, ξ are continuous functions, η is a vanishing perturbation term and ω_2 is an external input. Suppose that $||\eta(x,t)|| \leq \gamma||x||$, $\forall t \geq 0$, $\forall x \in \mathcal{D}$, where γ is a non-negative constant. Assume that $||\xi(x,t)|| \leq c$, $\forall x$, t and for some $c > 0$. If system Σ_1 is output strictly passive from $y_2 \to y_1$ with positive definite storage function $V_1(x_1)$ such that

$$\dot{V}_1 \leq -\lambda_1||y_1||^2 + c_1 y_2^T y_1, \quad \lambda_1 > 0 \tag{2.68}$$

and system Σ_2 is output strictly passive from $\omega_2 \to y_2$ with positive definite storage function $V_2(x_2)$ such that

$$\dot{V}_2 \leq -\lambda_2||y_2||^2 + c_2 \omega_2^T y_2, \quad \lambda_2 > 0. \tag{2.69}$$

Then, for $\omega_2 = 0$, the following properties hold:

- *(i)* $x_1, \; x_2 \in \mathcal{L}_\infty$;
- *(ii)* $lim_{t\to\infty}y_1(t) = 0, \;\; lim_{t\to\infty}t_2(t) = 0.$

Proof. Let $V_1(x_1)$ and $V_2(x_2)$ be the storage functions for the interconnected subsystems Σ_1 and Σ_2. Consider

$$V(x) = V_2(x_2) + \alpha V_1(x_1) \tag{2.70}$$

as the storage function for the feedback connection.

The derivative of $V(x)$ with respect to time, along the trajectories of both subsystems, and considering $\omega_2 = 0$ is given by

$$\dot{V} \leq -\lambda_2||y_2||^2 - \alpha\lambda_1||y_1||^2 + \alpha c_1 y_2^T y_1, \quad \alpha > 0 \tag{2.71}$$

$$\dot{V} \leq \left[\begin{array}{cc} ||y_1|| & ||y_2|| \end{array} \right] \left[\begin{array}{cc} -\alpha\lambda_1 & \frac{1}{2}\alpha c_1 \\ \frac{1}{2}\alpha c_1 & -\lambda_2 \end{array} \right] \left[\begin{array}{c} ||y_1|| \\ ||y_2|| \end{array} \right], \tag{2.72}$$

a Schur's complement property states that

$$\left[\begin{array}{cc} S_1 & S_2 \\ S_2^T & S_3 \end{array} \right] < 0 \Longleftrightarrow S_3 < 0, \;\; S_1 - S_2^T S_3^{-1} S_2 < 0, \tag{2.73}$$

then from equation (2.72), $\dot{V} < 0$ if

$$-\lambda_2 < 0, \qquad\qquad -\alpha\left(\lambda_1 + \frac{\alpha c_1^2}{4\lambda_2}\right), \tag{2.74}$$

then for some sufficiently small $\alpha > 0$, $\dot{V}(x)$ is negative definite with respect to outputs y_1 and y_2. Consequently, we have $x_1, \; x_2 \in \mathcal{L}_\infty$ and $\dot{x}_1, \; \dot{x}_2 \in \mathcal{L}_\infty$. The inequality equation for $\dot{V}(x)$ implies that $y_1, y_2 \in \mathcal{L}_2 \cap \mathcal{L}_\infty$. From Barbalat's lemma, it results that $lim_{t\to\infty}y_1(t) = 0$ and $lim_{t\to\infty}y_2(t) = 0$, which demonstrates the global asymptotic stability of closed-loop interconnected subsystems.

□

2.7 Conclusion

In this chapter, we present an overview of the kinematic and dynamic modeling of robot manipulators, emphasizing important properties that are useful for analyzing and projecting controller schemes. An inverse Jacobian scheme is introduced to illustrate control for the kinematic model, expanded to an adaptive case when considering uncertainties in the Jacobian.

For the manipulator with non-negligible dynamics the Slotine-Li adaptive scheme is presented. However, this control strategy cannot be used as is for Cartesian control of a manipulator with uncertainties on both dynamic and kinematic parameters. For this, we introduce a Cascade Control scheme, to achieve separation of the kinematic and dynamic control loops. By making use of this strategy proposed in (GUENTHER and HSU, 1993), we can connect the adaptive inverse Jacobian control to the Slotine-Li adaptive scheme, cascading into a stable closed-loop system.

Chapter 3

Adaptive Visual Servoing of Translational Motion

Visual servoing is a term coined to designate control based on feedback of visual measurements. Control schemes using visual servoing can be divided into two categories: Pose-based visual servoing, that realize visual servoing in the operational space; and image-based visual servoing, that realizes the same operation but in the image space. These situations are illustrated by Figure 3.1 and Figure 3.2

As seen in (SICILIANO *et al.*, 2011), in position-based visual servoing, measurements are used to estimate (in real time) the homogeneous transformation matrix T time, representing the relative pose of the object frame with respect to the camera frame. From T, the vector of independent coordinates p_i, containing the position of the object with respect to the camera frame and its relative orientation, can be obtained.

For the image-based visual servoing, the visual measurements are not processed to Cartesian space, and instead, the task itself is planned in the image-space, the pose of the manipulator in the inertial frame does not need to be known. In this case, control schemes need to guarantee that the image space error tends to zero.

If multiple cameras are used, it is possible to retrieve depth information with one image, a situation named stereo vision. However it is still possible to achieve

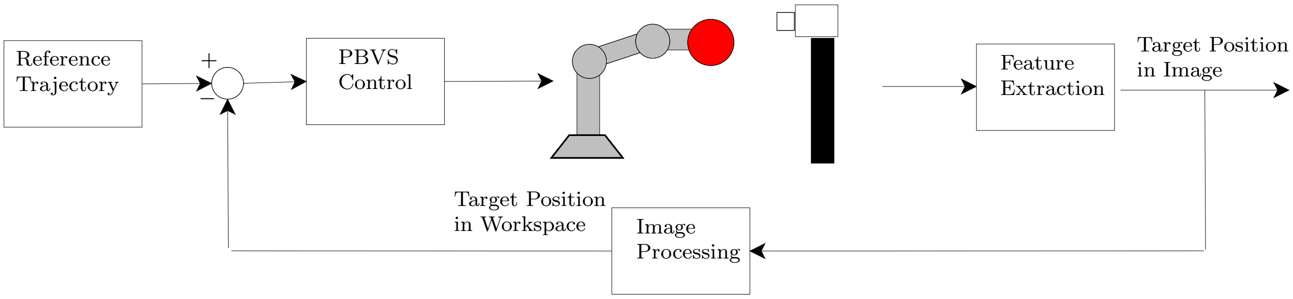

Figure 3.1: Schematics of a PBVS configuration

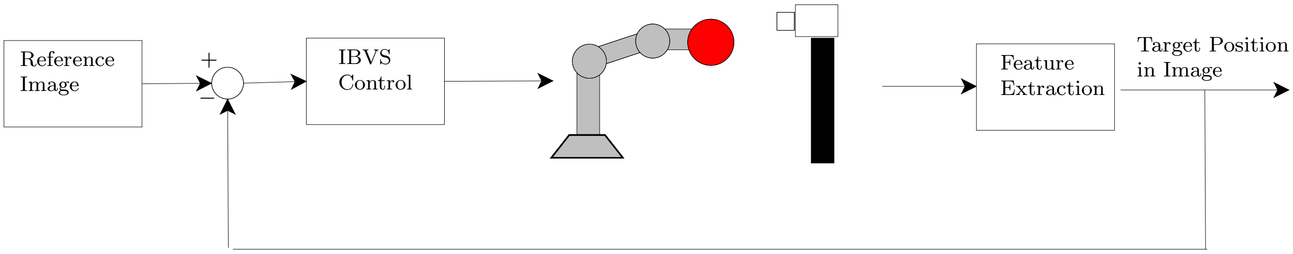

Figure 3.2: Schematics of a IBVS configuration

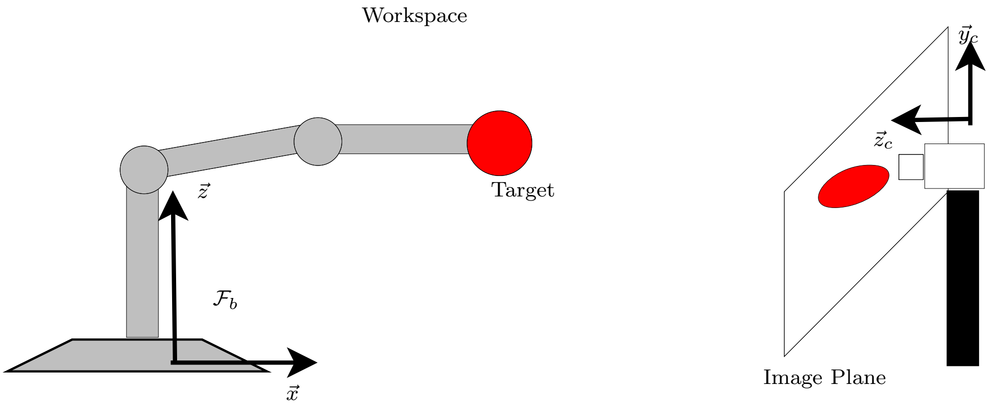

Figure 3.3: An eye-to-hand visual servoing setup.

3D vision with a single camera, as we shall use in this work, provided that a few geometrical characteristics of the object are known or prepared in advance. Mono-camera systems are easier to calibrate and set-up, even if they may present lower accuracy.

A visual servoing system can be further classified into two other systems, depending on where the camera is positioned:

An eye-to-hand system, where the camera is set up in a fixed pose, its field of view unchanging in relation to the base frame $\mathcal{F}_b$ of the manipulator. In this setup, the unchanging camera field of view makes the accuracy of image measurements, in most cases, constant (Figure 3.3). This setup, susceptible to object occlusion, as the manipulator itself may block the line of sight to the tracked objects (SICILIANO *et al.*, 2011).

An eye-in-hand system is a mobile camera setup, with the camera mounted on the robot, generally on the end-effector. Differently from the previous case, the field of view of this setup changes significantly during motion which may produce a high variability in the accuracy of measurements. However, when the end-effector is close to the target, the accuracy becomes almost constant and is usually higher than that achievable with eye-to-hand setups (SICILIANO *et al.*, 2011) (Figure 3.4).

Another point of note is that the camera itself has a series of intrinsic parameters that has to be taken into account, usually acquired by means of a process called camera calibration. In this work, we use an eye-to-hand mono-camera 3D image-

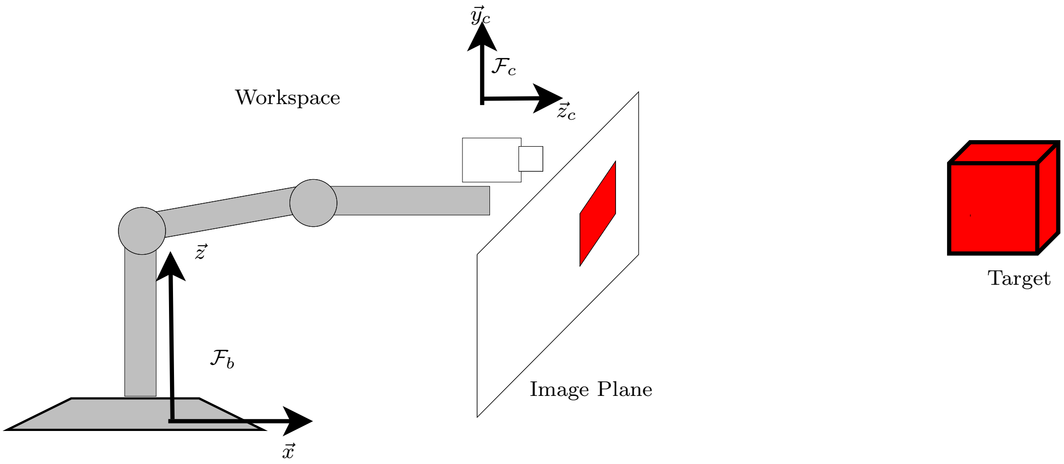

Figure 3.4: An eye-in-hand visual servoing setup

based visual servoing setup with a depth feature, with uncertain parameters, by making use of adaptive control schemes.

3.1 Visual Servoing System

Consider the visual tracking problem for an uncertain robot manipulator monitored by a fixed, pinhole camera with uncertain parameters, as illustrated by Figure 3.3. The control objective is tracking a reference trajectory along the x, y and z directions.

This task requires control of at least three degrees of freedom, and to accomplish that, the visual servoing system will need to extract at least three image features from a tracked target attached to the manipulator. In this work, a spherical target is assumed to be the target, so its projection in the image plane is invariant in response to rotations in the 3D environment and it is possible to partially decouple the control of x and y from the depth z (ZACHI *et al.*, 2006). The features to be extracted from this target are the centroid of its projection in the image plane and its area. The first feature is used to track a desired planar trajectory in the image plane, while the second relates to depth tracking.

3.1.1 System Description

Let $p_c = [x_c \; y_c \; z_c]^T \in \mathbb{R}^3$ be the position vector of the centroid of the tracked target and its depth, expressed in the image frame $\mathcal{F}_c$, and $p_b = [x_b \; y_b \; z_b]^T \in \mathbb{R}^3$ be the position vector of the centroid but expressed in base frame of the manipulator $\mathcal{F}_b$. From the frontal perspective projection model of a pinhole camera (ZACHI, 2007), these two vectors are related by

$$p_c = \begin{bmatrix} \frac{f\alpha_x}{z_c} & 0 & 0 \\ 0 & \frac{f\alpha_y}{z_c} & 0 \\ 0 & 0 & 1 \end{bmatrix} R(\phi_x, \phi_y, \phi_z)\, p_b + p_i \tag{3.1}$$

where $f \in \mathbb{R}^+$ is the camera focal length in mm, $\alpha_x,\ \alpha_y \in \mathbb{R}^+$ are the camera scaling factors in $pixel/mm$, $R \in SO(3)$ is the rotation matrix that represents the misalignment between camera and base frame and $p_i = [x_i\ y_i\ z_i]^T$ is the translational vector between the origin of the two frames.

Remark 11. *It is important to note that there is no requirement for the z-axis of the camera-frame and the base-frame to be aligned in this work. The sole assumption, regarding the pinhole camera, is that the target is always in the camera field of view.*

Consider the constant matrices $K_p^{\perp} = \begin{bmatrix} f\alpha_x & 0 & 0 \\ 0 & f\alpha_y & 0 \end{bmatrix} R$ and $K_{p_z} = [0\ 0\ 1]\ R$, so we can rewrite equation (3.1) in a compact notation

$$p_c = \begin{bmatrix} \frac{1}{z_c} K_p^{\perp} \\ K_{p_z} \end{bmatrix} p_b + p_i \tag{3.2}$$

The differential kinematics that describes the behavior of this system is obtained by directly calculating the derivative of equation (3.2) with respect to time:

$$\dot{p}_c = \begin{bmatrix} \frac{1}{z_c} K_p^{\perp} \\ K_{p_z} \end{bmatrix} \dot{p}_b - \frac{1}{z_c} \begin{bmatrix} p_{xy} - p_{xyi} \\ 0 \end{bmatrix} \dot{z}_c, \tag{3.3}$$

where $p_{xy} = [x_c\ y_c]^T$ and $p_{xyi} = [x_i\ y_i]^T$.

Yet, as $\dot{z}_c = K_{pz} \dot{p}_b$,

$$\dot{p}_c = \begin{bmatrix} \frac{1}{z_c}(K_p^{\perp} - (p_{xy} - p_{xyi}) K_{p_z}) \\ K_{p_z} \end{bmatrix} \dot{p}_b \tag{3.4}$$

3.1.2 Depth Tracking

Let us consider the Cartesian depth description z_c and the spherical target of the proposed formulation. Let $a_c \in \mathbb{R}^+$ be the projected area of the target object in $pixels^2$, expressed in the image frame $\mathcal{F}_c$. If so, the expression between those two measurements is given by:

$$(a_c)^{\frac{1}{2}} z_c = \frac{1}{\beta} \tag{3.5}$$

The following assumptions are considered hereafter:

($A1$) The projected area of the target a_c is bounded and greater than zero, for any time t in the interval $[0,\ \infty)$;

($A2$) The camera is uncalibrated and β is uncertain. Hence a measurement of z_c is unavailable;

($A3$) The sign of z_c is assumed to be constant and known. Hence, without loss of generality, we can assume that $z_c > 0$, and $\beta > 0$;

($A4$) The effects of radial distortion caused by the camera lens are considered negligible.

The differential kinematics of the depth-to-area transformation is given by directly deriving equation (3.5) with respect to time:

$$\dot{a}_c = -2\beta(a_c)^{\frac{3}{2}}\dot{z}_c \tag{3.6}$$

3.1.3 Complete translational model with area information

Let $p_v = [x_c\ y_c\ a_c]^T$ be the vector of image feature, expressed in terms of the centroid coordinates and the area of target object. From equations (3.4) and (3.6), we can rewrite the visual servoing system to have the following structure:

$$\dot{p}_v = \begin{bmatrix} \beta a_c^{\frac{1}{2}}(K_p^{\perp} - (p_{xy} - p_{xyi})K_{pz}) \\ -2\beta a_c^{\frac{3}{2}} K_{pz} \end{bmatrix} \dot{p}_b \tag{3.7}$$

Remark 12. *In (WANG* et al.*, 2018), multiple features can be tracked in the same manipulator. The number of degrees of freedom of the manipulator (n) and that of the feature points (m) are subjected to the constraint that $n \geq 2m$ and $m \leq 3$, and in the case $m = 3$, the three feature points are non-collinear. In this work, such a consideration is possible as well, however since we are also tracking depth the constraint is appropriately changed to $n \geq 3m$.*

Example 3. *Consider tracking two features ($n = 2$) in a manipulator with six degrees of freedom ($m = 6$). If the position of each feature is given by p_{v1} and p_{v2}, respectively, then the complete system can be described by:*

$$\begin{bmatrix} \dot{p}_{v1} \\ \dot{p}_{v2} \end{bmatrix} = \mathcal{A}_c \begin{bmatrix} \mathcal{K}_p^{\perp} - \mathcal{P}\mathcal{K}_z \end{bmatrix} \begin{bmatrix} \dot{p}_{b1} \\ \dot{p}_{b2} \end{bmatrix} \tag{3.8}$$

where

$$\mathcal{A}_c = \begin{bmatrix} \beta_1 a_{c_1}^{\frac{1}{2}} & 0 & 0 & 0 & 0 & 0 \\ 0 & \beta_1 a_{c_1}^{\frac{1}{2}} & 0 & 0 & 0 & 0 \\ 0 & 0 & -2\beta_1 a_{c_1}^{\frac{3}{2}} & 0 & 0 & 0 \\ 0 & 0 & 0 & \beta_2 a_{c_2}^{\frac{1}{2}} & 0 & 0 \\ 0 & 0 & 0 & 0 & \beta_2 a_{c_2}^{\frac{1}{2}} & 0 \\ 0 & 0 & 0 & 0 & 0 & -2\beta_2 a_{c_2}^{\frac{3}{2}} \end{bmatrix} \tag{3.9}$$

$$\mathcal{K}_p^{\perp} = \begin{bmatrix} K_p^{\perp} & 0 \\ 0 & 0 \\ 0 & K_p^{\perp} \\ 0 & 0 \end{bmatrix} \tag{3.10}$$

$$\mathcal{P} = \begin{bmatrix} (p_{xy_1} - p_{xyi_1}) & 0 \\ 1 & 0 \\ 0 & (p_{xy_2} - p_{xyi_2}) \\ 0 & 1 \end{bmatrix} \tag{3.11}$$

$$\mathcal{K}_z = \begin{bmatrix} K_z & 0 \\ 0 & K_z \end{bmatrix} \tag{3.12}$$

■

As mentioned earlier in this chapter, we consider the camera and robot parameters to be uncertain. In (LEITE and LIZARRALDE, 2016), linear parameterization of the depth and planar subsystems are done from this model for adaptation of the camera parameters. In this work, similar to what is presented in (WANG *et al.*, 2018), while we also separate the system in planar and depth subsystems, we parameterize the camera matrix K_p together with the Jacobian matrix J. However, since we already exemplified how parameterization is done in (LEITE and LIZARRALDE, 2016) for the kinematic and dynamic systems in the previous chapter, we also present how parameterization is done for the visual system here as well, a form that is useful for direct adaptation.

Considering that, in (LEITE and LIZARRALDE, 2016), the z-axis of the camera frame and robot frame are assumed to be aligned, the depth subsystem can be simplified as

$$\dot{a}_c = -2\beta(a_c)^{\frac{3}{2}}\dot{z}_b \tag{3.13}$$

So, the linear parameterization is given by

$$\dot{a}_c = Y_z(a_c, \dot{z}_b)a_z, \qquad a_z = \beta \tag{3.14}$$

Similarly, the planar subsystem can also be simplified as

$$\begin{aligned} \dot{p}_{xy} &= \left[\ \beta a_c^{\frac{1}{2}} (K_p^{\perp} - (p_{xy} - p_{xyi}) \, [0 \ 0 \ 1]) \ \right] \dot{p}_b \\ &= a_c^{\frac{1}{2}} \beta K_p^{\perp} \dot{p}_b - \beta a_c^{\frac{1}{2}} (p_{xy} - p_{xyi}) \dot{z}_b \end{aligned} \tag{3.15}$$

Then, according to (HSU *et al.*, 2001), if $K_p^{\perp}$ has non-zero leading principal minors, it is always possible to factorize $K_p^{\perp} = SDU$, where S denotes a symmetric and positive definite matrix, D is a diagonal matrix, and U is an upper triangular matrix with unitary diagonal elements.

3.2 Adaptive Visual Servo Control

In this section, we employ an adaptive visual servoing strategy in order to tackle a trajectory tracking problem, in the presence of an uncalibrated camera and parametric uncertainties in the robot manipulator. Here, the desired trajectory is decoupled in planar and depth trajectories, the former given in terms of the target centroid, the latter in terms of its projected area. Let $p_v \in \mathbb{R}^3$ be the vector of image feature and $p_d(t) \in \mathbb{R}^3$ be the translational reference trajectory, both represented in the image frame $\mathcal{F}_c$. The control goal can be described as:

$$p_v \to p_d(t), \qquad e_v(t) = p_v - p_d(t) \to 0 \tag{3.16}$$

where $e_v(t) \in \mathbb{R}^3$ represents the image feature error. The following assumptions are made to achieve this goal:

($A5$) The translational reference trajectory $p_d(t)$ is planned so it remains visible, within the robot workspace, and its first derivative, $\dot{p}_d(t)$, is known and bounded.

($A6$) The robot motions are away from singular configurations.

($A7$) The joint angle θ is measurable.

With these assumptions, we can consider that target occlusion problem does not occur and that inverse of the analytical Jacobian matrix always exists. Notice that as we use an indirect adaptive approach, to guarantee that the inverse of the estimated Jacobian matrix exists, we also use a projection method to keep the adaptive parameters bounded (HSU and COSTA, 1991).

3.2.1 Problem Formulation

Consider a visual servoing system with uncertain camera parameters, and a robot manipulator with three degrees-of-freedom, with non-negligible dynamics and similarly uncertain kinematic and dynamics parameters. The differential kinematics for a translational visual servoing system with depth feature is given by equation (3.7) and those for the position of a robot manipulator by equation (2.6), both repeated here for convenience:

$$\dot{p}_v = \begin{bmatrix} \beta a_c^{\frac{1}{2}}(K_p^{\perp} - (p_{xy} - p_{xyi})K_{pz}) \\ -2\beta a_c^{\frac{3}{2}} K_{pz} \end{bmatrix} \dot{p}_b \tag{3.17}$$

$$\dot{p}_b = J(\theta)\dot{\theta} \tag{3.18}$$

where $p_v = [x_c \; y_c \; a_c]^T$, $p_b = [x_b \; y_b \; z_b]^T$, $p_{xy} = [x_c \; y_c]^T$, $p_{xyi} = [x_i \; y_i]^T$, $K_p^{\perp}$ and K_{pz} are the planar and depth visual servoing system matrices respectively, β is the depth-to-area transformation constant, J is the Jacobian of the manipulator expressed in the base frame and θ are the configuration of its joints.

Substituting p_b from equation (3.18) into equation (3.17), we obtain the differential kinematics for the complete system.

$$\dot{p}_v = \begin{bmatrix} \beta a_c^{\frac{1}{2}}(K_p^{\perp} - (p_{xy} - p_{xyi})K_{pz}) \\ -2\beta a_c^{\frac{3}{2}} K_{pz} \end{bmatrix} J\dot{\theta} \tag{3.19}$$

$$\dot{p}_v = \underbrace{\begin{bmatrix} \beta a_c^{\frac{1}{2}}(J^{\perp} - (p_{xy} - p_{xyi})J_z) \\ -2\beta a_c^{\frac{3}{2}} J_z \end{bmatrix}}_{J^*(\theta, p_v)} \dot{\theta} \tag{3.20}$$

where $J^*(\theta, p_v)$ is called the feature Jacobian, $J^{\perp} = K_p^{\perp}J$ and $J_z = K_{pz}J$ are the image plane and depth Jacobian, respectively. These still maintain the linear parameterization property of the Jacobian, as follows:

($P1$) As an extension of the parameterization property of the Jacobian $J(\theta)$, the product of the image plane Jacobian $J^{\perp}(\theta)$ and the depth Jacobian J_z with any measurable vector $\phi(t)$ can be linearly parameterized as

$$\beta J^{\perp}\phi = Y^{\perp}(\theta, \phi)a^{\perp} \tag{3.21}$$

$$\beta J_z\phi = Y_z(\theta, \phi)a_z \tag{3.22}$$

where $Y^{\perp}(\theta, \phi) \in \mathbb{R}^{2\times p}$ and $Y_z(\theta, \eta) \in \mathbb{R}^{1\times q}$ are, respectively, the planar and depth kinematic regressor matrices, $a^{\perp} \in \mathbb{R}^p$ is a depth-independent parametric vector and $a_z \in \mathbb{R}^q$ is a constant depth parametric vector. The lower and upper bound $a^{\perp}_{min}$, $a^{\perp}_{max}$, $a_{z_{min}}$ and $a_{z_{max}}$, respectively, are assumed known for the camera and kinematic parameters and satisfy

$$||a^{\perp}_{min}|| \leq ||a^{\perp}|| \leq ||a^{\perp}_{max}|| \tag{3.23}$$

$$||a_{z_{min}}|| \leq ||a_z|| \leq ||a_{z_{max}}|| \tag{3.24}$$

3.2.2 Kinematic Translational Controller

Consider the kinematic visual servoing problem given by equation (3.20), that represents the differential kinematics of a target centroid and area. The task, here, is to have the robot manipulator end effector, effectively target centroid and area p_v measured in the camera, follow a desired trajectory $p_d(t)$, expressed in image coordinates. For this particular problem, we consider that the joints velocity $\dot{\theta}$ can be designed as a control signal $u \in \mathbb{R}^3$ so that the system is given by

$$p_v = \begin{bmatrix} \beta a_c^{\frac{1}{2}}(J^{\perp} - (p_{xy} - p_{xyi})J_z) \\ -2\beta a_c^{\frac{3}{2}} J_z \end{bmatrix} u + \omega_1(t) = J^* u + \omega_1(t) \tag{3.25}$$

which can be rewritten with parameterizations (3.21) and (3.22) as

$$p_v = \begin{bmatrix} a_c^{\frac{1}{2}} Y^{\perp}(\theta, u) \\ 0 \end{bmatrix} a^{\perp} - \begin{bmatrix} a_c^{\frac{1}{2}}(p_{xy} - p_{xyi}) \\ 2a_c^{\frac{3}{2}} \end{bmatrix} Y_z(\theta, u) a_z + \omega_1 \tag{3.26}$$

Assuming, θ is measurable, it is possible to calculate the regressor matrices $Y^{\perp}$ and Y_z.

Finally, to reach the desired task goal, we propose the following control law u

$$u = \hat{J}^{*-1}(\dot{p}_d - K_k e_v) \tag{3.27}$$

where $e_v = p_v - p_d$ is the tracking error, K_k is a positive gain and $\hat{J}^*$ is an estimate of the image Jacobian J^* using a parameter vectors estimates $\hat{a}^{\perp}$ and $\hat{a}_z$. Those estimated parameter vectors are updated by the following laws:

$$\dot{\hat{a}}^{\perp} = \Gamma^{\perp} \begin{bmatrix} a_c^{\frac{1}{2}} Y^{\perp} \\ 0 \end{bmatrix}^T e_v \tag{3.28}$$

$$\dot{\hat{a}}_z = -\Gamma_z Y_z^T \begin{bmatrix} a_c^{\frac{1}{2}}(p_{xy} - p_{xyi}) \\ 2a_c^{\frac{3}{2}} \end{bmatrix}^T e_v \tag{3.29}$$

Projection Algorithm

As mentioned in Chapter 1 and earlier in this chapter, to ensure that the inverse of the estimated Jacobian exists in an indirect adaptation scheme, a projection algorithm is needed to avoid the singularity at the origin of the parameter vector. In this work, we introduce a projection to accomplish this, and another objective as well:

- Avoid the singularity point at the origin;
- Avoid large parameter drifting during the transient phase.

Consider the following projection algorithm:

$$\Lambda(g,h) = h - \frac{(h^T g)h}{h^T h} \tag{3.30}$$

Then, we can update the adaptation laws (3.28) and (3.29) as:

$$\dot{\hat{a}}^{\perp} = \begin{cases} \Lambda(\dot{\hat{a}}^{\perp}, \hat{a}^{\perp}), & for \;\; ||\hat{a}^{\perp}|| >= ||a^{\perp}||_{max}, \;\; \hat{a}^{\perp T}\dot{\hat{a}}^{\perp} > 0 \\ \Lambda(\dot{\hat{a}}^{\perp}, \hat{a}^{\perp}), & for \;\; ||\hat{a}^{\perp}|| <= ||a^{\perp}||_{min}, \;\; \hat{a}^{\perp T}\dot{\hat{a}}^{\perp} < 0 \\ \dot{\hat{a}}^{\perp}, \quad otherwise. \end{cases} \tag{3.31}$$

$$\dot{\hat{a}}_z = \begin{cases} \Lambda(\dot{\hat{a}}_z, \hat{a}_z), & for \;\; ||\hat{a}_z|| >= ||a_z||_{max}, \;\; \hat{a}_z^T\dot{\hat{a}}_z > 0 \\ \Lambda(\dot{\hat{a}}_z, \hat{a}_z), & for \;\; ||\hat{a}_z|| <= ||a_z||_{min}, \;\; \hat{a}_z^T\dot{\hat{a}}_z < 0 \\ \dot{\hat{a}}_z, \quad otherwise. \end{cases} \tag{3.32}$$

It is necessary to know $||a^{\perp}||_{max}, ||a^{\perp}||_{min}, ||a_z||_{max}, ||a_z||_{min}$, upper and lower bounds for parameter vectors $a^{\perp}$ and a_z respectively.

Stability Analysis

Now, we proceed with the stability analysis of the proposed controller scheme. First, we calculate the dynamic equation of the tracking error $\dot{e}_v = \dot{p}_v - \dot{p}_d$ so:

$$\dot{e}_v = J^* u + \omega_1 - \dot{p}_d \tag{3.33}$$

Considering the parametric errors $\tilde{a}^{\perp} = \hat{a}^{\perp} - a^{\perp}$ and $\tilde{a}_z = \hat{a}_z - a_z$, we can rewrite $J^*u = \hat{J}^*u - \tilde{J}^*u$ as:

$$J^*u = \hat{J}^*u - \begin{bmatrix} a_c^{\frac{1}{2}} Y^{\perp}(\theta,u) \\ 0 \end{bmatrix} \tilde{a}^{\perp} + \begin{bmatrix} a_c^{\frac{1}{2}}(p_{xy} - p_{xyi}) \\ 2a_c^{\frac{3}{2}} \end{bmatrix} Y_z(\theta,u)\tilde{a}_z \tag{3.34}$$

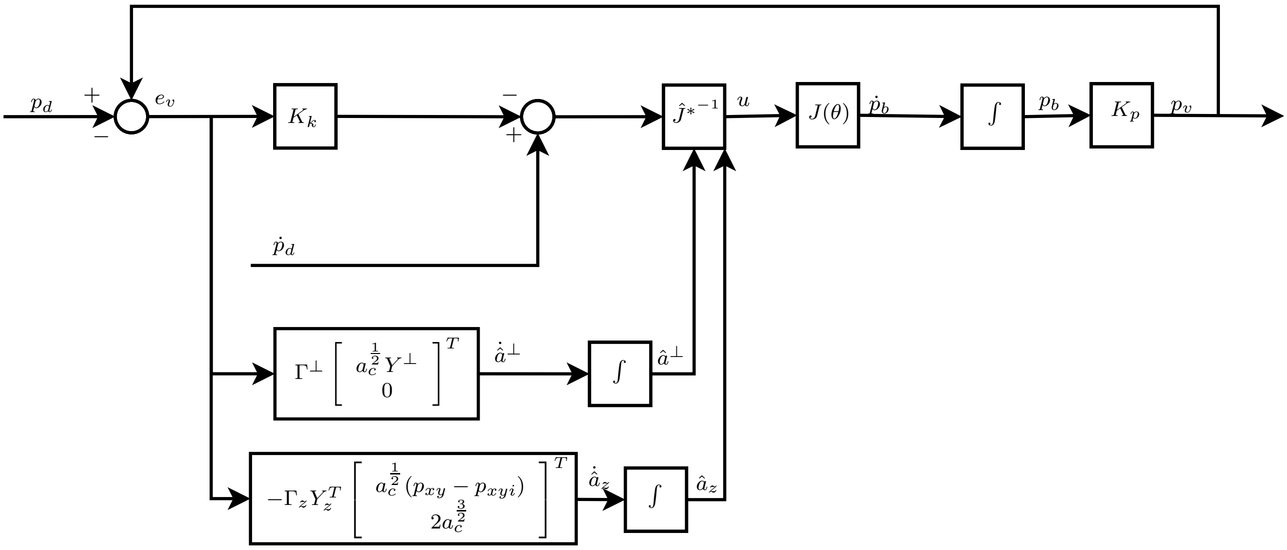
p_d
+
−
e_v
K_k
−
+
$\hat{J}^{*^{-1}}$
u
$J(\theta)$
$\dot{p}_b$
$\int$
p_b
K_p
p_v
$\dot{p}_d$
$\Gamma^{\perp}\begin{bmatrix} a_c^{\frac{1}{2}} Y^{\perp} \\ 0 \end{bmatrix}^T$
$\dot{\hat{a}}^{\perp}$
$\int$
$\hat{a}^{\perp}$
$-\Gamma_z Y_z^T \begin{bmatrix} a_c^{\frac{1}{2}}(p_{xy} - p_{xyi}) \\ 2a_c^{\frac{3}{2}} \end{bmatrix}^T$
$\dot{\hat{a}}_z$
$\int$
$\hat{a}_z$

Figure 3.5: Block Diagram for an Adaptive Kinematic Visual Servoing Scheme

Rewriting equation (3.33) with the algebraic manipulation from equation (3.34), we obtain:

$$\dot{e}_v = \hat{J}^{*}u - \begin{bmatrix} a_c^{\frac{1}{2}} Y^{\perp} \\ 0 \end{bmatrix} \tilde{a}^{\perp} + \begin{bmatrix} a_c^{\frac{1}{2}}(p_{xy} - p_{xyi}) \\ 2a_c^{\frac{3}{2}} \end{bmatrix} Y_z \tilde{a}_z + \omega_1 - \dot{p}_d \tag{3.35}$$

Using control law (3.27) into equation (3.35), results in the error dynamics equation:

$$\dot{e}_v = \hat{J}^{*}\hat{J}^{*-1}(\dot{p}_d - K_k e_v) - \begin{bmatrix} a_c^{\frac{1}{2}} Y^{\perp} \\ 0 \end{bmatrix} \tilde{a}^{\perp} + \begin{bmatrix} a_c^{\frac{1}{2}}(p_{xy} - p_{xyi}) \\ 2a_c^{\frac{3}{2}} \end{bmatrix} Y_z \tilde{a}_z + \omega_1 - \dot{p}_d \tag{3.36}$$

$$\dot{e}_v = -K_k e_v - \begin{bmatrix} a_c^{\frac{1}{2}} Y^{\perp} \\ 0 \end{bmatrix} \tilde{a}^{\perp} + \begin{bmatrix} a_c^{\frac{1}{2}}(p_{xy} - p_{xyi}) \\ 2a_c^{\frac{3}{2}} \end{bmatrix} Y_z \tilde{a}_z + \omega_1 \tag{3.37}$$

Table 3.1 presents the algorithm for the kinematics controller, and Figure 3.5 shows its block diagram. The following theorem establishes passivity properties and stability analysis of the closed-loop system.

Remark 13. *In this work, we consider a non-redundant manipulator. However, this could be expanded to a redundant manipulator by using the standard generalized inverse of the Jacobian matrix, $\hat{J}^{*^{\dagger}} = \hat{J}^{*^{T}}(\hat{J}^{*}\hat{J}^{*^{T}})^{-1}$, in the control law u.*

Theorem 5. *Consider the uncertain visual servoing problem, modeled by equation (3.25), the control law given by (3.27), the parameterizations given by (3.21) and (3.22) , and the parameter adaptation laws given by (3.28) and (3.29). Assume that*

Table 3.1: Algorithm for Adaptive Image-based Visual Servoing with Position and Depth Features

IBVS Kinematic Model	$\dot{p}_v = J^* u + \omega_1(t)$
Control Law	$u = \hat{J}^{*-1}(\dot{p}_d - K_k e_v)$
Parameterization	$\beta J^\perp u = Y^\perp(\theta, u) a^\perp \quad \beta J_z u = Y_z(\theta, u) a_z$
Kinematic Adaptation Law	$\dot{\hat{a}}^\perp = \Gamma^\perp \begin{bmatrix} a_c^{\frac{1}{2}} Y^\perp \\ 0 \end{bmatrix}^T e_v \quad \dot{\hat{a}}_z = -\Gamma_z Y_z^T \begin{bmatrix} a_c^{\frac{1}{2}}(p_{xy} - p_{xyi}) \\ 2a_c^{\frac{3}{2}} \end{bmatrix}^T e_v$
Model Errors	$e_v = p_v - p_d \quad \tilde{a}^\perp = \hat{a}^\perp - a^\perp \quad \tilde{a}_z = \hat{a}_z - a_z$
Closed-loop Equation	$\dot{e}_v = -K_k e_v - \begin{bmatrix} a_c^{\frac{1}{2}} Y^\perp \\ 0 \end{bmatrix} \tilde{a}^\perp + \begin{bmatrix} a_c^{\frac{1}{2}}(p_{xy} - p_{xyi}) \\ 2a_c^{\frac{3}{2}} \end{bmatrix} Y_z \tilde{a}_z + \omega_1$

θ is measured, so that regressor matrices $Y^\perp$ and Y_z can be calculated. Then, the map $\omega_1 \rightarrow e_v$ is output strictly passive with positive definite storage function

$$2V_k(e_v, \tilde{a}^\perp, \tilde{a}_z) = e_v^T e_v + \tilde{a}^{\perp T} \Gamma^{\perp -1} \tilde{a}^\perp + \tilde{a}_z^T \Gamma_z^{-1} \tilde{a}_z \tag{3.38}$$

Moreover, for $\omega_1 = 0$, the following properties hold:

- *(i) All system signals are uniformly bounded;*
- *(ii) $lim_{t \rightarrow \infty} e_v(t) = 0$*

Proof. The derivative with respect to time of the storage function V_k (3.38) is given by:

$$\dot{V}_k(e_v, \tilde{a}^\perp, \tilde{a}_z) = e_v^T \dot{e_v} + \tilde{a}^{\perp T} \Gamma^{\perp -1} \dot{\tilde{a}}^\perp + \tilde{a}_z^T \Gamma_z^{-1} \dot{\tilde{a}}_z \tag{3.39}$$

Using the closed-loop error dynamics given by equation (3.37), we obtain:

$$\begin{aligned} \dot{V}_k(e_v, \tilde{a}^\perp, \tilde{a}_z) = -e_v^T K_k e_v - e_v^T \begin{bmatrix} a_c^{\frac{1}{2}} Y^\perp \\ 0 \end{bmatrix} \tilde{a}^\perp + e_v^T \begin{bmatrix} a_c^{\frac{1}{2}}(p_{xy} - p_{xyi}) \\ 2a_c^{\frac{3}{2}} \end{bmatrix} Y_z \tilde{a}_z + e_v^T \omega_1 \\ + \tilde{a}^{\perp T} \Gamma^{\perp -1} \dot{\tilde{a}}^\perp + \tilde{a}_z^T \Gamma_z^{-1} \dot{\tilde{a}}_z \end{aligned} \tag{3.40}$$

With the adaptation laws (3.28) and (3.29), we obtain:

$$\dot{V}_k(e_v, \tilde{a}^\perp, \tilde{a}_z) = -e_v^T K_k e_v + e_v^T \omega_1 \tag{3.41}$$

This defines an output strictly passive mapping from $\omega_1 \rightarrow e_v$. As such, with $\omega_1 = 0$, $\dot{V}_k \leq 0$. This implies, by Lyapunov theory, that e_v, $\tilde{a}^\perp$ and $\tilde{a}_z \in \mathcal{L}_\infty$ and thus, the equilibrium state is uniformly stable. As e_v, $\tilde{a}^\perp$ and $\tilde{a}_z$ are limited, the derivative with respect to time $\ddot{V}_k = -2e_v^T K_k \dot{e}_v$ is uniformly limited. So, by using the Barbalat's Lemma, we can conclude that $lim_{t\to\infty} e_v(t) \to 0$. □

Next, we would like to extend the kinematic controller to a system with non-negligible dynamics. Considering the passivity property of the Slotine-Li dynamic adaptive scheme and the passivity property of the kinematic visual servoing control proposed, we can use Theorem 4 to propose a stable cascade controller for the complete system. However, the calculation of τ (2.54) in the Slotine-Li control requires knowledge of $\dot{u}$. As $u \to h(p_v)$, as seen in equation (3.27), its derivative with respect to time $\dot{u}$ will be a function of the image velocity $\dot{p}_v$. Image-space velocity obtained by standard numerical differentiation approach is a signal known to contain much noise and as such it is desirable to avoid it. To circumvent this problem, we first propose an observer for the kinematic system in the next subsection, so we can design u in terms of signal $p_o = [p_{xyo}^T \;\; a_c]^T$, where p_{xyo} is the observer measure of p_{xy}. In this work, we will assume that a numerical differential approach is still used for the variation of the target area $\dot{a}_c$.

3.2.3 Kinematic Controller with Observer

Consider the kinematic visual servoing problem presented in the previous section, given by equation (3.25) and the parameterization given in equations (3.21) and (3.22). The idea of using an observer to avoid explicitly using p_{xy} in the expression of u, and consequently $\dot{p}_{xy}$ in $\dot{u}$ when designing control for a system with non-negligible dynamics was introduced in (WANG *et al.*, 2018), where it is also used to guarantee the passivity of the complete system. Here, we simplify the observer proposed in (WANG *et al.*, 2018) and guarantee that the kinematic subsystem with the observer is still output strict passive.

We design a kinematic observer p_{xyo} as follows, a copy of the system using the Jacobian estimate and two terms related to the observation error and tracking error:

$$\dot{p}_{xyo} = [\hat{\beta} a_c^{\frac{1}{2}} (\hat{J}^{\perp} - (p_{xy} - p_{xyi} + e_{xy})\hat{J}_z)]u - K_o e_o + K_k(p_{xy} - p_{xyd}) + \omega_1 \tag{3.42}$$

or equivalently,

$$\dot{p}_{xyo} = \hat{J}_{xyo} u - K_o e_o + K_k(p_{xy} - p_{xyd}) + \omega_1 \tag{3.43}$$

where $e_o = (p_{xyo} - p_{xy})$ is the observation error, $e_{xy} = (p_{xy} - p_{xyd})$ is the target's centroid position error and $K_o \neq K_k > 0$ is a positive gain. Now, we rewrite the control law u as follows:

$$u = \begin{bmatrix} \hat{\beta} a_c^{\frac{1}{2}} (\hat{J}^{\perp} - (p_{xyo} - p_{xyi}) \hat{J}_z) \\ -2\hat{\beta} a_c^{\frac{3}{2}} \hat{J}_z \end{bmatrix}^{-1} (\dot{p}_d - K_k(p_o - p_d)) = \hat{J}_o^{*^{-1}} (\dot{p}_d - K_k(p_o - p_d)) \tag{3.44}$$

where the structure of $\hat{J}_o^*(\theta, p_o)$ is very similar to $hatJ^*(\theta, p_v)$, but uses p_{xyo}, the observed position, instead of p_{xy}

Remark 14. *For the estimated parameter updates, we consider the following adaptation laws and the projection algorithm given by equations (3.30), (3.31) and (3.32) are applied here as well.*

$$\dot{\hat{a}}^{\perp} = \Gamma^{\perp} a_c^{\frac{1}{2}} Y^{\perp T} (e_{xy} - e_o) \tag{3.45}$$

$$\dot{\hat{a}}_z = \Gamma_z Y_z^T \left(a_c^{\frac{1}{2}} e_o^T e_{xy} + a_c^{\frac{1}{2}} (p_{xy} - p_{xyi})^T e_o - \begin{bmatrix} a_c^{\frac{1}{2}} (p_{xy} - p_{xyi}) \\ 2a_c^{\frac{3}{2}} \end{bmatrix}^T e_v \right) \tag{3.46}$$

Consider dynamic equation for the tracking error e_v, and that $p_{xy} = p_{xyo} - e_o$

$$\dot{e}_v = \begin{bmatrix} \beta a_c^{\frac{1}{2}} (J^{\perp} - (p_{xyo} - p_{xyi} - e_o) J_z) \\ -2\beta a_c^{\frac{3}{2}} J_z \end{bmatrix} u + \omega_1 - \dot{p}_d \tag{3.47}$$

Using the control law (3.44) and the parameterizations (3.21) and (3.22), we obtain:

$$\dot{e}_v = -K_k(p_o - p_d) + a_c^{\frac{1}{2}} \beta \begin{bmatrix} e_o \\ 0 \end{bmatrix} J_z u - \begin{bmatrix} a_c^{\frac{1}{2}} Y^{\perp} \\ 0 \end{bmatrix} \tilde{a}^{\perp} + \begin{bmatrix} a_c^{\frac{1}{2}} (p_{xy} - p_{xyi}) \\ 2a_c^{\frac{3}{2}} \end{bmatrix} Y_z \tilde{a}_z + \omega_1 \tag{3.48}$$

Finally, considering that $p_{xyo} = p_{xy} + e_o$, we obtain the tracking error e_v dynamic:

$$\begin{aligned} \dot{e}_v = -K_k(e_v) - K_k \begin{bmatrix} e_o \\ 0 \end{bmatrix} + a_c^{\frac{1}{2}} \beta \begin{bmatrix} e_o \\ 0 \end{bmatrix} J_z u - \begin{bmatrix} a_c^{\frac{1}{2}} Y^{\perp} \\ 0 \end{bmatrix} \tilde{a}^{\perp} \\ + \begin{bmatrix} a_c^{\frac{1}{2}} (p_{xy} - p_{xyi}) \\ 2a_c^{\frac{3}{2}} \end{bmatrix} Y_z \tilde{a}_z + \omega_1 \end{aligned} \tag{3.49}$$

For the observation error e_o, its dynamic equation $\dot{e}_o = \dot{p}_{xyo} - \dot{p}_{xy}$ is given as follows

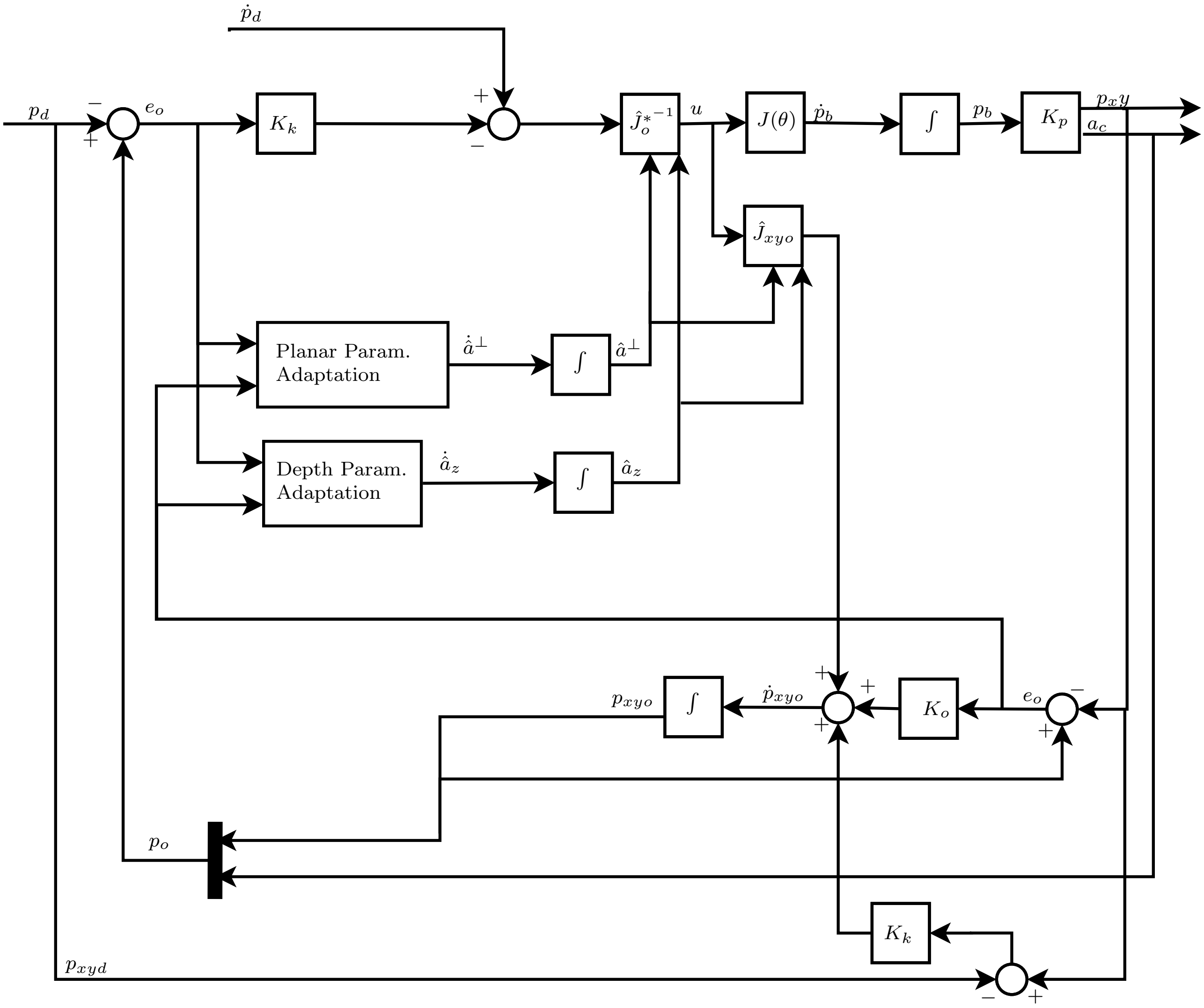

Figure 3.6: Block Diagram for an Adaptive Kinematic Scheme with Observer

$$\dot{e}_o = \dot{p}_{xyo} = [\hat{\beta} a_c^{\frac{1}{2}} (\hat{J}^{\perp} - (p_{xy} - p_{xyi} + e_{xy})\hat{J}_z)]u - K_o e_o + K_k(p_{xy} - p_{xyd}) \\ - [\beta a_c^{\frac{1}{2}} (J^{\perp} - (p_{xy} - p_{xyi})J_z)]u \quad (3.50)$$

Considering the parameterization errors $\tilde{a}^{\perp}$ and $\tilde{a}_z$, equation (3.50) can be rewritten as:

$$\dot{e}_o = -K_o e_o - e_{xy} \hat{\beta} a_c^{\frac{1}{2}} \hat{J}_z u + K_k(p_{xy} - p_{xyd}) + a_c^{\frac{1}{2}} Y^{\perp} \tilde{a}^{\perp} + a_c^{\frac{1}{2}} (p_{xy} - p_{xyi}) Y_z \tilde{a}_z \quad (3.51)$$

Table 3.2 presents the updated algorithm for the kinematic problem with an observer, and Figure 3.6 the complete kinematic model block diagram. The following theorem shows results on passivity properties and stability analysis of the system.

Table 3.2: Algorithm for Adaptive IBVS with Observer using position and depth features

IBVS Kinematic Model	$\dot{p}_v = J^* u + \omega_1(t)$
Observer Model	$\dot{p}_{xyo} = [\hat{J}_{xyo} u + \omega_1 - K_o e_o + K_k(p_{xy} - p_{xyd})$
Control Law	$u = {\hat{J}_o^*}^{-1}(\dot{p}_d - K_k(p_o - p_d))$
Parameterization	$\beta J^\perp u = Y^\perp(\theta, u) a^\perp \quad \beta J_z u = Y_z(\theta, u) a_z$
Kinematic Adaptation Law	$\dot{\hat{a}}^\perp = \Gamma^\perp a_c^{\frac{1}{2}} Y^{\perp T}\left(e_{xy} - e_o\right)$ $\dot{\hat{a}}_z = \Gamma_z Y_z^T (e_o^T e_{xy} + a_c^{\frac{1}{2}}(p_{xy} - p_{xyi})^T e_o$ $- \begin{bmatrix} a_c^{\frac{1}{2}}(p_{xy} - p_{xyi}) \\ 2a_c^{\frac{3}{2}} \end{bmatrix}^T e_v)$
Model Errors	$e_v = p_v - p_d \quad e_o = p_{xyo} - p_{xy} \quad \tilde{a}^\perp = \hat{a}^\perp - a^\perp \quad \tilde{a}_z = \hat{a}_z - a_z$
Closed-loop Equation	$\dot{e}_v = -K_k(e_v) - K_k \begin{bmatrix} e_o \\ 0 \end{bmatrix} + a_c^{\frac{1}{2}} \beta \begin{bmatrix} e_o \\ 0 \end{bmatrix} J_z u + \omega_1$ $- \begin{bmatrix} a_c^{\frac{1}{2}} Y^\perp \\ 0 \end{bmatrix} \tilde{a}^\perp + \begin{bmatrix} a_c^{\frac{1}{2}}(p_{xy} - p_{xyi}) \\ 2a_c^{\frac{3}{2}} \end{bmatrix} Y_z \tilde{a}_z$ $\dot{e}_o = -K_o e_o - e_{xy} \hat{\beta} a_c^{\frac{1}{2}} \hat{J}_z u + K_k(p_{xy} - p_{xyd})$ $+ a_c^{\frac{1}{2}} Y^\perp \tilde{a}^\perp + a_c^{\frac{1}{2}}(p_{xy} - p_{xyi}) Y_z \tilde{a}_z$

Theorem 6. *Consider the uncertain visual servoing problem, modeled by equation (3.25), the observer described in equation (3.42), the control law given by (3.44), the parameterizations given by (3.21) and (3.22) , and the parameter adaptation laws given by (3.45) and (3.46). Assume that θ is measured, so that regressor matrices $Y^\perp$ and Y_z can be calculated. Then, the map $\omega_1 \to e_v$ is output strictly passive with positive definite storage function*

$$2V_{ko}(e_v, e_o, \tilde{a}^\perp, \tilde{a}_z) = e_v^T e_v + e_o^T e_o + \tilde{a}^{\perp T} {\Gamma^\perp}^{-1} \tilde{a}^\perp + \tilde{a}_z^T \Gamma_z^{-1} \tilde{a}_z \tag{3.52}$$

Moreover, for $\omega_1 = 0$, the following properties hold:

(i) All system signals are uniformly bounded;

(ii) $lim_{t \to \infty} e_v(t) = 0$

(ii) $lim_{t \to \infty} e_o(t) = 0$

Proof. The derivative with respect to time of the storage function V_k (3.52) is given by:

$$\dot{V}_{ko}(e_v, e_o, \tilde{a}^\perp, \tilde{a}_z) = e_v^T \dot{e}_v + e_o^T \dot{e}_o \tilde{a}^{\perp T} {\Gamma^\perp}^{-1} \dot{\tilde{a}}^\perp + \tilde{a}_z^T \Gamma_z^{-1} \dot{\tilde{a}}_z \tag{3.53}$$

Using the closed-loop error dynamics given by equations (3.49) and (3.51), we obtain:

$$\begin{aligned}\dot{V}_{ko}(e_v, e_o, \tilde{a}^{\perp}, \tilde{a}_z) = -e_v^T K_k e_v - e_v^T \begin{bmatrix} a_c^{\frac{1}{2}} Y^{\perp} \\ 0 \end{bmatrix} \tilde{a}^{\perp} + e_v^T \begin{bmatrix} a_c^{\frac{1}{2}}(p_{xy} - p_{xyi}) \\ 2a_c^{\frac{3}{2}} \end{bmatrix} Y_z \tilde{a}_z + e_v^T \omega_1 \\ - e_o^T K_o e_o - a_c^{\frac{1}{2}} e_o^T e_{xy} Y_z \tilde{a}_z + e_o^T a_c^{\frac{1}{2}} Y^{\perp} \tilde{a}^{\perp} + e_o^T a_c^{\frac{1}{2}} (p_{xy} - p_{xyi}) Y_z \tilde{a}_z \\ + \tilde{a}^{\perp T} \Gamma^{\perp -1} \dot{\tilde{a}}^{\perp} + \tilde{a}_z^T \Gamma_z^{-1} \dot{\tilde{a}}_z \quad (3.54)\end{aligned}$$

With the adaptation laws (3.45) and (3.46), we obtain:

$$\dot{V}_{ko}(e_v, e_o, \tilde{a}^{\perp}, \tilde{a}_z) = -e_v^T K_k e_v - e_o^T K_o e_o + e_v^T \omega_1 \qquad (3.55)$$

which defines an output strictly passive map, from $\omega_1 \rightarrow e_v$. Thus, $\omega_1 = 0$, $\dot{V}_{ko} \leq 0$ which implies, by Lyapunov theory, that e_v, e_o, $\tilde{a}^{\perp}$ and $\tilde{a}_z \in \mathcal{L}_\infty$ and thus, the equilibrium state is uniformly stable. As e_v,e_o, $\tilde{a}^{\perp}$ and $\tilde{a}_z$ are limited, the derivative with respect to time $\ddot{V}_{ko} = -2e_v^T K_k \dot{e}_v - 2e_o^T K_o \dot{e}_o$ is uniformly limited. So, by using the Barbalat's Lemma, we can conclude that $lim_{t\rightarrow\infty} e_v(t) \rightarrow 0$ and $lim_{t\rightarrow\infty} e_o(t) \rightarrow 0$. □

3.2.4 Cascade Control

Now, we finally extend the kinematic visual servoing controller to the case of a robot manipulator with non-negligible dynamics. First, to illustrate the problem, consider a case where the camera depth is fixed

$$p_c = K_p p_b + p_{xyi} \qquad (3.56)$$

If K_p is known, then it would be simple to obtain the desired trajectory p_d expressed in robot base coordinate frame, p_{db}, by

$$p_{db} = K_p^{-1}(p_d - p_{xyi}) \qquad (3.57)$$

and apply an adaptive or robust control strategy for dynamic manipulators.

However, as we consider the case with an uncalibrated camera, i.e. K_p is unknown, p_{db} cannot be calculated. Considering equation (3.56) and the manipulator dynamic model expressed in Cartesian coordinates (2.46),

$$M_c(\theta)\ddot{p} + C_c(\theta, \dot{\theta})\dot{p} + G_c(\theta) = \tau_c \qquad (3.58)$$

we can write the dynamic model in camera frame coordinates as:

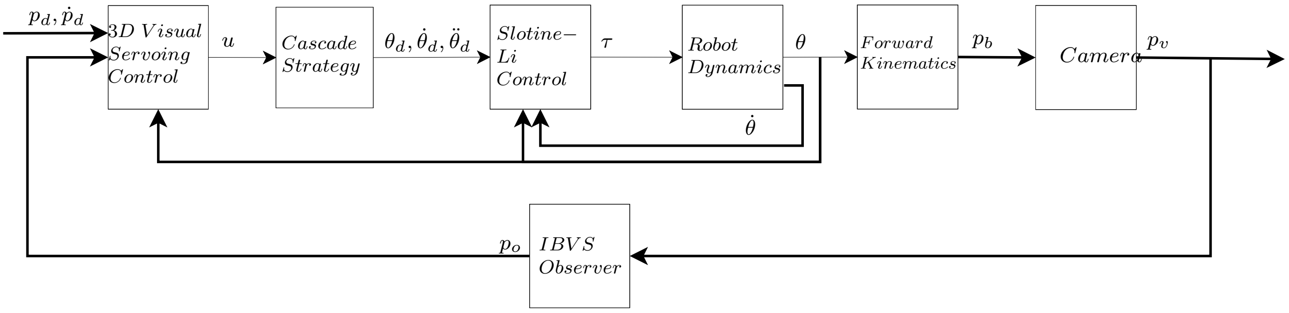

Figure 3.7: Cascade Strategy for Visual Servoing system

$$\bar{M}_c(\theta)\ddot{p}_c + \bar{C}_c(\theta, \dot{\theta})\dot{p}_c + \bar{G}_c(\theta) = \bar{Y}_c(\theta, \dot{\theta}, \dot{p}_c, \ddot{p}_c)\bar{a}_c = K_p^{-T}\tau_c \tag{3.59}$$

where $\bar{M}_c = K_p^{-T} M_c K_p^{-1}$, $\bar{C}_c = K_p^{-T} C_c Kp^{-1}$ and $\bar{G}_c = K_p^{-T} G_c$. This situation is similar to what was illustrated in the previous chapter. To use a standard adaptation on this model, it is necessary to adapt both $\bar{a}_c$ and K_p^{-1} separately.

Remark 15. *It is also important to note that while the robot is passive from $K_p^{-T}\tau_c \to \dot{p}_c$, it may not be from from $\tau_c \to p_c$*

We adopt the cascade control strategy previously presented in Section 2.6 and choose a control τ which can guarantee a goal $p_v \to p_d$ is reached, as seen in the kinematic loop. A block diagram of the complete closed-loop system is given by Figure 3.7. The following assumptions are done, with respect to the complete system:

($A5$) The translational reference trajectory $p_d(t)$ is planned so it remains visible, within the robot workspace, and its first and second derivatives, $\dot{p}_d(t)$ and $\ddot{p}_d(t)$ are known and bounded.

($A6$) The robot motions are away from singular configurations.

($A7$) The joint angles θ and joint velocities $\dot{\theta}$ are measurable.

Considering that $\dot{\theta} = \dot{\theta}_r + \sigma$, and the cascade strategy we have

$$\dot{p}_v = J^*\dot{\theta}_r + J^*\sigma \tag{3.60}$$

where σ is a vanishing term, as seen in Theorem 3. This is similar to the kinematic system (3.25) as we make $\omega_1 = J^*\sigma$. Then, by taking the control law presented in (3.44), the cascade control strategy can be implemented by setting:

$$\dot{\theta}_d = \dot{\theta}_r + \lambda_d e \tag{3.61}$$

$$\ddot{\theta}_d = \ddot{\theta}_r + \lambda_d \dot{e} \tag{3.62}$$

with reference signal $\dot{\theta}_r$ as the cascade so

$$\dot{\theta}_r = u = \hat{J}_o^{*^{-1}}(\dot{p}_d - K_k(p_o - p_d)) \tag{3.63}$$

And finally, we adopt the Slotine-Li adaptive scheme to solve the dynamic loop, given by control law (2.54) and adaptation law (2.55), restated here for convenience. The Table 3.3 illustrates the algorithm complete system.

$$\tau = Y_d(\theta, \dot{\theta}, \dot{\theta}_r, \ddot{\theta}_r)\hat{a}_d - K_D\sigma + \omega_2, \tag{3.64}$$

$$\dot{\hat{a}}_d = -\Gamma_d Y_d^T \sigma, \quad \Gamma_d = \Gamma_d^T > 0 \tag{3.65}$$

Remark 16. *It is important to remind that while we use the Slotine-Li adaptive scheme in this work any other passive control loop, like robust control, could also be used for this cascade strategy.*

Consider now the passivity properties of the adaptive dynamic control system, stated by Theorem 3, and of adaptive visual servoing kinematic control system, stated by Theorem 6. Thus, we can apply Theorem 4 to analyze the stability properties of the overall closed-loop cascade system, where the driven system Σ_1 and the driving system Σ_2 are identified as follows:

$$\Sigma_1 : x_1^T = [e_v^T \;\; a^{\perp^T} \;\; a_z^T], \quad y_1 = e_v, \tag{3.66}$$

$$\Sigma_2 : x_2^T = [e^T \;\; \dot{e}^T \;\; a_d^T], \quad y_2 = \sigma, \tag{3.67}$$

with storage functions $V_1(x_1) = V_{ko}$ and $V_2 x_2 = V_d$ as seen in equations (3.52) and (2.58) respectively. Then, from Theorem 4, we can conclude that, for the complete adaptive visual servoing system with non-negligible dynamics:

- (i) All signals of the interconnected system are bounded;
- (ii) $lim_{t\to\infty}\sigma(t) = 0$, $lim_{t\to\infty}e(t) = 0$, $lim_{t\to\infty}e_v(t) = 0$, and $lim_{t\to\infty}e_o(t) = 0$.

3.3 Conclusion

In this chapter, we proposed an adaptive visual servoing control approach for the task of tracking a translational trajectory to control position and depth. First, we introduced a few basic concepts about visual servoing, before presenting the camera model equation.

Table 3.3: Algorithm for Adaptive IBVS for manipulator with non-negligible dynamics using position and depth features.

IBVS Kinematic Model	$\dot{p}_v = J^* u + \omega_1(t)$
Observer Model	$\dot{p}_{xyo} = \hat{J}_{xyo} u + \omega_1 - K_o e_o + K_k(p_{xy} - p_{xyd})$
Control Law	$u = \hat{J}_o^{*^{-1}}(\dot{p}_d - K_k(p_o - p_d))$
Parameterization	$\beta J^{\perp} u = Y^{\perp}(\theta, u) a^{\perp} \quad\quad \beta J_z u = Y_z(\theta, u) a_z$
Kinematic Adaptation Law	$\dot{\hat{a}}^{\perp} = \Gamma^{\perp} a_c^{\frac{1}{2}} Y^{\perp T}(e_{xy} - e_o)$ $\dot{\hat{a}}_z = \Gamma_z Y_z^T (e_o^T e_{xy} + a_c^{\frac{1}{2}}(p_{xy} - p_{xyi})^T e_o$ $-\begin{bmatrix} a_c^{\frac{1}{2}}(p_{xy} - p_{xyi}) \\ 2a_c^{\frac{3}{2}} \end{bmatrix}^T e_v)$
Model Errors	$e_v = p_v - p_d \quad e_o = p_{xyo} - p_{xy} \quad \tilde{a}^{\perp} = \hat{a}^{\perp} - a^{\perp} \quad \tilde{a}_z = \hat{a}_z - a_z$
Closed-loop Equation	$\dot{e}_v = -K_k(e_v) - K_k \begin{bmatrix} e_o \\ 0 \end{bmatrix} + a_c^{\frac{1}{2}} \beta \begin{bmatrix} e_o \\ 0 \end{bmatrix} J_z u + \omega_1$ $- \begin{bmatrix} a_c^{\frac{1}{2}} Y^{\perp} \\ 0 \end{bmatrix} \tilde{a}^{\perp} + \begin{bmatrix} a_c^{\frac{1}{2}}(p_{xy} - p_{xyi}) \\ 2a_c^{\frac{3}{2}} \end{bmatrix} Y_z \tilde{a}_z$ $\dot{e}_o = -K_o e_o - e_{xy} \hat{\beta} a_c^{\frac{1}{2}} \hat{J}_z u + K_k(p_{xy} - p_{xyd})$ $+a_c^{\frac{1}{2}} Y^{\perp} \tilde{a}^{\perp} + a_c^{\frac{1}{2}}(p_{xy} - p_{xyi}) Y_z \tilde{a}_z$
Cascade Strategy	$\dot{\theta}_r = u$ $\ddot{\theta}_r = \hat{J}_o^{*^{-1}}(\ddot{p}_d - K_k(\dot{p}_o - \dot{p}_d)) - \hat{J}_o^{*^{-1}} \dot{\hat{J}}_o \hat{J}_o^{*^{-1}}(\dot{p}_d - K_k(p_o - p_d))$ $\dot{\theta}_d = \dot{\theta}_r + \lambda_d e \quad\quad \ddot{\theta}_d = \ddot{\theta}_r + \lambda_d \dot{e}$
Robot Dynamic Model	$M(\theta)\ddot{\theta} + C(\theta, \dot{\theta})\dot{\theta} + G(\theta) = \tau$
Dynamic Control Law	$\tau = Y_d(\theta, \dot{\theta}, \dot{\theta}_r, \ddot{\theta}_r)\hat{a}_d - K_D \sigma + \omega_2$
Parameterization	$M(\theta)\dot{\eta} + C(\theta, \dot{\theta})\eta + G(\theta) = Y_d(\theta, \dot{\theta}, \eta, \dot{\eta}) a_d$
Dynamic Adaptation Law	$\dot{\hat{a}}_d = -\Gamma_d Y_d^T \sigma$
Model Errors	$\sigma = \dot{\theta} - \dot{\theta}_r = \dot{e} + \lambda_d e \quad\quad \tilde{a}_d = \hat{a}_d - a_d$ $e = \theta - \theta_d \quad\quad \dot{\theta}_r = \dot{\theta}_d - \lambda_d e$
Closed-loop Equation	$M(\theta)\dot{\sigma} + (C(\theta, \dot{\theta}) + K_D)\sigma = Y_d(\theta, \dot{\theta}, \dot{\theta}_r, \ddot{\theta}_r)\tilde{a}_d + \omega_2$

Following, we formulate the visual servoing problem for a robot manipulator with negligible dynamics, and propose an adaptive control scheme, with an indirect adaptation method, that can following a desired goal in the camera image. We introduce a projection algorithm to the parameter update laws, with two objectives: avoid large parameter drifting during the transient state and avoid the estimate Jacobian singularity at the origin.

An observer is designed to avoid use of image-space velocities when controlling a robot with non-negligible dynamics. And finally, the cascade strategy introduced in the previous chapter is used to extend the adaptive kinematic visual servoing to a robot with non-negligible dynamics, cascading the proposed control and the Slotine-Li adaptive scheme.

Chapter 4

Simulation Results

In this chapter, several simulations and experiments are presented to illustrate the adaptive visual servoing control adopted, both for a kinematic manipulator scheme and for a manipulator with non-negligible dynamics, by means of a cascade strategy, as presented in Chapter 3. Simulations are done with the Matlab/Simulink software, for a 3R anthropomorphic arm. Experimental results are presented, using the Tetis, a 4R manipulator, and a webcam.

4.1 Kinematic Anthropomorphic Arm

In this section, we present equations and nominal parameters for simulation of the camera/arm setup. First, consider the following visual servoing system, as seen in Figure 4.1:

- A 3R manipulator, an anthropomorphic arm, as seen in (SICILIANO *et al.*, 2011), where $l_1, l_2, l_3 \in \mathbb{R}^+$ are the robot dimensions, $\theta = [\theta_1\ \theta_2\ \theta_3]^T \in \mathbb{R}^3$ are its joint angles and $p_{be} \in \mathbb{R}^3$ is the end-effector position, in robot base frame;

- a pinhole camera, where $f \in \mathbb{R}^+$ is its focal length, $\alpha \in \mathbb{R}^+$ is the camera scaling factor. Consider that $p_c \in \mathbb{R}^3$ is the position of target centroid $p_v \in \mathbb{R}^3$ are coordinates after a depth-to-area transformation, where $\beta \in \mathbb{R}^+$ is the depth-to-area transformation constant. For simplicity, consider as well that the image frame and robot base frame z-axis are aligned, however, misaligned by a rotation $R(\phi)$ around the z-axis.

Now, consider the forward kinematics mapping for an anthropomorphic arm, following the model given in equation (2.4)

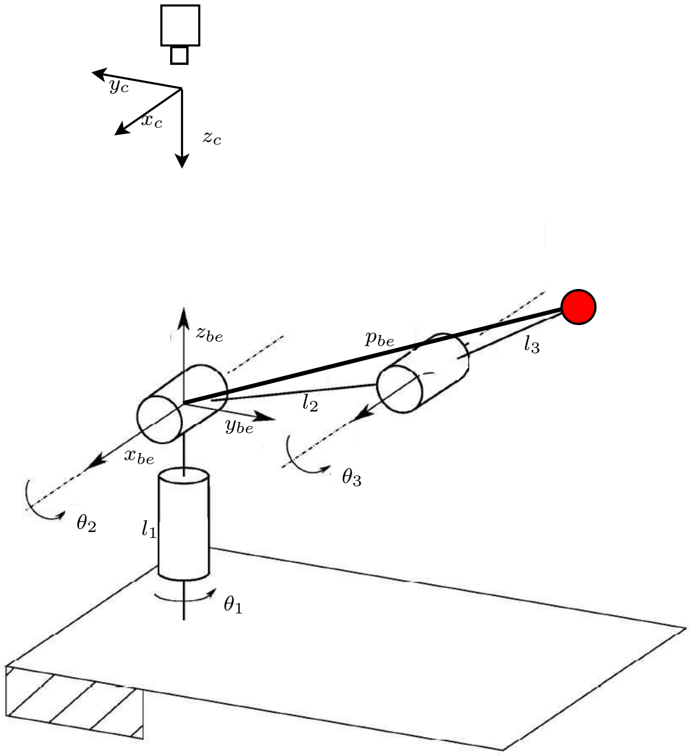

Figure 4.1: A camera and anthropomorphic robot arm setup

$$p_{be} = \begin{bmatrix} c_1(l_2c_2 + l_3c_{23}) \\ s_1(l_2c_2 + l_3c_{23}) \\ l_2s_2 + l_3s_{23} \end{bmatrix} \tag{4.1}$$

where $c_i = \cos(\theta_i)$, $s_i = \sin(\theta_i)$, $c_{ij} = \cos(\theta_i + \theta_j)$ and $s_{ij} = \sin(\theta_i + \theta_j)$.

The camera transformation mapping, from p_{be} to p_c, is given according to model (3.1)

$$p_c = \begin{bmatrix} \frac{1}{z_c}f\alpha c_\phi & \frac{1}{z_c}f\alpha s_\phi & 0 \\ \frac{1}{z_c}f\alpha s_\phi & -\frac{1}{z_c}f\alpha c_\phi & 0 \\ 0 & 0 & -1 \end{bmatrix} R^T(\phi)p_{be} + \begin{bmatrix} 0 \\ 0 \\ z_i \end{bmatrix} \tag{4.2}$$

where z_i is a displacement from the origin of camera frame to the base frame, along the z_c axis. Finally, we can describe the visual servoing differential kinematics, as given by the model after depth-to-area transformation (3.20)

$$\dot{p}_v = \begin{bmatrix} \beta a_c^{\frac{1}{2}}(J^\perp - (p_{xy}J_z) \\ -2\beta a_c^{\frac{3}{2}}J_z \end{bmatrix} u \tag{4.3}$$

where $u \in \mathbb{R}^3$ is the control signal, the elements of matrix $J^{\perp}(\theta)\mathcal{R}^{2\times 3}$ are given by

$$\begin{aligned}
J^{\perp}_{11} &= -f\alpha c_{\phi}(l_2 s_1 c_2 + l_3 s_1 c23) + f\alpha s_{\phi}(l_2 c_1 c_2 + l_3 c_1 c_{23}) \\
J^{\perp}_{12} &= -f\alpha c_{\phi}(l_2 c_1 s_2 + l_3 c_1 s23) - f\alpha s_{\phi}(l_2 s_1 s_2 + l_3 s_1 s_{23}) \\
J^{\perp}_{13} &= -f\alpha c_{\phi} l_3 c_1 s23 - f\alpha s_{\phi} l_3 s_1 s_{23} \\
J^{\perp}_{21} &= -f\alpha c_{\phi}(l_2 c_1 c_2 + l_3 c_1 c23) - f\alpha s_{\phi}(l_2 s_1 c_2 + l_3 s_1 c_{23}) \\
J^{\perp}_{22} &= +f\alpha c_{\phi}(l_2 s_1 s_2 + l_3 s_1 s23) - f\alpha s_{\phi}(l_2 c_1 s_2 + l_3 c_1 s_{23}) \\
J^{\perp}_{23} &= +f\alpha c_{\phi} l_3 s_1 s23) - f\alpha s_{\phi} l_3 c_1 s_{23})
\end{aligned}$$

and, similarly, $J_z \in \mathbb{R}^{1\times 3}$ is given by

$$J_z = \begin{bmatrix} 0 & -l_2 c_2 - l_3 c_{23} & -l_3 c_{23} \end{bmatrix} \tag{4.4}$$

Furthermore, following the parameterization models given in equations (3.21) and (3.22)

$$\beta J^{\perp}(\theta)u = Y^{\perp}(\theta, u)a^{\perp} = \begin{bmatrix} Y_{11} & Y_{12} & Y_{13} & Y_{14} \\ Y_{21} & Y_{22} & Y_{23} & Y_{24} \end{bmatrix} \begin{bmatrix} \beta f\alpha c_{\phi} l_2 \\ \beta f\alpha c_{\phi} l_3 \\ \beta f\alpha s_{\phi} l_2 \\ \beta f\alpha c_{\phi} l_3 \end{bmatrix} \tag{4.5}$$

where the elements of $Y^{\perp}(\theta, u)$ are given by

$$\begin{aligned}
Y_{11} &= -s_1 c_2 u_1 - c_1 s_2 u_2; \\
Y_{12} &= -s_1 c_{23} u_1 - c_1 s_{23} u_2 - c_1 s_{23} u_3; \\
Y_{13} &= c_1 c_2 u_1 - s_1 s_2 u_2; \\
Y_{14} &= c_1 c_{23} u_1 - s_1 s_{23} u_2 - s_1 s_{23} u_3; \\
Y_{21} &= -c_1 c_2 u_1 + s_1 s_2 u_2; \\
Y_{22} &= -c_1 c_{23} u_1 + s_1 s_{23} u_2 + s_1 s_{23} u_3; \\
Y_{23} &= -s_1 c_2 u_1 - c_1 s_2 u_2; \\
Y_{24} &= -s_1 c_{23} u_1 - c_1 s_{23} u_2 - c_1 s_{23} u_3;
\end{aligned}$$

and

$$J_z(\theta)u = Y_z(\theta, u)a_z = \begin{bmatrix} -c_2 u_2 & -c_{23}(u_2 + u_3) \end{bmatrix} \begin{bmatrix} \beta l_2 \\ \beta l_3 \end{bmatrix} \tag{4.6}$$

The kinematic and camera nominal parameters are given in Table (4.1).

Table 4.1: Nominal Parameters for the camera and kinematic manipulator

l_2	0.26m
l_3	0.26m
f	8mm
α	72727 pixel/m
ϕ	0 rad
z_i	1m
β	0.1

Table 4.2: Simulation Look and move: Initial conditions

$\theta(0)$	$\left[0\ -\frac{\pi}{4}\ \frac{\pi}{2}\right]^T$
$\hat{a}^{\perp}$	$[9.8207\ 7.5292\ 5.6700\ 4.3470]^T$
$\hat{a}_z$	$[0.0270\ 0.0207]^T$
$p_c(0)$	$[213.93\ 0\ 100]^T$

4.1.1 Non-Adaptive Control

First, to illustrate the significance of adaptive schemes, we do a few simulations with a non-adaptive approach, in the presence of kinematic uncertainties and a camera with uncertain parameters. Consider the following tracking goal $p_d(t)$

$$p_d(t) = \begin{bmatrix} 210 + 30\sin(\frac{\pi}{5}t) + 30\sin(1.5\frac{\pi}{5}t) \\ -60 + 30\sin(\frac{\pi}{5}t + 1.6) + 30\sin(1.5\frac{\pi}{5}t + 1.6) \\ 95 + 3\sin(0.1t) \end{bmatrix} \tag{4.7}$$

The look and move control should minimize a tracking error $e_v = p_c - p_d \to 0$, and can be expressed as

$$u = \hat{J}^{*^{-1}}(\dot{p}_d - K_k(p_{be} - p_d)) \tag{4.8}$$

where $\hat{J}^*$ is the image Jacobian with uncertainties on the kinematic and camera parameters. Consider the following deviations for each parameter, from their nominal values: $\hat{l}_2 = 0.3$m, $\hat{l}_3 = 0.23$m, $\hat{f} = 6$ mm, $\hat{\alpha} = 70000$ pixel/m and $\hat{\beta} = 0.09$. Given $K_k = 7$ as the control gain, we simulate the a non-adaptive kinematic control scheme for $\hat{\phi} = \frac{\pi}{6}$.

Case - $\hat{\phi} = \frac{\pi}{6}$

Here, we present simulation results for an estimated misalignment $\hat{phi} = \frac{\pi}{6}$. The system initial conditions are given in Table 4.2.

The simulation results are presented in Figures 4.2-4.4. The plane and area

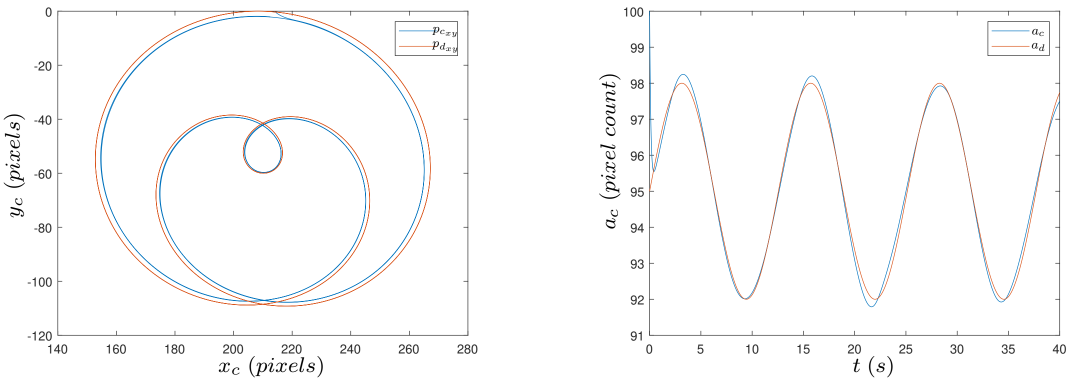

Figure 4.2: Simulation Look and move: Image plane Trajectory and Area

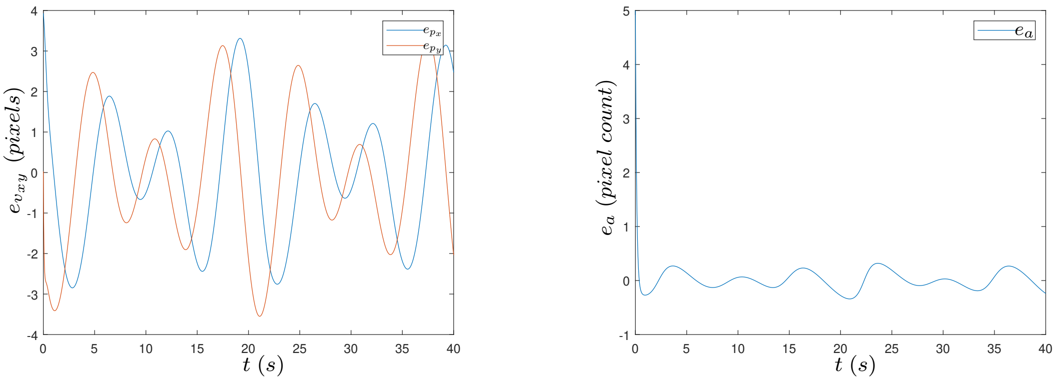

Figure 4.3: Simulation Look and move: Tracking Error

trajectory tracking in image space are presented in Figure 4.2. The error for plane and area trajectory tracking is illustrated in Figure 4.3 and is important to note the error does not seem to tend towards zero over time. Figure 4.4 illustrates the joint angles and the control signal during this task. These results are useful as comparison to the performance of adaptive visual servoing in the next subsection.

4.1.2 Adaptive Visual Servoing Simulations

Now that we have seen the performance of control without adaptation for a visual servoing system with parametric uncertainties, we present the performance of the adaptive visual servoing with kinematic observer for translational trajectory tracking, developed in Chapter 3, for the task of tracking the same goal $p_d(t)$ (4.7). Let us consider the same parameters used for the look and move scheme: $\hat{l}_2 = 0.3$m, $\hat{l}_3 = 0.23$m, $\hat{f} = 6$ mm, $\hat{\alpha} = 70000$ pixel/m and $\hat{\beta} = 0.09$. Consider the following parametric updates, as given in (3.28) and (3.29), and the kinematic observer, as given in (3.42)

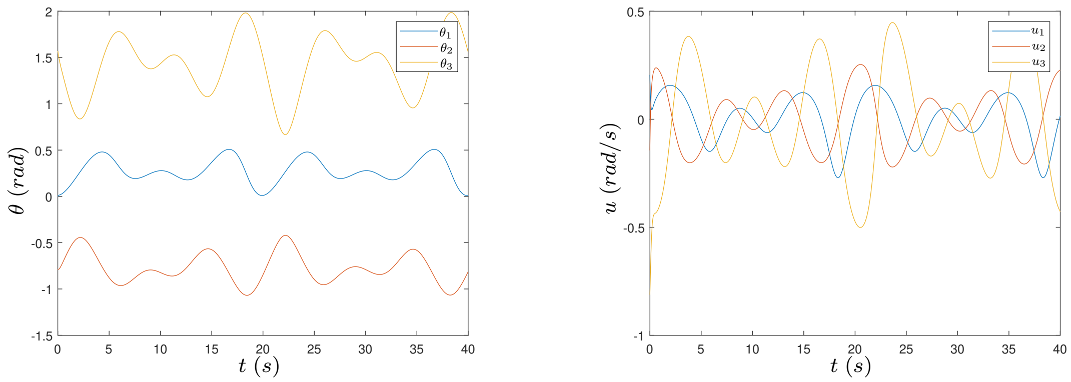

Figure 4.4: Simulation Look and move: Joint angles and control signals

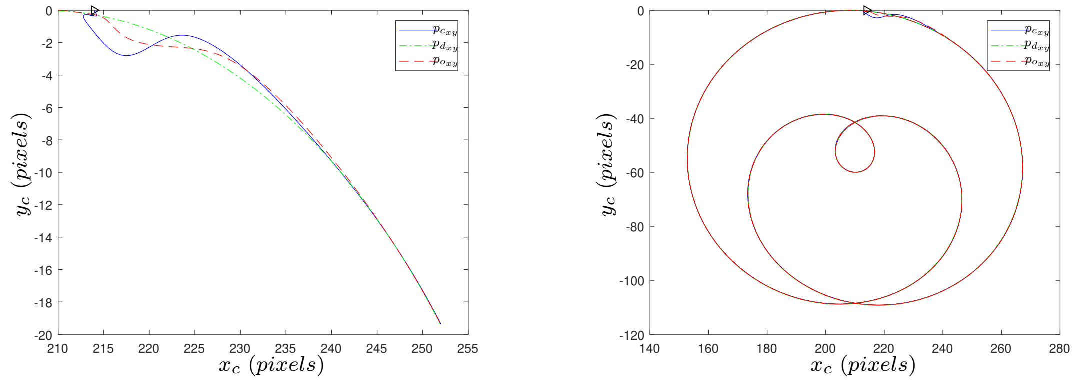

Figure 4.5: Simulation Adaptive Control Case $\frac{\pi}{6}$: Image plane Trajectory

$$\dot{\hat{a}}^{\perp} = \Gamma^{\perp} \begin{bmatrix} a_c^{\frac{1}{2}} Y^{\perp} \\ 0 \end{bmatrix}^T e_v \tag{4.9}$$

$$\dot{\hat{a}}_z = -\Gamma_z Y_z^T \begin{bmatrix} a_c^{\frac{1}{2}} (p_{xy} - p_{xyi}) \\ 2a_c^{\frac{3}{2}} \end{bmatrix}^T e_v \tag{4.10}$$

For this adaptive controller scheme, we simulate for two estimated values of $\hat{\phi}$: $\hat{\phi} = \frac{\pi}{6}$, as done before for the non-adaptive scheme, and $\hat{\phi} = \frac{2\pi}{3}$, to highlight the lack of the usual restriction on camera misalignment, as a significant advantage of indirect adaptation schemes over direct adaptation counterparts, on a visual servoing scenario.

Case 1 - $\hat{\phi} = \frac{\pi}{4}$

Here, we present simulation results for an estimated misalignment $\hat{\phi} = \frac{\pi}{6}$. The system initial conditions and control gains are given in Table 4.3.

Simulation results are presented in Figures 4.5-4.13. The planar trajectory track-

Table 4.3: Simulation Adaptive Control- Case $\frac{\pi}{6}$: Initial conditions

$\theta(0)$	$\left[0 \ -\frac{\pi}{4} \ \frac{\pi}{2}\right]^T$
$\hat{a}^{\perp}(0)$	$[9.8207 \ 7.5292 \ 5.6700 \ 4.3470]^T$
$\hat{a}_z(0)$	$[0.0270 \ 0.0207]^T$
$p_c(0)$	$[213.93 \ 0 \ 100]^T$
$p_{o_{xy}}(0)$	$[210 \ 0]^T$
K_k	$7\begin{bmatrix} 1 & 0 & 0 \\ 0 & 1 & 0 \\ 0 & 0 & 1 \end{bmatrix}$
K_o	$6\begin{bmatrix} 1 & 0 \\ 0 & 1 \end{bmatrix}$
$\Gamma^{\perp}$	$8\begin{bmatrix} 3 & 0 & 0 & 0 \\ 0 & 3 & 0 & 0 \\ 0 & 0 & 1 & 0 \\ 0 & 0 & 0 & 1 \end{bmatrix}$
Γ_z	$10^{-6}\begin{bmatrix} 0.5 & 0 \\ 0 & 1 \end{bmatrix}$
$[\|\|a^{\perp}_{max}\|\| \ \|\|a^{\perp}_{min}\|\|]$	$[28.28 \ 2]$
$[\|\|a^{z_{max}}\|\| \ \|\|a^{z_{min}}\|\|]$	$[0.13 \ 0.03]$

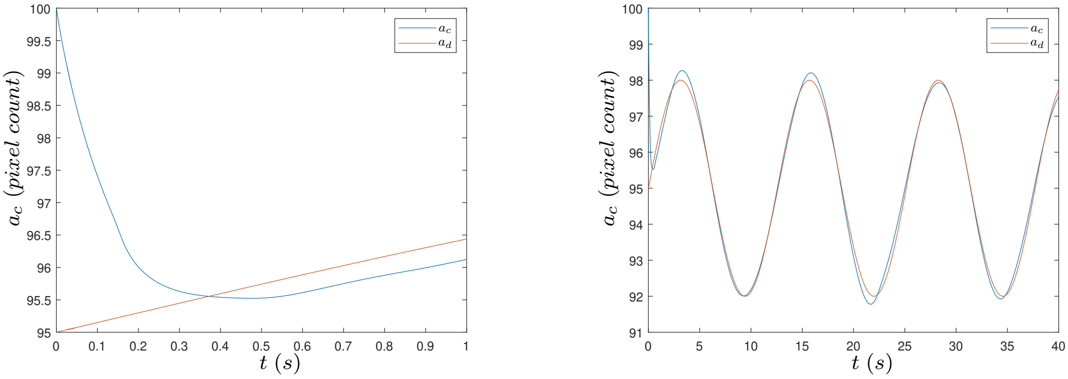

Figure 4.6: Simulation Adaptive Control Case $\frac{\pi}{6}$: Area Tracking

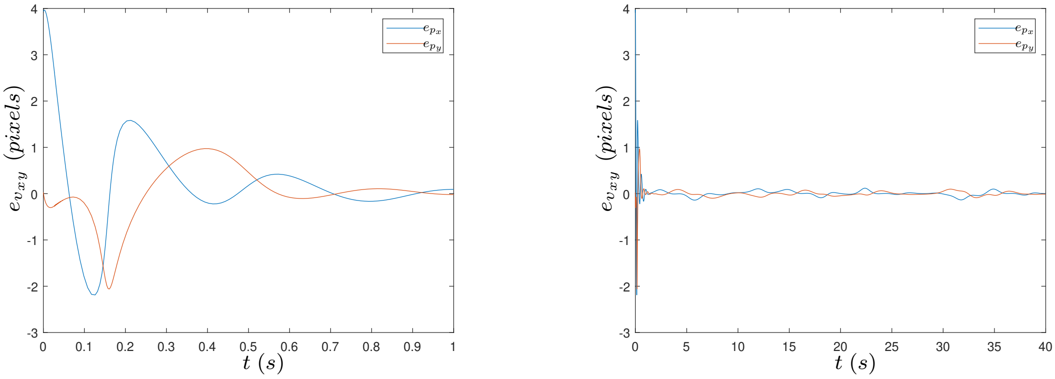

Figure 4.7: Simulation Adaptive Control Case $\frac{\pi}{6}$: Image plane tracking error

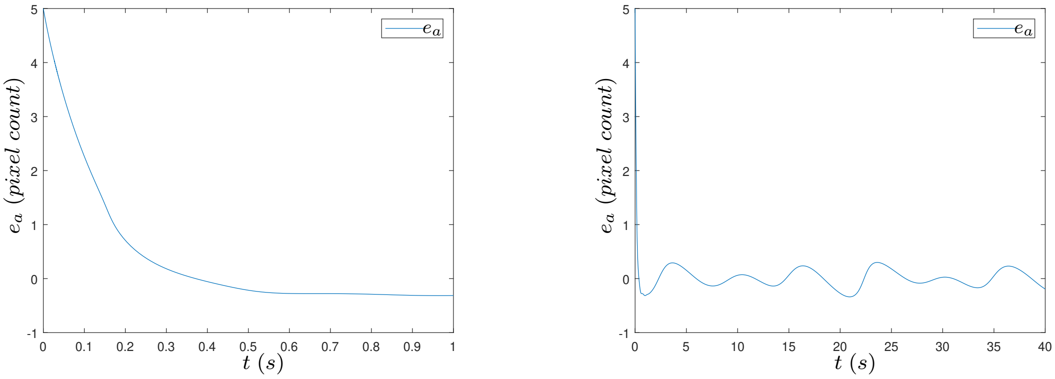

Figure 4.8: Simulation Adaptive Control Case $\frac{\pi}{6}$: Area tracking error

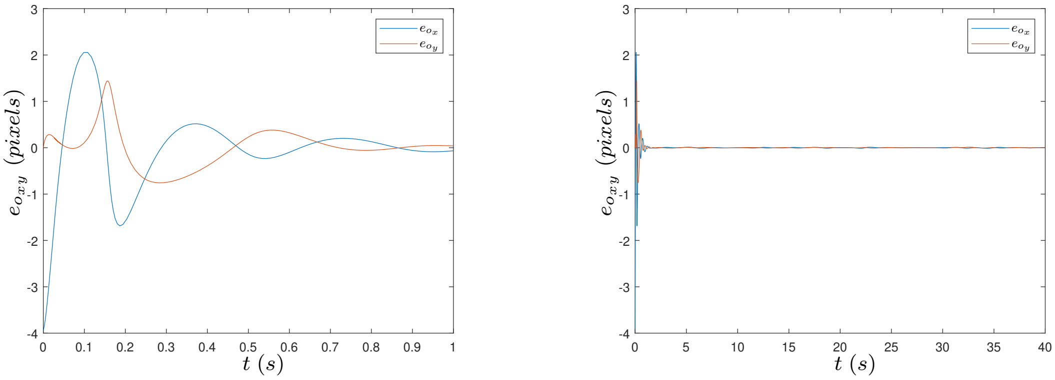

Figure 4.9: Simulation Adaptive Control Case $\frac{\pi}{6}$: Observer error

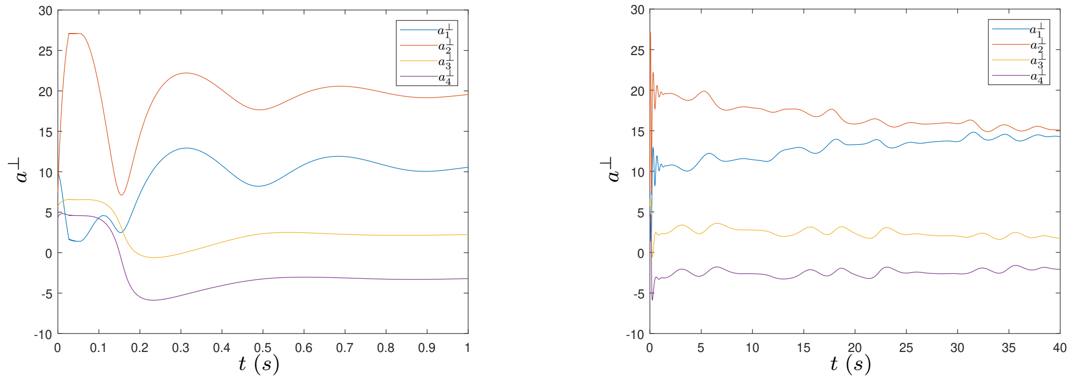

Figure 4.10: Simulation Adaptive Control Case $\frac{\pi}{6}$: Depth-independent Parameters

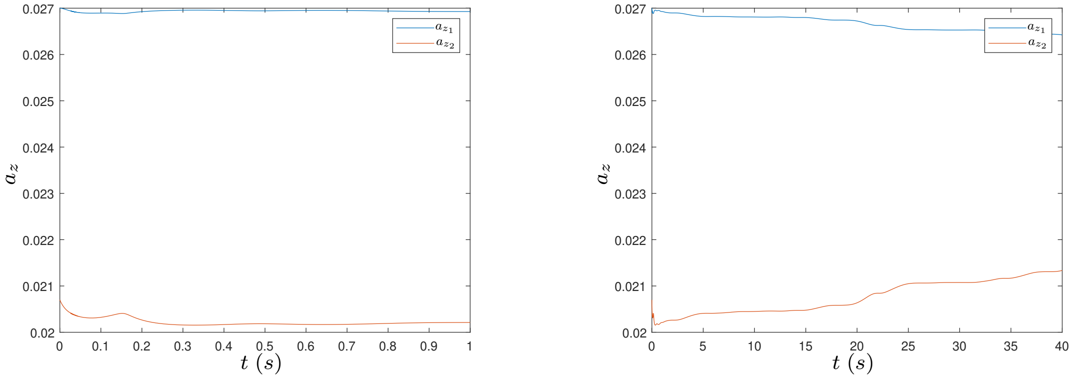

Figure 4.11: Simulation Adaptive Control Case $\frac{\pi}{6}$: Depth-dependent Parameters

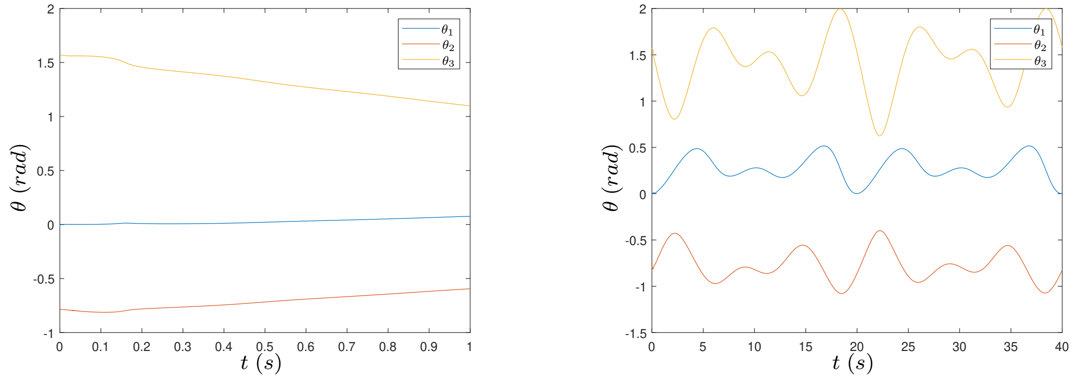

Figure 4.12: Simulation Adaptive Control Case $\frac{\pi}{6}$: Joint angles

ing in image space is presented in Figure 4.5, for the robot and observer, as the area tracking is similarly presented in Figure 4.6. The error for plane and area trajectory tracking are illustrated in Figure 4.7 and Figure 4.8. In around 1 second, the tracking error has been significantly reduced, and it is important to note while the error seems to tend towards zero over time, it is not an asymptotic decrease, as expect from the stability analysis in Chapter 3. Figure 4.9 illustrates the observer error. As previously mentioned, the observer is useful to avoid using image space velocity in the controller for manipulators with non-negligible dynamics, which are simulated in the next section. Figures 4.10 and 4.11 show the evolution of estimated parameters $\hat{a}^{\perp}$ and $\hat{a}_z$ over time. Observe that after as the parameter updates are based on trajectory tracking error, there is a greater and faster variation at the parameters on the first second of simulations, before slowly down as the norm of the tracking error decreases. Figures 4.12 and 4.13 show the joint angles and control signals respectively. Overall, a feasible control signal with a satisfying performance was reached.

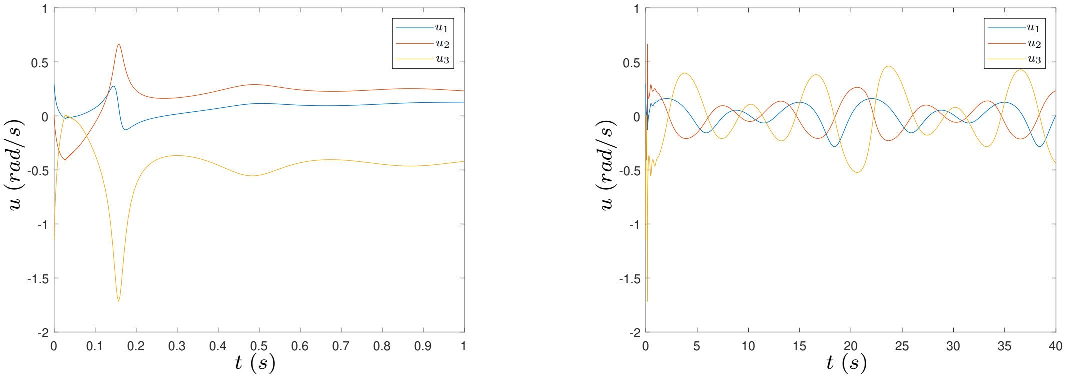

Figure 4.13: Simulation Adaptive Control Case $\frac{\pi}{6}$: Control signals

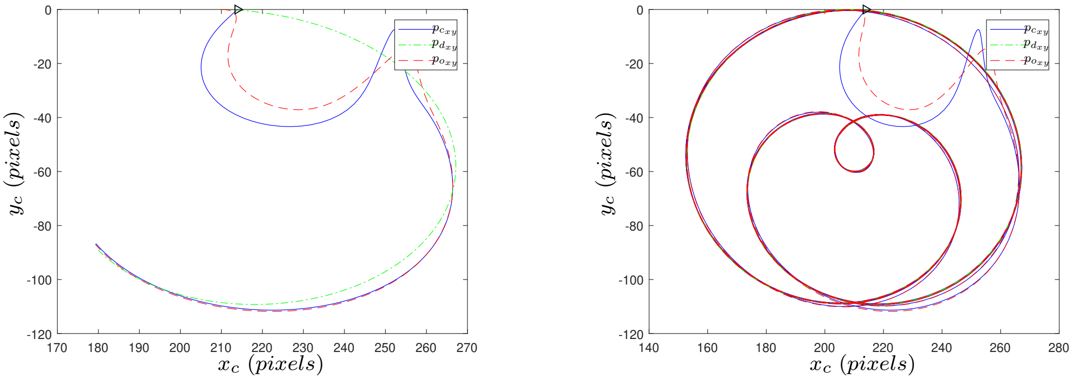

Figure 4.14: Simulation Adaptive Control Case $\frac{2\pi}{3}$: Image plane Trajectory

Case 2 - $\hat{\phi} = \frac{2\pi}{3}$

Here, we present simulation results for an estimated misalignment $\hat{\phi} = \frac{2\pi}{3}$. The system initial conditions and control gains are given in Table 4.4.

Simulation results are presented in Figures 4.14-4.22. The planar trajectory tracking in image space is presented in Figure 4.14, for the robot and observer, as the area tracking is similarly presented in Figure 4.15. The increasing tracking error for the initial assumption of $\hat{\phi} = \frac{2\pi}{3}$ is visible on the trajectory. Figures 4.19 and 4.20 show the evolution of estimated parameters $\hat{a}^{\perp}$ and $\hat{a}_z$ over time. Observe that it takes around 0.5 seconds for the estimated parameters $\hat{a}^{\perp}$ to change signals from their initial estimation. The error for plane and area trajectory tracking are illustrated in Figure 4.16 and Figure 4.17. Worthy of note that the error increases until around the 0.5 second mark, where the parameters change signals, before tending towards zero as in the previous case. Figure 4.18 illustrates the observer error. Figures 4.21 and 4.22 show the joint angles and control signals respectively. Overall, a feasible control signal with a satisfying performance was reached, even in the presence of a misalignment angle greater than $\frac{\pi}{2}$.

Table 4.4: Simulation Adaptive Control- Case $\frac{2\pi}{3}$: Initial conditions

$\theta(0)$	$\left[0 \ -\frac{\pi}{4} \ \frac{\pi}{2}\right]^T$
$\hat{a}^{\perp}(0)$	$[-5.67 \ -4.347 \ 9.8207 \ 7.5292]^T$
$\hat{a}_z(0)$	$[0.0270 \ 0.0207]^T$
$p_c(0)$	$[213.93 \ 0 \ 100]^T$
$p_{o_{xy}}(0)$	$[210 \ 0]^T$
K_k	$3\begin{bmatrix} 1 & 0 & 0 \\ 0 & 1 & 0 \\ 0 & 0 & 1 \end{bmatrix}$
K_o	$6\begin{bmatrix} 1 & 0 \\ 0 & 1 \end{bmatrix}$
$\Gamma^{\perp}$	$8 \times 10^{-2}\begin{bmatrix} 3 & 0 & 0 & 0 \\ 0 & 3 & 0 & 0 \\ 0 & 0 & 1 & 0 \\ 0 & 0 & 0 & 1 \end{bmatrix}$
Γ_z	$10^{-6}\begin{bmatrix} 1 & 0 \\ 0 & 2 \end{bmatrix}$
$[\|\|a^{\perp}_{max}\|\| \ \|\|a^{\perp}_{min}\|\|]$	$[28.28 \ 2]$
$[\|\|a^{z_{max}}\|\| \ \|\|a^{z_{min}}\|\|]$	$[0.13 \ 0.03]$

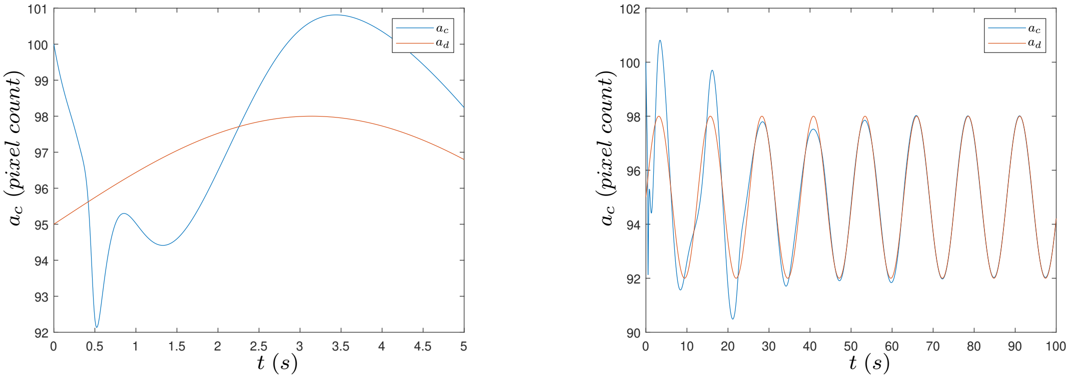

Figure 4.15: Simulation Adaptive Control Case $\frac{2\pi}{3}$: Area Tracking

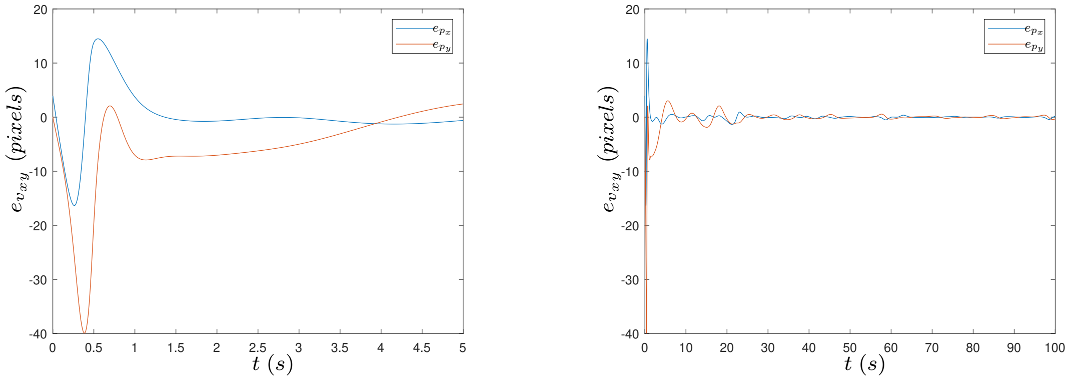

Figure 4.16: Simulation Adaptive Control Case $\frac{2\pi}{3}$: Image plane tracking error

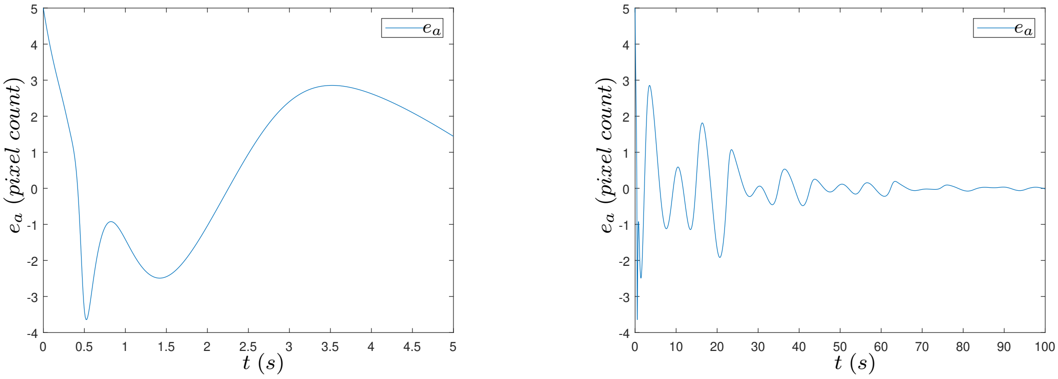

Figure 4.17: Simulation Adaptive Control Case $\frac{2\pi}{3}$: Area tracking error

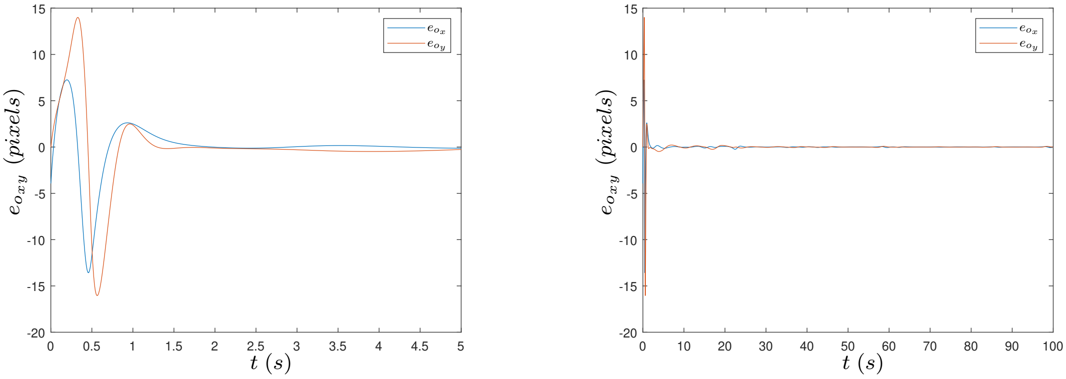

Figure 4.18: Simulation Adaptive Control Case $\frac{2\pi}{3}$: Observer error

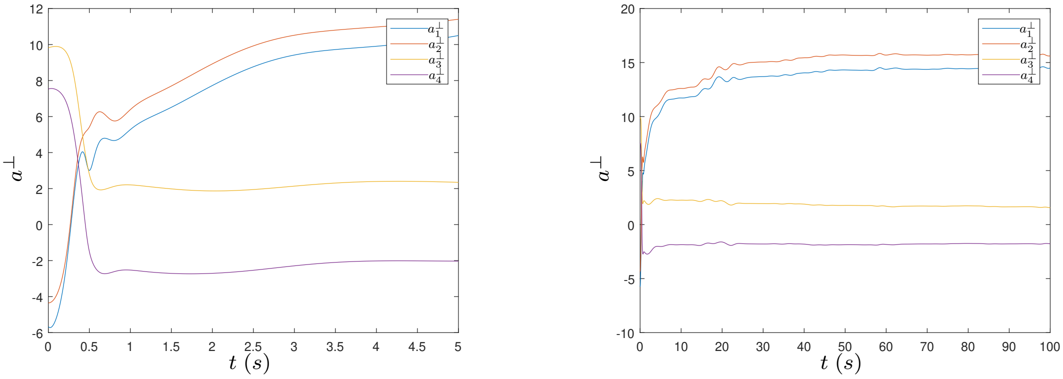

Figure 4.19: Simulation Adaptive Control Case $\frac{2\pi}{3}$: Depth-independent Parameters

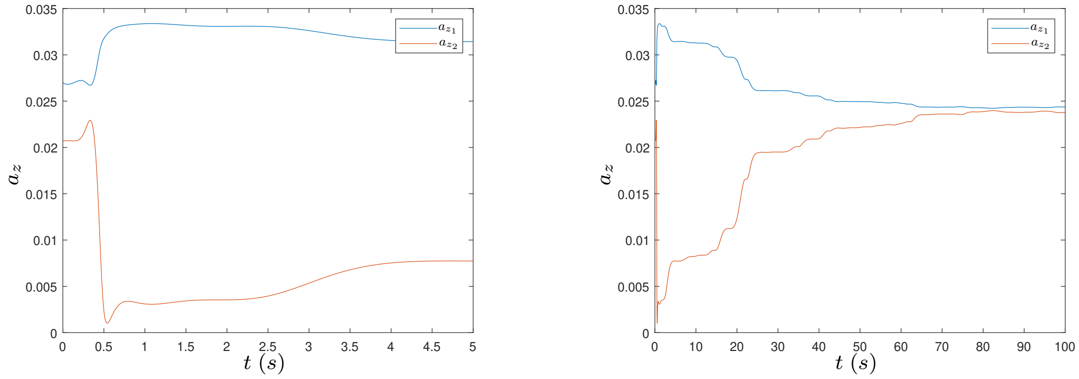

Figure 4.20: Simulation Adaptive Control Case $\frac{2\pi}{3}$: Depth-dependent Parameters

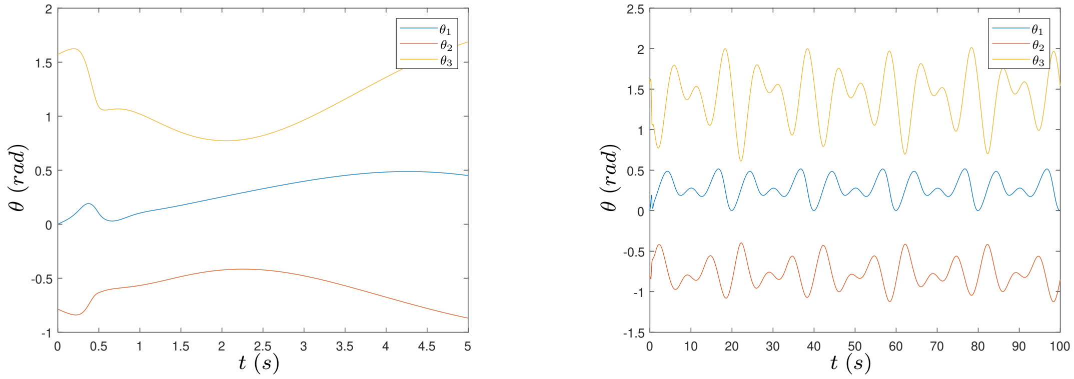

Figure 4.21: Simulation Adaptive Control Case $\frac{2\pi}{3}$: Joint angles

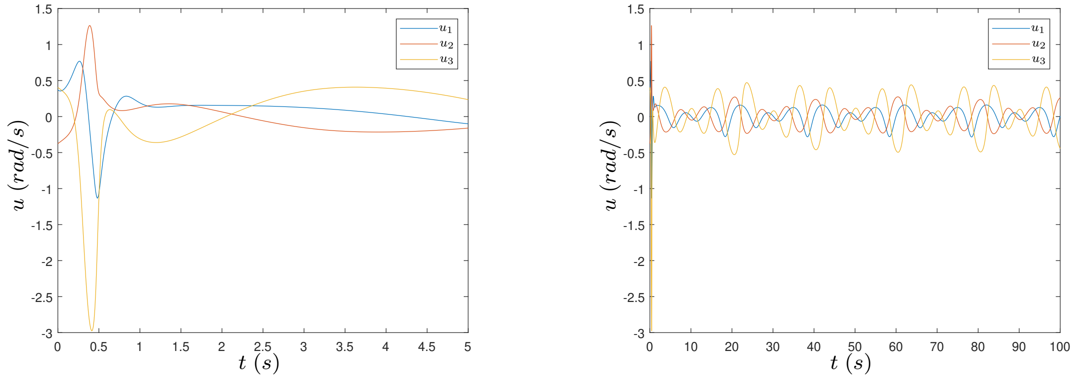

Figure 4.22: Simulation Adaptive Control Case $\frac{2\pi}{3}$: Control signals

4.2 Dynamic Anthropomorphic Arm

In this section, the anthropomorphic arm dynamics are non-negligible. Consider the same visual servoing setup from the previous section, as seen in Figure 4.1. The inertia Matrix $M(\theta)$, the Coriolis and centrifugal forces matrix $C(\theta, \dot{\theta})$ and the gravity vector $g(\theta)$ for an anthropomorphic arm are given as seen in (LEITE and LIZARRALDE, 2016):

$$M(\theta) = \begin{bmatrix} a_1 & 0 & 0 \\ 0 & a_2 + 2a_3c_3 & a_4 + a_3c_3 \\ 0 & a_4 + a_3c_3 & a_4 \end{bmatrix} \tag{4.11}$$

$$C(\theta, \dot{\theta}) = \begin{bmatrix} 0 & 0 & 0 \\ 0 & -a_3s_3\dot{\theta}_3 & -a_3s_3(\dot{\theta}_2 + \dot{\theta}_3) \\ 0 & a_3s_3\dot{\theta}_2 & 0 \end{bmatrix} \tag{4.12}$$

$$g(\theta) = \begin{bmatrix} 0 \\ a_5s_2 + a_6s_{23} \\ a_6s_{23} \end{bmatrix} \tag{4.13}$$

where $a_1 = I_1 + m_1l_{c1}^2$, $a_2 = I_2 + m_2l_{c2}^2 + m_3l_{c3}^2 + m_3l_2^2$, $a_3 = m_3l_2l_{c3}$, $a_4 = I_3 + m_3l_{c3}^2$, $a_5 = g(m_2l_{c2} + m_3l_2)$ and $a_6 = gm_3l_{c3}$. I_i, m_i are the inertia and mass of link i, l_{ci} is the center of mass of link i and g is the gravity acceleration.

Furthermore, by considering $a_d = [a_1\ a_2\ a_3\ a_4\ a_5\ a_6]^T$, we can parameterize the dynamic model, as seen in equation (2.53) with

$$M(\theta)\ddot{\theta}_r + C(\theta, \dot{\theta})\dot{\theta}_r + g(\theta) = Y_d(\theta, \dot{\theta}, \dot{\theta}_r, \ddot{\theta})a_d \tag{4.14}$$

Table 4.5: Nominal Parameters for the camera and dynamic manipulator

l_1	0.26m
l_2	0.26m
l_3	0.26m
l_{c1}	0.0983m
l_{c2}	0.0983m
l_{c3}	0.0223m
m_1	6.5225kg
m_2	6.5225kg
m_3	2.0458kg
I_1	0.1213 kg m^2
I_2	0.1213 kg m^2
I_3	0.0116 kg m^2
g	9.81 m/s^2
f	8mm
α	72727 pixel/m
ϕ	0 rad
z_i	1m
β	0.1

where $Y_d \in \mathbb{R}^{3\times 6}$ has elements given by

$$
\begin{aligned}
&Y_{d_{12}} = Y_{d_{13}} = Y_{d_{14}} = Y_{d_{15}} = Y_{d_{16}} = Y_{d_{21}} = Y_{d_{31}} = Y_{d_{32}} = Y_{d_{35}} = 0\\
&Y_{d_{11}} = \ddot{\theta}_{r_1}\\
&Y_{d_{22}} = \ddot{\theta}_{r_2}\\
&Y_{d_{23}} = (2\ddot{\theta}_{r_2} + \ddot{\theta}_{r_3})c_3 - (\dot{\theta}_{r_3}\dot{\theta}_2 + \dot{\theta}_3\dot{\theta}_{r_2} + \dot{\theta}_3\dot{\theta}_{r_3})s_3\\
&Y_{d_{24}} = \ddot{\theta}_{r_3}\\
&Y_{d_{25}} = s_2\\
&Y_{d_{26}} = s_{23}\\
&Y_{d_{33}} = \ddot{\theta}_{r_2}c_3 + \dot{\theta}_2\dot{\theta}_{r_2}s_3\\
&Y_{d_{34}} = \ddot{\theta}_{r_2} + \ddot{\theta}_{r_3}\\
&Y_{d_{36}} = s_{23}
\end{aligned}
$$

The parameters for the camera and the manipulator with non-negligible dynamics are given in Table 4.5.

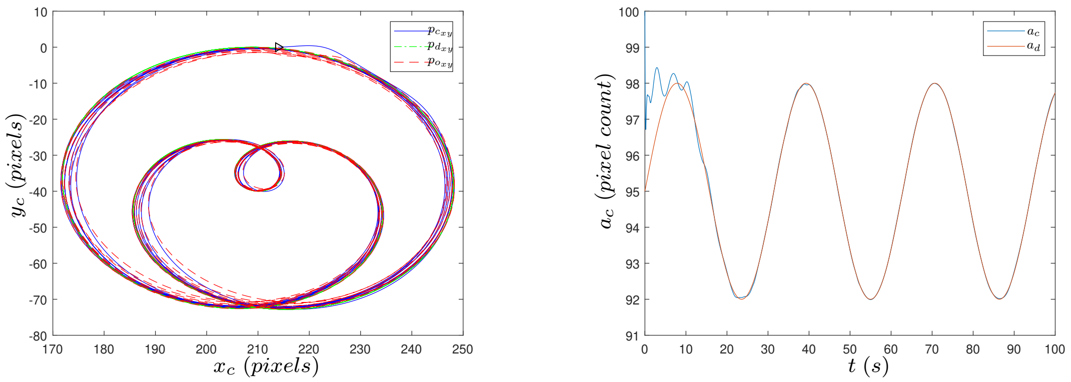

Figure 4.23: Simulation Dynamic Control Case $\frac{\pi}{6}$: Image plane Trajectory and Area Tracking

4.2.1 Adaptive Visual Servoing Simulations - Cascade Strategy

Here, we present the performance of the adaptive visual servoing for a manipulator with non-negligible dynamics and a kinematic observer for translational trajectory tracking, as developed in Chapter 3, for the task of tracking the same goal $p_d(t)$ (4.7) from the previous section. Consider as well the following control and parameter update laws, as presented in Table 3.3 in the previous chapter.

$$\tau = Y_d(\theta, \dot{\theta}, \dot{\theta}_r, \ddot{\theta}_r)\hat{a}_d - K_D\sigma \tag{4.15}$$

$$\dot{\theta}_r = \hat{J}_o^{*^{-1}}(\dot{p}_d - K_k(p_o - p_d)) \tag{4.16}$$

$$\dot{\hat{a}}^{\perp} = \Gamma^{\perp} \begin{bmatrix} a_c^{\frac{1}{2}} Y^{\perp} \\ 0 \end{bmatrix}^T e_v \tag{4.17}$$

$$\dot{\hat{a}}_z = -\Gamma_z Y_z^T \begin{bmatrix} a_c^{\frac{1}{2}}(p_{xy} - p_{xyi}) \\ 2a_c^{\frac{3}{2}} \end{bmatrix}^T e_v \tag{4.18}$$

$$\dot{\hat{a}}_d = -\Gamma_d Y_d^T \sigma \tag{4.19}$$

Similar to the the kinematic case, we present simulations for two estimated values of $\hat{\phi}$: $\hat{\phi} = \frac{\pi}{6}$ and $\hat{\phi} = \frac{2\pi}{3}$.

Case 1 - $\hat{\phi} = \frac{\pi}{6}$

Here, we present simulation results for an estimated misalignment $\hat{\phi} = \frac{\pi}{6}$. The system initial conditions and control gains are given in Table 4.6.

Simulation results are presented in Figures 4.23-4.28. The planar trajectory tracking in image space, for both manipulator and observer, and area tracking are

Table 4.6: Simulation Adaptive Dynamic Control- Case $\frac{\pi}{6}$: Initial conditions

$\theta(0)$	$\left[0 \;\; -\frac{\pi}{4} \;\; \frac{\pi}{2}\right]^T$
$\dot{\theta}(0)$	$[0\ 0\ 0]^T$
$\hat{a}^{\perp}(0)$	$[9.8207\ 7.5292\ 5.6700\ 4.3470]^T$
$\hat{a}_z(0)$	$[0.0270\ 0.0207]^T$
$\hat{a}_d(0)$	$[0.1659\ 0.3018\ 0.0110\ 0.0114\ 10.3570; 0.4136]^T$
$p_c(0)$	$[213.93\ 0\ 100]^T$
$p_{o_{xy}}(0)$	$[210\ 0]^T$
K_k	$7\begin{bmatrix} 1 & 0 & 0 \\ 0 & 1 & 0 \\ 0 & 0 & 1 \end{bmatrix}$
K_o	$8\begin{bmatrix} 1 & 0 \\ 0 & 1 \end{bmatrix}$
K_d	$2\begin{bmatrix} 1 & 0 & 0 \\ 0 & 1 & 0 \\ 0 & 0 & 1 \end{bmatrix}$
$\Gamma^{\perp}$	$0.2\begin{bmatrix} 3 & 0 & 0 & 0 \\ 0 & 3 & 0 & 0 \\ 0 & 0 & 1 & 0 \\ 0 & 0 & 0 & 1 \end{bmatrix}$
Γ_z	$3 \times 10^{-6}\begin{bmatrix} 1 & 0 \\ 0 & 2 \end{bmatrix}$
Γ_d	$\mathbb{R}^{6\times 6}$ Identity matrix
$[\lvert\lvert a^{\perp}_{max}\rvert\rvert\ \lvert\lvert a^{\perp}_{min}\rvert\rvert]$	$[28.28\ 2]$
$[\lvert\lvert a^{z_{max}}\rvert\rvert\ \lvert\lvert a^{z_{min}}\rvert\rvert]$	$[0.13\ 0.03]$

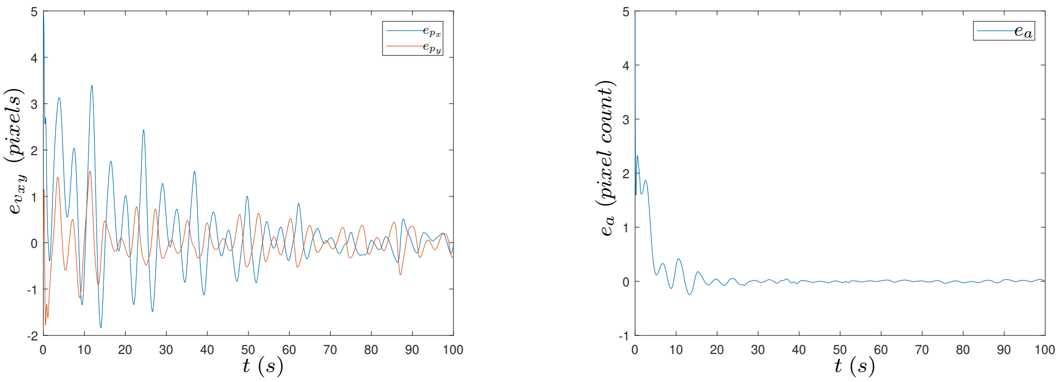

Figure 4.24: Simulation Dynamic Control Case $\frac{\pi}{6}$: Image plane and area tracking error

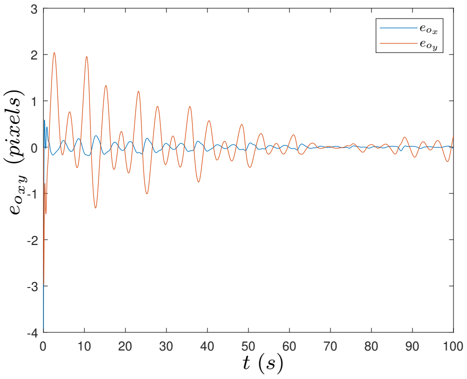

Figure 4.25: Simulation Dynamic Control Case $\frac{\pi}{6}$: Observer error

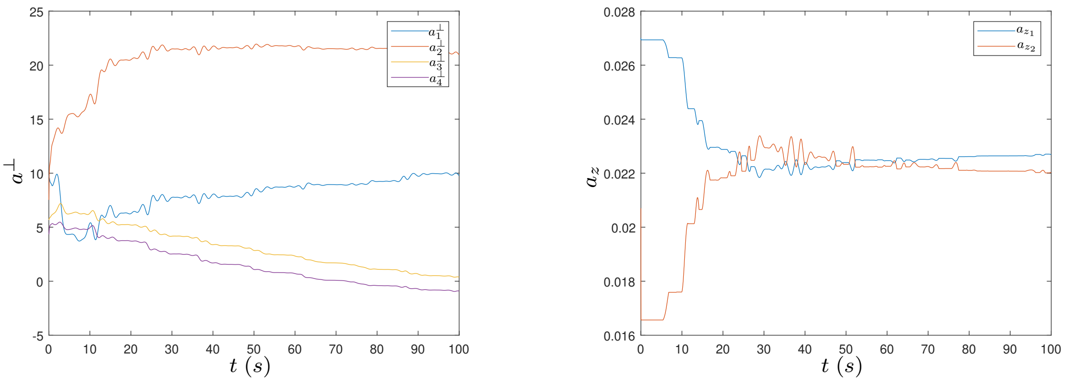

Figure 4.26: Simulation Dynamic Control Case $\frac{\pi}{6}$: Depth-independent and Depth-dependent Parameters

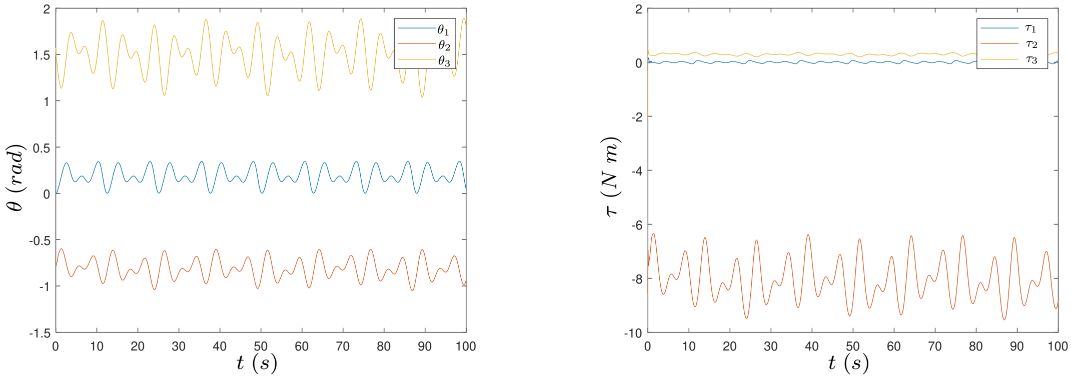

Figure 4.27: Simulation Dynamic Control Case $\frac{\pi}{6}$: Joint angles and control signals

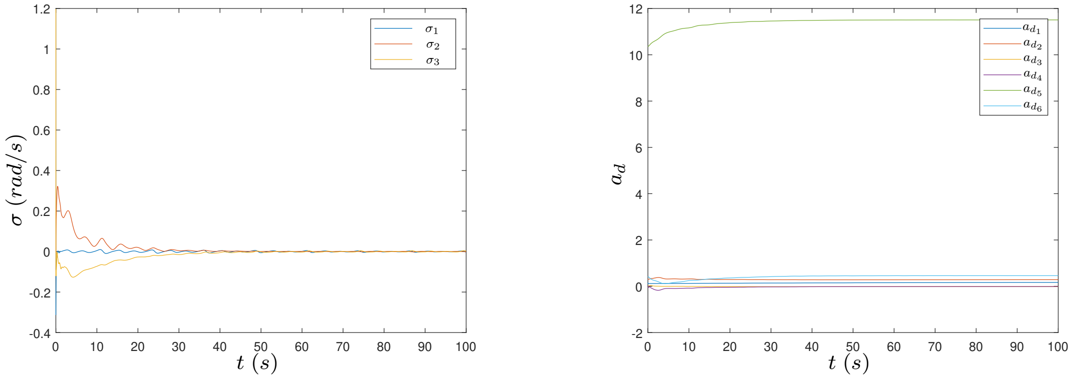

Figure 4.28: Simulation Dynamic Control Case $\frac{\pi}{6}$: Velocity tracking error and dynamic parameters

presented in Figure 4.23. The error for plane and area trajectory tracking are illustrated in Figure 4.24. The area tracking error is already significantly reduced in around 5 seconds, while the trajectory tracking error takes longer. Figure 4.25 illustrates the observer error. Figure 4.26 show the evolution of estimated parameters $\hat{a}^{\perp}$ and $\hat{a}_z$ over time. As the parameters take longer to converge in this case, we can observe that error reduction is also slower. Figure 4.27 shows the joint angles and control signals which are visibly bounded as expected. Figure 4.28 show the velocity tracking error and the dynamic parameters over time. Overall, a feasible control signal and performance were reached.

Case 2 - $\hat{\phi} = \frac{2\pi}{3}$

Here, we present simulation results for an estimated misalignment $\hat{\phi} = \frac{2\pi}{3}$. The system initial conditions and control gains are given in Table 4.7.

Simulation results are presented in Figures 4.29-4.34. The planar trajectory tracking in image space, for both manipulator and observer, and area tracking are presented in Figure 4.29. The error for plane and area trajectory tracking are illustrated in Figure 4.30. An increasing tracking error is visible at the beginning

Table 4.7: Adaptive Dynamic - Case $\frac{2\pi}{3}$: Initial conditions

$\theta(0)$	$\left[0\ -\frac{\pi}{4}\ \frac{\pi}{2}\right]^T$
$\dot{\theta}(0)$	$[0\ 0\ 0]^T$
$\hat{a}^{\perp}(0)$	$[-5.6700\ -4.3470\ 9.8207\ 7.5292]^T$
$\hat{a}_z(0)$	$[0.0270\ 0.0207]^T$
$\hat{a}_d(0)$	$[0.1659\ 0.3018\ 0.0110\ 0.0114\ 10.3570; 0.4136]^T$
$p_c(0)$	$[213.93\ 0\ 100]^T$
$p_{o_{xy}}(0)$	$[210\ 0]^T$
K_k	$2\begin{bmatrix}1 & 0 & 0\\ 0 & 1 & 0\\ 0 & 0 & 1\end{bmatrix}$
K_o	$4\begin{bmatrix}1 & 0\\ 0 & 1\end{bmatrix}$
K_d	$2\begin{bmatrix}1 & 0 & 0\\ 0 & 1 & 0\\ 0 & 0 & 1\end{bmatrix}$
$\Gamma^{\perp}$	$0.2\begin{bmatrix}3 & 0 & 0 & 0\\ 0 & 3 & 0 & 0\\ 0 & 0 & 1 & 0\\ 0 & 0 & 0 & 1\end{bmatrix}$
Γ_z	$3\times 10^{-6}\begin{bmatrix}1 & 0\\ 0 & 2\end{bmatrix}$
Γ_d	$\mathbb{R}^{6\times 6}$ Identity matrix
$[\lvert\lvert a^{\perp}_{max}\rvert\rvert\ \lvert\lvert a^{\perp}_{min}\rvert\rvert]$	$[28.28\ 2]$
$[\lvert\lvert a^{z_{max}}\rvert\rvert\ \lvert\lvert a^{z_{min}}\rvert\rvert]$	$[0.13\ 0.03]$

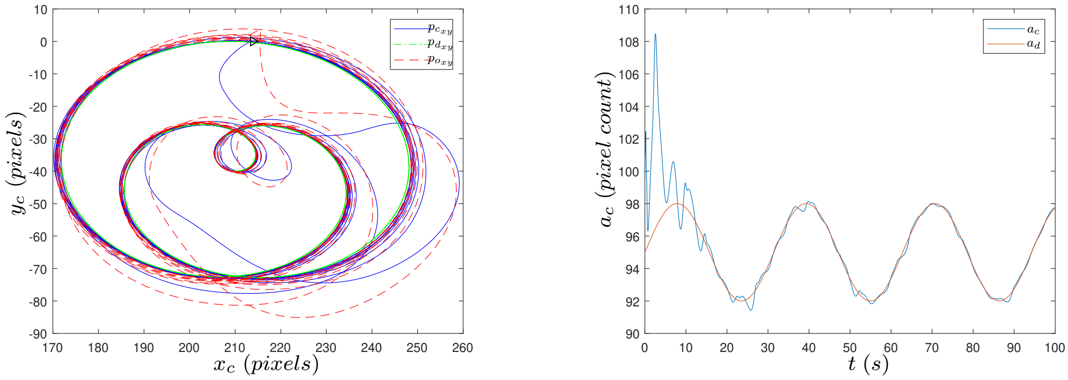

Figure 4.29: Simulation Dynamic Control Case $\frac{2\pi}{3}$: Image plane Trajectory and Area Tracking

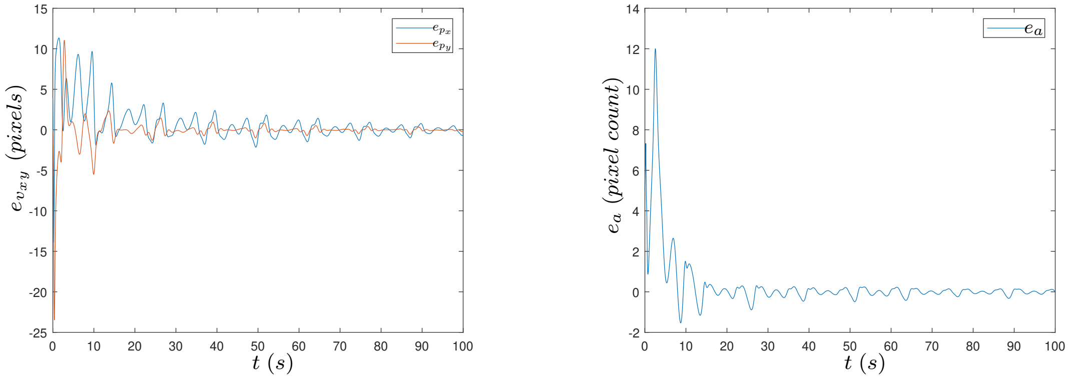

Figure 4.30: Simulation Dynamic Control Case $\frac{2\pi}{3}$: Image plane and area tracking error

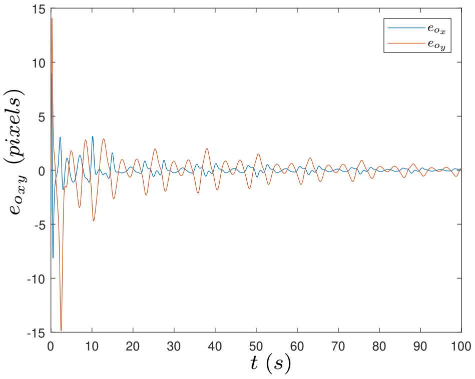

Figure 4.31: Simulation Dynamic Control Case $\frac{2\pi}{3}$: Observer error

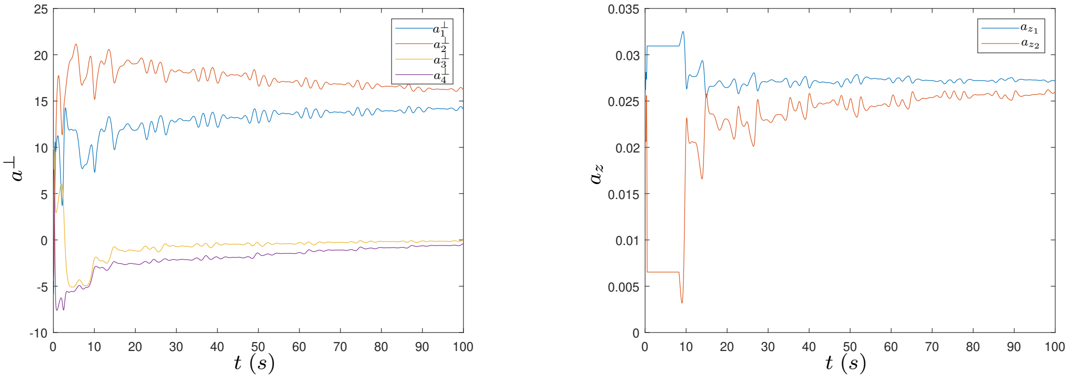

Figure 4.32: Simulation Dynamic Control Case $\frac{2\pi}{3}$: Depth-independent and Depth-dependent Parameters

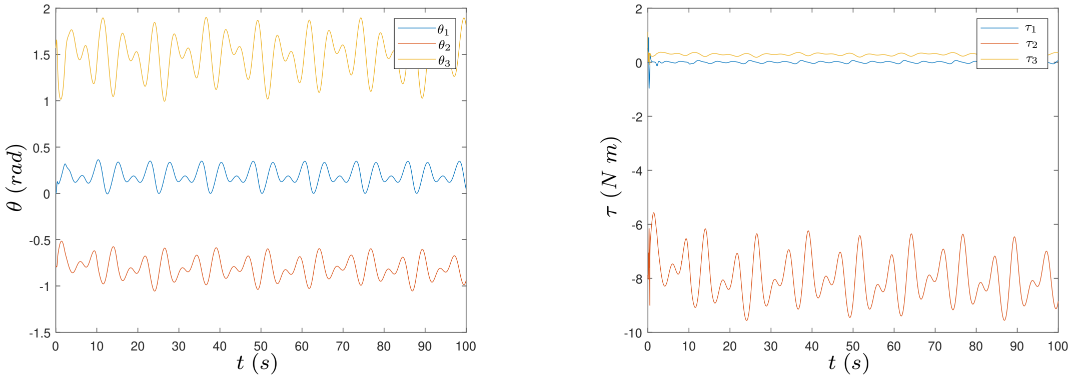

Figure 4.33: Simulation Dynamic Control Case $\frac{2\pi}{3}$: Joint angles and control signals

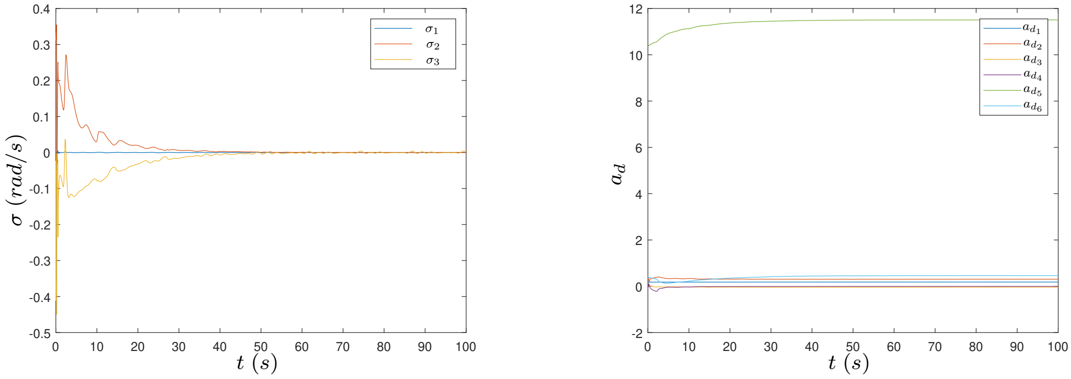

Figure 4.34: Simulation Dynamic Control Case $\frac{2\pi}{3}$: Velocity tracking error and dynamic parameters

as the robot starts moving in the opposite direction than it should, due to the initial assumption of $\hat{\phi} = \frac{2\pi}{3}$. Figure 4.31 illustrates the observer error. Figure 4.32 show the evolution of estimated parameters $\hat{a}^{\perp}$ and $\hat{a}_z$ over time. Similarly to the kinematic case, the parameters estimated with wrong sign quickly adapt at the start, changing signs near the 1 second mark. Figure 4.33 shows the joint angles and control signals which are visibly bounded as expected. Figure 4.34 show the velocity tracking error and the dynamic parameters over time. Overall, a feasible control signal and performance were reached.

4.3 Initial Experimental Results - Planar Case

In this section, experimental results are presented for the adaptive visual servoing scheme, in an eye-to-hand setup. The manipulator used is the Tetis, a robot arm with four revolute joints, along a fixed webcam for capturing images, with uncertain parameters, as shown in Figure 4.35.

The Tetis has links made of carbon fiber tubes and its joints are 3D printed in titanium alloy Ti64. The actuators are from the Harmonic Drive Ag Mini series,

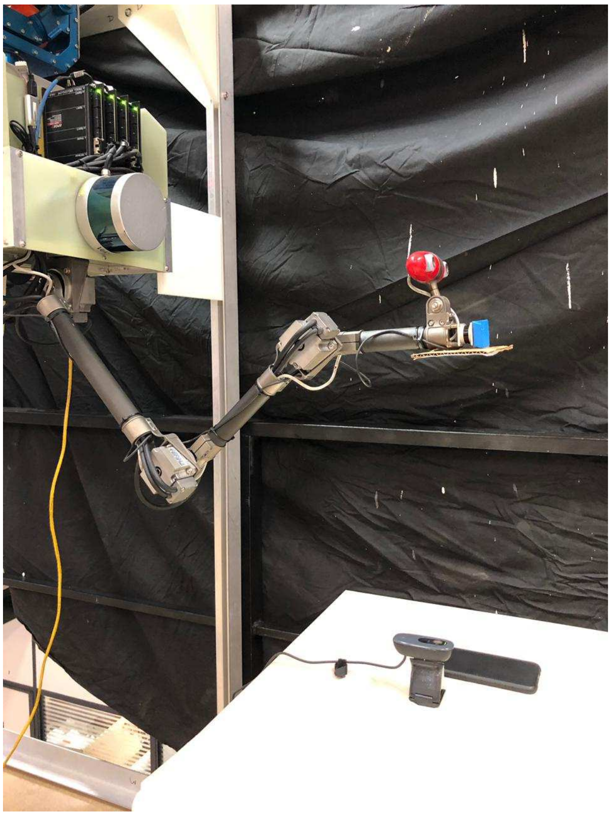

Figure 4.35: Experimental setup: Tetis Manipulator and Webcam

and drivers are the EPOS2 70/10 model from Maxon Motor. The software used to operate the Tetis is based on the Robot Operating System (ROS) platform, and allows for Cartesian velocities in the robot base frame to be given as commands to move the end-effector. Thus, in the following experiments, the robot Jacobian is considered known and solved in an inner control loop, only the camera parameters are considered uncertain.

The webcam is also sending images through the ROS usb_cam package. The target to be tracked is a QR Code as seen in Figure 4.36. Image processing and target detection are done with the ROS package visp_auto_tracker.

The position of the target centroid is received by the Matlab software, in which control is calculated and then sent to the Tetis software. Control is transmitted at a rate of 50 Hz and calculated in SI units. The Tetis software however, receives velocity control in mm/s, so care with unit conversions should be taken during the experiment. The kinematic observer proposed in this thesis is implemented in Matlab to show its validity. The full experimental setup is illustrated in diagram 4.37.

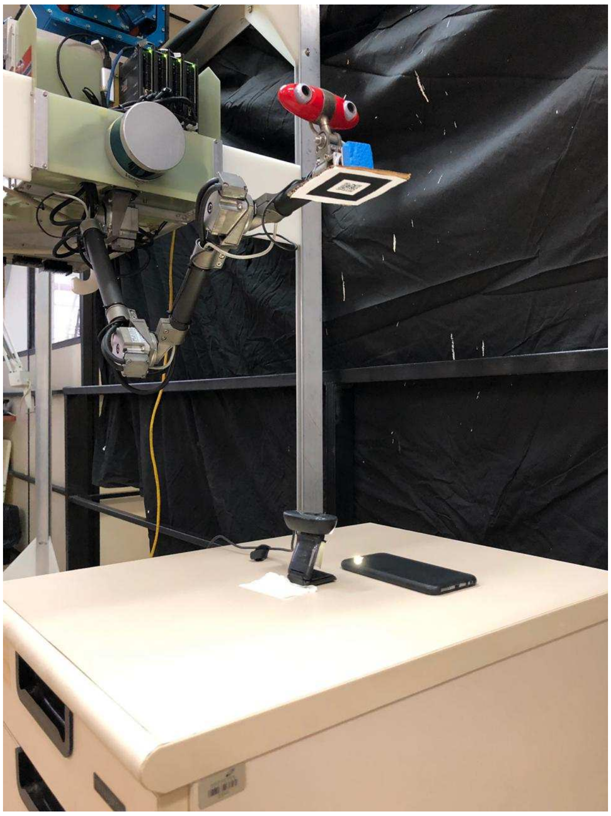

Figure 4.36: Experimental setup: QR Code target

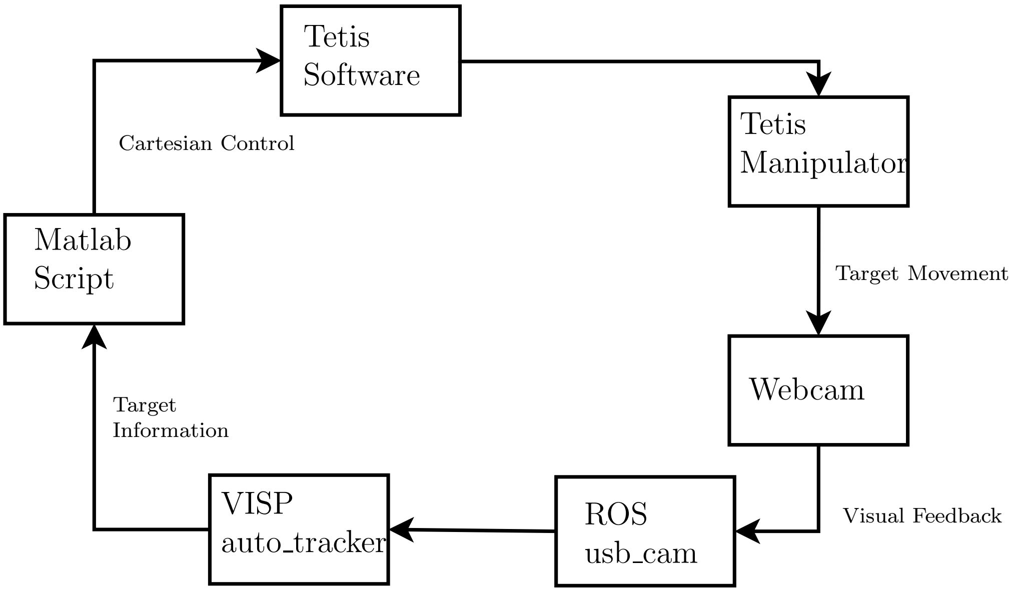

Figure 4.37: Block diagram of the experimental setup

4.3.1 Planar Control

We present experimental results for a image planar configuration, with constant depth. A constant depth z_c can be considered an unknown parameter part of the camera matrix K_p and taking in consideration that the Tetis is controlled with Cartesian control, the system can be simplified as:

$$\dot{p_c'} = \begin{bmatrix} \frac{f\alpha}{z_c} & 0 \\ 0 & \frac{f\alpha}{z_c} \end{bmatrix} R(\phi)\dot{p}_{be} = K_p \ v \tag{4.20}$$

Similarly, Cartesian control v is given by

$$v = \hat{K_p}^{-1}(\dot{p}_d - K_k(p_c - p_d)) \tag{4.21}$$

where $\hat{K_p}$ is an estimative of the camera matrix. Parameterization is simplified to a single vector of parameters, and is given by:

$$K_p \ v = \begin{bmatrix} v(1) & v(2) \\ v(2) & -v(1) \end{bmatrix} \begin{bmatrix} \frac{\hat{f}\hat{\alpha}}{\hat{z}_c}\cos(\hat{\phi}) \\ \frac{\hat{f}\hat{\alpha}}{\hat{z}_c}\sin(\hat{\phi}) \end{bmatrix} \tag{4.22}$$

$$K_p \ v = Y(v)\hat{a} \tag{4.23}$$

Finally, the kinematic observer is expressed by

$$\dot{p}_o = \hat{K_p} \ v - K_o(p_o - p_c) + K_k(p_c - p_d) \tag{4.24}$$

For this system, we show performance of the adaptive control with parameters update.

Adaptive Controller

In this simplified planar configuration, estimated parameters are updated with the following law:

$$\dot{\hat{a}} = \Gamma \ Y^T(p_c - p_d) \tag{4.25}$$

The desired trajectory is $p_d = [0.06 + 0.01\sin(\frac{5}{\pi}t) \quad -0.021 + 0.01\cos(\frac{5}{\pi}t)]^T$, as measured in the camera frame. The controller gains are $K_k = 1$, $K_o = 2$ and $\Gamma = 10$. The observer initial position is given by $p_o = [0.5 \ \ 0]^T$.

Experimental results are presented with Figures 4.38-4.41. Figure 4.38 shows the target current and desired position as well as the observer state over the duration of the experiment. Figure 4.41 show that the parameters were still in transient state and adapting slowly, a higher Γ gain could have been used, or a longer experiment run to see more effects in the adaptation of parameters. With small variation in the

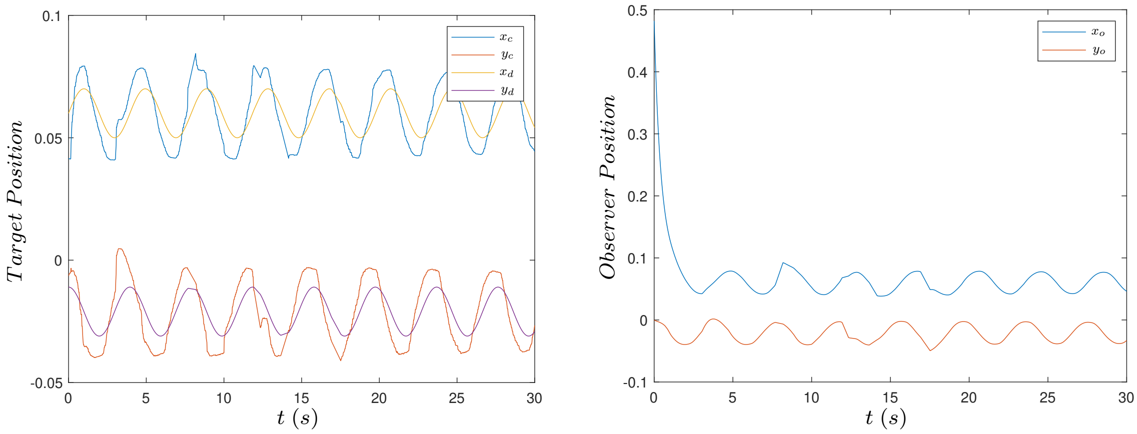

Figure 4.38: Adaptive Control experimental results: Target and Observer position over time

parameters, the tracking and observer errors themselves have slow variation in their overall magnitude, while still being bounded as expected.

Here, it is important to point out a few problems observed in this experimental setup, especially over the choice for target data acquisition, QR code identification through visp_auto_tracker, as it might not have been an optimal choice. First, as quantity of binary information is high, processing its information can be slow for the controller, rate at which the position of its centroid is acquired getting as low as 10 Hz at times, as the ROS package calculates various parameters which are not of interest to this problem, like orientation. For a similar reason, movement may cause the package to lose track or wrongly locate the target. A third major problem is the sensibility to variance in ambient lighting, which required saturation with an external flashlight (as seen with the phone in Figure 4.36) to increase performance in that sense. Even then, there were still noticeable errors in target localization in the experiment and some less noticeable loss of tracking (if the package loses track of the QRCode, it repeats the last known position until it finds the QRCode again).

A possible solution to the rate of target acquisition would be using a simpler identification tag like an ArUco marker, however, it still requires further testing.

4.4 Conclusions

In this chapter, we presented simulations and experimental to illustrate the performance of the controller scheme developed in this paper. First, we presented performance for the Look-and-move algorithm, for a kinematic model and an assumed camera misalignment of $\hat{\phi} = \frac{\pi}{6}$. Then, we presented the adaptive kinematic controller scheme for the same case, followed of a case where the parameters are assumed with a wrong sign $\hat{\phi} = \frac{2pi}{3}$. We extend the problem to a problem with non-negligible dynamics, showing the performance of the cascade controller scheme

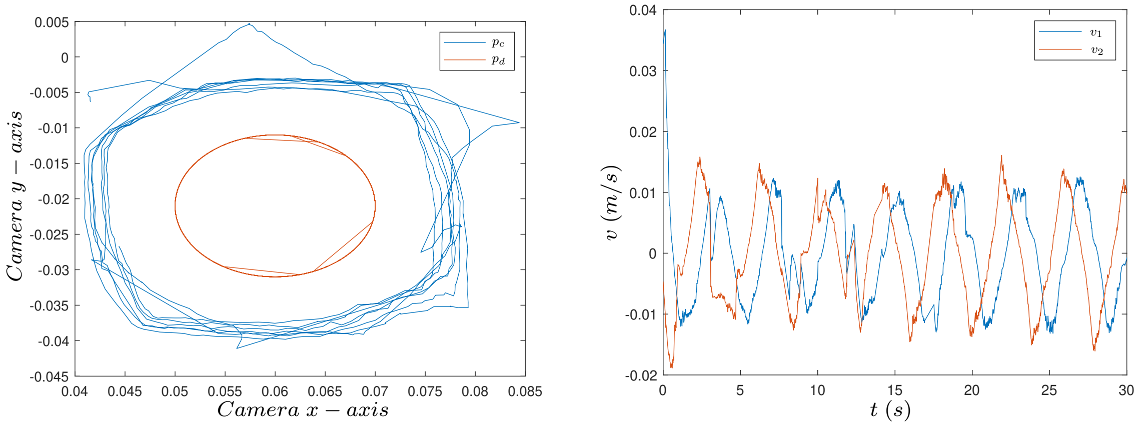

Figure 4.39: Adaptive Control experimental results: Planar Trajectory and Control Signal

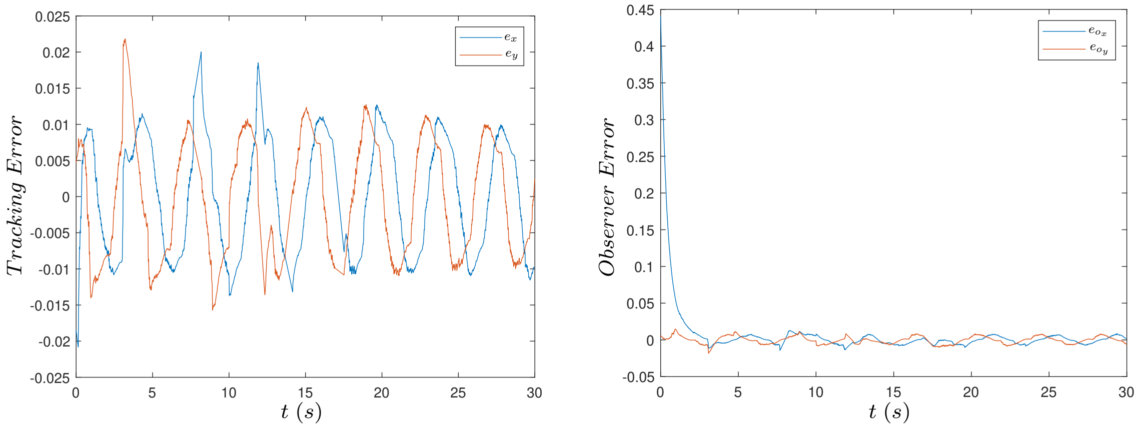

Figure 4.40: Adaptive Control experimental results: Image and Observer errors

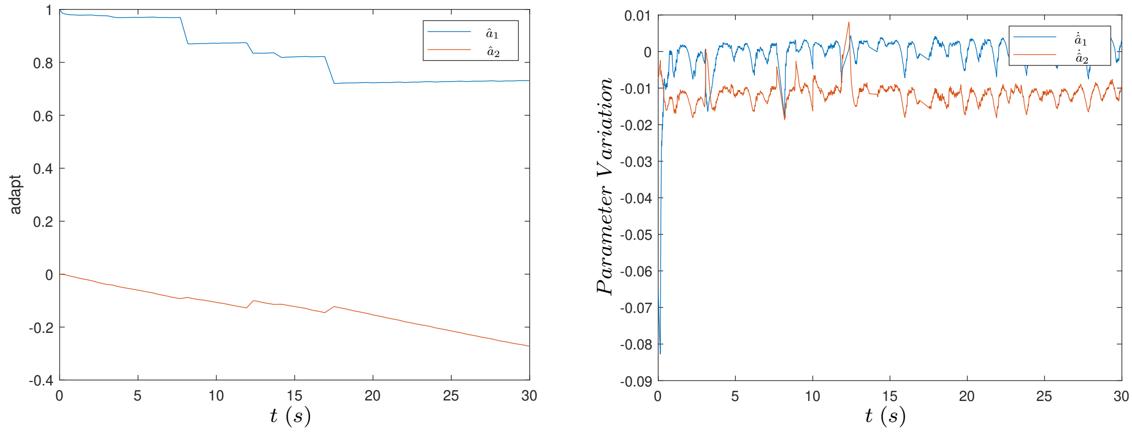

Figure 4.41: Adaptive Control experimental results: Estimated Parameters and Estimated Parameters variation signal

for previous two $\hat{\phi}$ cases. Finally, we present experimental results using the Tetis manipulator, for planar control with constant depth.

Chapter 5

Conclusions and Future Work

In this chapter, we present the conclusions and final considerations about the research theme considered in this thesis, along with a brief summary over what has been discussed in the previous chapters. Finally, we present some suggestions and proposals to be developed in future work.

5.1 Conclusions

- In this work, we considered the problem of adaptive 3D image based visual servoing for a manipulator with uncertain parameters and an uncalibrated camera. The controller scheme is first developed for a kinematic problem and then extended for the case with non-negligible dynamics. The idea is to use indirect adaptive methods to estimate the unknown parameters and then project control laws to allow for planar trajectory and depth tracking simultaneously.

- First, we have considered a setup with an open-chain robot manipulator and the frontal perspective model of a pinhole fixed camera. A target was chosen ad the end-effector manipulator, with defining features to be extracted being the target's centroid and projected area, as the area is inversely proportional to the square potency of camera depth. An assumption was made for an spherical target, so that the target area is invariant to the orientation of the robot manipulator.

- The task goal consists of tracking a reference trajectory and area variation, in the camera image frame. No special considerations are made about the alignment between the camera and robot, aside from the target staying inside the camera field of view during the whole task, with no occlusions. A kinematic adaptive controller is developed using the parameters estimated through an indirect adaptive scheme, in a inverse-Jacobian control law. Parameterizations are presented, separating the depth-dependent from the depth-independent image Jacobian.

- To avoid measuring image velocity, we introduce a kinematic observer to the system, using the observer states in the control law instead. An stability analysis is then done for the full visual servoing kinematic system with an observer. The passivity property of the complete system is also analyzed.

- We then extended the controller to a case with non-negligible dynamics. The cascade control strategy presented in (GUENTHER and HSU, 1993) is used, which can connect a passive driving subsystem to a passive driven subsystem. We use the theorem for interconnected passive subsystems with external disturbances to cascade the developed adaptive kinematic control to the well-known Slotine-Li adaptive scheme for dynamic manipulators, proved to have passivity properties, while also remarking that any passive dynamic control scheme could also be used.

- Lastly, we presented simulations done in the Matlab/Simulink software and experimental results using a setup with Tetis manipulator and a webcam, to illustrate the performance of the proposed control schemes. With simulation, the performance of a Look-and-move scheme was first presented for comparison, followed by the results of the adaptive kinematic control scheme, both for a camera misalignment smaller and greater than $\frac{\pi}{2}$ to properly illustrate the lack of a camera misalignment restriction for the proposed work. Similar results are then presented for the case with non-negligible dynamics, cascading with the Slotine-Li adaptive scheme. With the experimental setup, results are presented for the adaptive controller for a simplified tracking problem with constant depth and unknown camera parameters.

5.2 Future Work

Considering the problem of image-based indirect adaptive visual servoing for translational trajectories, the following topics can be investigated:

- Develop an adaptive visual servoing scheme using an observer for the tracked area and provide stability analysis for it. In this work, as previously mentioned, the observer was used to estimate only the image planar velocity and the area variation was supposed to be measured.

- Develop an adaptive scheme for tracking moving targets using an eye-in-hand camera system, without measuring image-space velocity, using the indirect adaptive methods presented in this work.

- Extend the problem from trajectory tracking to pose tracking, considering camera occlusion and manipulator singularities.
- Relax the condition of area being invariant to camera angle, essentially accepting non-spherical targets for tracking. Similarly, use the depth-to-area transformation to propose a goal directly as camera depth instead of target area.
- Consider other image characteristics of features that could be used for tracking. Only geometric features are used in this work, however literature presents other approaches for target recognition, such as luminance of image pixels as seen in (COLLEWET and MARCHAND, 2011) or intensity of image pixels (SILVEIRA, 2014).
- Consider different camera models, like a fisheye camera, instead of the perspective model of a pinhole camera used in this work.

Bibliography

[1] KRUPA, A., GANGLOFF, J., DOIGNON, C., DE MATHELIN, M. F., MOREL, G., LEROY, J., SOLER, L., MARESCAUX, J. "Autonomous 3-D positioning of surgical instruments in robotized laparoscopic surgery using visual servoing", *IEEE Transactions on Robotics and Automation*, v. 19, n. 5, pp. 842–853, Oct 2003. ISSN: 1042-296X. doi: 10.1109/TRA.2003.817086.

[2] OUYANG, B., MO, H., CHEN, H., LIU, Y., SUN, D. "Robust Model-Predictive Deformation Control of a Soft Object by Using a Flexible Continuum Robot". In: *2018 IEEE/RSJ International Conference on Intelligent Robots and Systems (IROS)*, pp. 613–618, Oct 2018. doi: 10.1109/IROS.2018.8593880.

[3] ZHANG, X., FANG, Y., ZHANG, X., JIANG, J., CHEN, X. "A Novel Geometric Hierarchical Approach for Dynamic Visual Servoing of Quadrotors", *IEEE Transactions on Industrial Electronics*, pp. 1–1, 2019. ISSN: 0278-0046. doi: 10.1109/TIE.2019.2917420.

[4] SICILIANO, B., SCIAVICCO, L., LUIGI, V., ORIOLO, G. *Robotics: Modelling, Planning and Control.* 01 2011. doi: 10.1007/978-1-84628-642-1.

[5] LI, G., SU, H., COLE, G. A., SHANG, W., HARRINGTON, K., CAMILO, A., PILITSIS, J. G., FISCHER, G. S. "Robotic System for MRI-Guided Stereotactic Neurosurgery", *IEEE Transactions on Biomedical Engineering*, v. 62, n. 4, pp. 1077–1088, April 2015. ISSN: 0018-9294. doi: 10.1109/TBME.2014.2367233.

[6] KARTHIKEYAN, K. B., NITHYA, V. "Implementation of surgical robot instrument with a force feedback". In: *2017 IEEE Region 10 Humanitarian Technology Conference (R10-HTC)*, pp. 101–104, Dec 2017. doi: 10.1109/R10-HTC.2017.8288916.

[7] LEE, Y., CHOI, J., JUNG, J., KIM, T., CHOI, H. "Underwater robot exploration and identification using dual imaging sonar : Basin test".

In: *2017 IEEE Underwater Technology (UT)*, pp. 1–4, Feb 2017. doi: 10.1109/UT.2017.7890335.

[8] VIDAL, E., HERNÁNDEZ, J. D., PALOMERAS, N., CARRERAS, M. "Online Robotic Exploration for Autonomous Underwater Vehicles in Unstructured Environments". In: *2018 OCEANS - MTS/IEEE Kobe Techno-Oceans (OTO)*, pp. 1–4, May 2018. doi: 10.1109/OCEANSKOBE.2018.8559224.

[9] TANAKA, Y., LEE, H., WALLACE, D., JUN, Y., OH, P., INABA, M. "Toward deep space humanoid robotics inspired by the NASA Space Robotics Challenge". In: *2017 14th International Conference on Ubiquitous Robots and Ambient Intelligence (URAI)*, pp. 14–19, June 2017. doi: 10.1109/URAI.2017.7992877.

[10] WANG, X., XIA, B., LI, G., LIU, H., LIANG, B. "Modelling and control of dual-arm free-floating space robot using virtual decomposition control for capturing target". In: *2017 IEEE International Conference on Robotics and Biomimetics (ROBIO)*, pp. 2021–2026, Dec 2017. doi: 10.1109/ROBIO.2017.8324716.

[11] TOKEKAR, P., HOOK, J. V., MULLA, D., ISLER, V. "Sensor Planning for a Symbiotic UAV and UGV System for Precision Agriculture", *IEEE Transactions on Robotics*, v. 32, n. 6, pp. 1498–1511, Dec 2016. ISSN: 1552-3098. doi: 10.1109/TRO.2016.2603528.

[12] SA, I., LEHNERT, C., ENGLISH, A., MCCOOL, C., DAYOUB, F., UPCROFT, B., PEREZ, T. "Peduncle Detection of Sweet Pepper for Autonomous Crop Harvesting—Combined Color and 3-D Information", *IEEE Robotics and Automation Letters*, v. 2, n. 2, pp. 765–772, April 2017. ISSN: 2377-3766. doi: 10.1109/LRA.2017.2651952.

[13] NÄGELI, T., ALONSO-MORA, J., DOMAHIDI, A., RUS, D., HILLIGES, O. "Real-Time Motion Planning for Aerial Videography With Dynamic Obstacle Avoidance and Viewpoint Optimization", *IEEE Robotics and Automation Letters*, v. 2, n. 3, pp. 1696–1703, July 2017. ISSN: 2377-3766. doi: 10.1109/LRA.2017.2665693.

[14] ZACHARIADIS, O., MYGDALIS, V., MADEMLIS, I., NIKOLAIDIS, N., PITAS, I. "2D visual tracking for sports UAV cinematography applications". In: *2017 IEEE Global Conference on Signal and Information Processing (GlobalSIP)*, pp. 36–40, Nov 2017. doi: 10.1109/GlobalSIP.2017.8308599.

[15] PATIC, P. C., MAINEA, M., PASCALE, L., MANTESCU, G. "Designing a Mobile Robot used for Access to Dangerous Areas". In: *2017 International Conference on Control, Artificial Intelligence, Robotics Optimization (ICCAIRO)*, pp. 60–65, May 2017. doi: 10.1109/ICCAIRO.2017.21.

[16] PHAM, H. X., LA, H. M., FEIL-SEIFER, D., DEANS, M. "A distributed control framework for a team of unmanned aerial vehicles for dynamic wildfire tracking". In: *2017 IEEE/RSJ International Conference on Intelligent Robots and Systems (IROS)*, pp. 6648–6653, Sep. 2017. doi: 10.1109/IROS.2017.8206579.

[17] BOZKURT, A., LOBATON, E., SICHITIU, M. "A Biobotic Distributed Sensor Network for Under-Rubble Search and Rescue", *Computer*, v. 49, n. 5, pp. 38–46, May 2016. ISSN: 0018-9162. doi: 10.1109/MC.2016.136.

[18] WANG, R., CHEN, G. "Design and Experimental Research of Underwater Maintenance Vehicle for Seabed Pipelines". In: *2018 3rd International Conference on Robotics and Automation Engineering (ICRAE)*, pp. 146–149, Nov 2018. doi: 10.1109/ICRAE.2018.8586764.

[19] HUTCHINSON, S., HAGER, G. D., CORKE, P. I. "A tutorial on visual servo control", *IEEE Transactions on Robotics and Automation*, v. 12, n. 5, pp. 651–670, Oct 1996. ISSN: 1042-296X. doi: 10.1109/70.538972.

[20] SHIRAI, Y., INOUE, H. "Guiding a robot by visual feedback in assembling tasks", *Pattern Recognition*, v. 5, pp. 99–108, 1973.

[21] HILL, J., PARK, W. T. "Real time control of a robot with a mobile camera". In: *Proc. 9th ISIR, Washington, D.C.*, pp. 233–246, Mar 1979.

[22] WEISS, L. E., SANDERSON, A. C., NEUMAN, C. P. "Dynamic visual servo control of robots: An adaptive image-based approach". In: *Proceedings. 1985 IEEE International Conference on Robotics and Automation*, v. 2, pp. 662–668, March 1985. doi: 10.1109/ROBOT.1985.1087296.

[23] WALLACE, R., MATSUZAKI, K., GOTO, Y., CRISMAN, J., WEBB, J., KANADE, T. "Progress in robot road-following". In: *Proceedings. 1986 IEEE International Conference on Robotics and Automation*, v. 3, pp. 1615–1621, April 1986. doi: 10.1109/ROBOT.1986.1087503.

[24] WEISS, L., SANDERSON, A., NEUMAN, C. "Dynamic sensor-based control of robots with visual feedback", *IEEE Journal on Robotics and Automation*, v. 3, n. 5, pp. 404–417, October 1987. ISSN: 0882-4967. doi: 10.1109/JRA.1987.1087115.

[25] KOIVO, A. J., HOUSHANGI, N. “Real-time vision feedback for servoing robotic manipulator with self-tuning controller”, *IEEE Transactions on Systems, Man, and Cybernetics*, v. 21, n. 1, pp. 134–142, Jan 1991. ISSN: 0018-9472. doi: 10.1109/21.101144.

[26] HOSODA, K., ASADA, M. “Versatile visual servoing without knowledge of true Jacobian”. In: *Proceedings of IEEE/RSJ International Conference on Intelligent Robots and Systems (IROS'94)*, v. 1, pp. 186–193 vol.1, Sep. 1994. doi: 10.1109/IROS.1994.407392.

[27] KELLY, R. “Robust asymptotically stable visual servoing of planar robots”, *IEEE Transactions on Robotics and Automation*, v. 12, n. 5, pp. 759–766, Oct 1996. ISSN: 1042-296X. doi: 10.1109/70.538980.

[28] CORKE, P. I., GOOD, M. C. “Dynamic effects in visual closed-loop systems”, *IEEE Transactions on Robotics and Automation*, v. 12, n. 5, pp. 671–683, Oct 1996. ISSN: 1042-296X. doi: 10.1109/70.538973.

[29] WILSON, W. J., HULLS, C. C. W., BELL, G. S. “Relative end-effector control using Cartesian position based visual servoing”, *IEEE Transactions on Robotics and Automation*, v. 12, n. 5, pp. 684–696, Oct 1996. ISSN: 1042-296X. doi: 10.1109/70.538974.

[30] JAGERSAND, M., FUENTES, O., NELSON, R. “Experimental evaluation of uncalibrated visual servoing for precision manipulation”. In: *Proceedings of International Conference on Robotics and Automation*, v. 4, pp. 2874–2880 vol.4, April 1997. doi: 10.1109/ROBOT.1997.606723.

[31] WHAITE, P., FERRIE, F. P. “Autonomous exploration: driven by uncertainty”, *IEEE Transactions on Pattern Analysis and Machine Intelligence*, v. 19, n. 3, pp. 193–205, March 1997. ISSN: 0162-8828. doi: 10.1109/34.584097.

[32] DEGUCHI, K. “Optimal motion control for image-based visual servoing by decoupling translation and rotation”. In: *Proceedings. 1998 IEEE/RSJ International Conference on Intelligent Robots and Systems. Innovations in Theory, Practice and Applications (Cat. No.98CH36190)*, v. 2, pp. 705–711 vol.2, Oct 1998. doi: 10.1109/IROS.1998.727274.

[33] KELLY, R. “Regulation of manipulators in generic task space: an energy shaping plus damping injection approach”, *IEEE Transactions on Robotics and Automation*, v. 15, n. 2, pp. 381–386, April 1999. ISSN: 1042-296X. doi: 10.1109/70.760361.

[34] MA, Y., KOSECKA, J., SASTRY, S. S. "Vision guided navigation for a nonholonomic mobile robot", *IEEE Transactions on Robotics and Automation*, v. 15, n. 3, pp. 521–536, June 1999. ISSN: 1042-296X. doi: 10.1109/70.768184.

[35] WINTERS, N., GASPAR, J., LACEY, G., SANTOS-VICTOR, J. "Omnidirectional vision for robot navigation". In: *Proceedings IEEE Workshop on Omnidirectional Vision (Cat. No.PR00704)*, pp. 21–28, June 2000. doi: 10.1109/OMNVIS.2000.853799.

[36] GASPAR, J., WINTERS, N., SANTOS-VICTOR, J. "Vision-based navigation and environmental representations with an omnidirectional camera", *IEEE Transactions on Robotics and Automation*, v. 16, n. 6, pp. 890–898, Dec 2000. ISSN: 1042-296X. doi: 10.1109/70.897802.

[37] CORKE, P. I., HUTCHINSON, S. A. "A new partitioned approach to image-based visual servo control", *IEEE Transactions on Robotics and Automation*, v. 17, n. 4, pp. 507–515, Aug 2001. ISSN: 1042-296X. doi: 10.1109/70.954764.

[38] COWAN, N. J., WEINGARTEN, J. D., KODITSCHEK, D. E. "Visual servoing via navigation functions", *IEEE Transactions on Robotics and Automation*, v. 18, n. 4, pp. 521–533, Aug 2002. ISSN: 1042-296X. doi: 10.1109/TRA.2002.802202.

[39] MALIS, E. "Visual servoing invariant to changes in camera-intrinsic parameters", *IEEE Transactions on Robotics and Automation*, v. 20, n. 1, pp. 72–81, Feb 2004. ISSN: 1042-296X. doi: 10.1109/TRA.2003.820847.

[40] FANG, Y., DIXON, W. E., DAWSON, D. M., CHAWDA, P. "Homography-based visual servo regulation of mobile robots", *IEEE Transactions on Systems, Man, and Cybernetics, Part B (Cybernetics)*, v. 35, n. 5, pp. 1041–1050, Oct 2005. ISSN: 1083-4419. doi: 10.1109/TSMCB.2005.850155.

[41] HSU, L., COSTA, R. R., LIZARRALDE, F. "Lyapunov/passivity-based adaptive control of relative degree two MIMO systems with an application to visual servoing". In: *2006 American Control Conference*, pp. 6 pp.–, June 2006. doi: 10.1109/ACC.2006.1656628.

[42] CHAUMETTE, F., HUTCHINSON, S. "Visual servo control. I. Basic approaches", *IEEE Robotics Automation Magazine*, v. 13, n. 4, pp. 82–90, Dec 2006. ISSN: 1070-9932. doi: 10.1109/MRA.2006.250573.

[43] CHAUMETTE, F., HUTCHINSON, S. "Visual servo control. II. Advanced approaches [Tutorial]", *IEEE Robotics Automation Magazine*, v. 14, n. 1, pp. 109–118, March 2007. ISSN: 1070-9932. doi: 10.1109/MRA.2007.339609.

[44] GUENARD, N., HAMEL, T., MAHONY, R. "A Practical Visual Servo Control for an Unmanned Aerial Vehicle", *IEEE Transactions on Robotics*, v. 24, n. 2, pp. 331–340, April 2008. ISSN: 1552-3098. doi: 10.1109/TRO.2008.916666.

[45] COLLEWET, C., MARCHAND, E. "Photometric Visual Servoing", *IEEE Transactions on Robotics*, v. 27, n. 4, pp. 828–834, Aug 2011. ISSN: 1552-3098. doi: 10.1109/TRO.2011.2112593.

[46] BECERRA, H. M., LÓPEZ-NICOLÁS, G., SAGÜÉS, C. "A Sliding-Mode-Control Law for Mobile Robots Based on Epipolar Visual Servoing From Three Views", *IEEE Transactions on Robotics*, v. 27, n. 1, pp. 175–183, Feb 2011. ISSN: 1552-3098. doi: 10.1109/TRO.2010.2091750.

[47] CHEN, S. Y. "Kalman Filter for Robot Vision: A Survey", *IEEE Transactions on Industrial Electronics*, v. 59, n. 11, pp. 4409–4420, Nov 2012. ISSN: 0278-0046. doi: 10.1109/TIE.2011.2162714.

[48] SILVEIRA, G. "On intensity-based 3D visual servoing", *Robotics and Autonomous Systems*, v. 62, n. 11, pp. 1636 – 1645, 2014. ISSN: 0921-8890. doi: https://doi.org/10.1016/j.robot.2014.03.008. Disponível em: <`http://www.sciencedirect.com/science/article/pii/S0921889014000529`>. Special Issue on Visual Control of Mobile Robots.

[49] WANG, K., LIU, Y., LI, L. "Visual Servoing Trajectory Tracking of Non-holonomic Mobile Robots Without Direct Position Measurement", *IEEE Transactions on Robotics*, v. 30, n. 4, pp. 1026–1035, Aug 2014. ISSN: 1552-3098. doi: 10.1109/TRO.2014.2317891.

[50] PUTRA, M. A., PITOWARNO, E., RISNUMAWAN, A. "Visual servoing line following robot: Camera-based line detecting and interpreting". In: *2017 International Electronics Symposium on Engineering Technology and Applications (IES-ETA)*, pp. 123–128, Sep 2017. doi: 10.1109/ELECSYM.2017.8240390.

[51] KAUFMANN, E., GEHRIG, M., FOEHN, P., RANFTL, R., DOSOVITSKIY, A., KOLTUN, V., SCARAMUZZA, D. "Beauty and the Beast: Optimal

Methods Meet Learning for Drone Racing", *CoRR*, v. abs/1810.06224, 2018.

[52] ZHOU, S., MIAO, Z., LIU, Z., ZHAO, H., WANG, H., CHEN, H., LIU, Y. "Vision-Based State Estimation and Trajectory Tracking Control of Car-Like Mobile Robots with Wheel Skidding and Slipping". pp. 4270–4275, 10 2018. doi: 10.1109/IROS.2018.8593982.

[53] CUEVAS-VELASQUEZ, H., LI, N., TYLECEK, R., SAVAL-CALVO, M., FISHER, R. B. "Hybrid Multi-camera Visual Servoing to Moving Target", *CoRR*, v. abs/1803.02285, 2018.

[54] LAMPARIELLO, R., MISHRA, H., OUMER, N., SCHMIDT, P., STEFANO, M. D., ALBU-SCHÄFFER, A. "Tracking Control for the Grasping of a Tumbling Satellite With a Free-Floating Robot", *IEEE Robotics and Automation Letters*, v. 3, n. 4, pp. 3638–3645, Oct 2018. ISSN: 2377-3766. doi: 10.1109/LRA.2018.2855799.

[55] CHERUBINI, A., ZHU, J., FRAISSE, P., CROSNIER, A., NAVARRO, B. "Dual-arm robotic manipulation of flexible cables". 07 2018. doi: 10.1109/IROS.2018.8593780.

[56] ZHENG, D., WANG, H., CHEN, W., WANG, Y. "Planning and Tracking in Image Space for Image-Based Visual Servoing of a Quadrotor", *IEEE Transactions on Industrial Electronics*, v. 65, n. 4, pp. 3376–3385, April 2018. ISSN: 0278-0046. doi: 10.1109/TIE.2017.2752124.

[57] YANG, L., LIU, Z., WANG, X., XU, Y. "An Optimized Image-Based Visual Servo Control for Fixed-Wing Unmanned Aerial Vehicle Target Tracking with Fixed Camera", *IEEE Access*, pp. 1–1, 2019. ISSN: 2169-3536. doi: 10.1109/ACCESS.2019.2918686.

[58] BECHLIOULIS, C. P., HESHMATI-ALAMDARI, S., KARRAS, G. C., KYRIAKOPOULOS, K. J. "Robust Image-Based Visual Servoing With Prescribed Performance Under Field of View Constraints", *IEEE Transactions on Robotics*, pp. 1–8, 2019. ISSN: 1552-3098. doi: 10.1109/TRO.2019.2914333.

[59] FERRO, M., PAOLILLO, A., CHERUBINI, A., VENDITTELLI, M. "Vision-Based Navigation of Omnidirectional Mobile Robots", *IEEE Robotics and Automation Letters*, v. 4, n. 3, pp. 2691–2698, July 2019. ISSN: 2377-3766. doi: 10.1109/LRA.2019.2913077.

[60] YAHYA, M. F., ARSHAD, M. R. "Position-based visual servoing for underwater docking of an autonomous underwater vehicle". In: *2016 IEEE International Conference on Underwater System Technology: Theory and Applications (USYS)*, pp. 121–126, Dec 2016. doi: 10.1109/USYS.2016.7893924.

[61] LEITE, A. C., LIZARRALDE, F. "Passivity-based adaptive 3D visual servoing without depth and image velocity measurements for uncertain robot manipulators", *International Journal of Adaptive Control and Signal Processing*, v. 30, n. 8-10, pp. 1269–1297, 2016.

[62] COSTA, R. R., HSU, L., IMAI, A. K., KOKOTOVIĆ, P. "Lyapunov-based adaptive control of MIMO systems", *Automatica*, v. 39, n. 7, pp. 1251 – 1257, 2003. ISSN: 0005-1098. doi: https://doi.org/10.1016/S0005-1098(03)00085-2. Disponível em: <http://www.sciencedirect.com/science/article/pii/S0005109803000852>.

[63] GUENTHER, R., HSU, L. "Variable structure adaptive cascade control of rigid-link electrically-driven robot manipulators". In: *Proceedings of 32nd IEEE Conference on Decision and Control*, pp. 2137–2142 vol.3, Dec 1993. doi: 10.1109/CDC.1993.325574.

[64] WANG, H., CHEAH, C. C., REN, W., XIE, Y. "Passive Separation Approach to Adaptive Visual Tracking for Robotic Systems", *IEEE Transactions on Control Systems Technology*, v. 26, n. 6, pp. 2232–2241, Nov 2018. ISSN: 1063-6536. doi: 10.1109/TCST.2017.2748061.

[65] SLOTINE, J.-J. E., OTHERS. *Applied nonlinear control*. 1991.

[66] CHEAH, C. C., LIU, C., SLOTINE, J. J. E. "Adaptive Jacobian vision based control for robots with uncertain depth information", *Automatica*, v. 46, n. 7, pp. 1228 – 1233, 2010. ISSN: 0005-1098.

[67] ZACHI, A. R. L. *Servovisao Adaptativa 2D e 3D para Manipuladores Roboticos*. Tese de Doutorado, Federal University of Rio de Janeiro, 2007.

[68] YAHYA, M. F., ARSHAD, M. R. "Image-based visual servoing for docking of an autonomous underwater vehicle". In: *2017 IEEE 7th International Conference on Underwater System Technology: Theory and Applications (USYS)*, pp. 1–6, Dec 2017. doi: 10.1109/USYS.2017.8309453.

[69] MURRAY, R. M., SASTRY, S. S., ZEXIANG, L. *A Mathematical Introduction to Robotic Manipulation*. 1st ed. Boca Raton, FL, USA, CRC Press, Inc., 1994. ISBN: 0849379814.

[70] MAREELS, I., POLDERMAN, J. W. *Adaptive systems: an introduction.* Springer Science & Business Media, 2012.

[71] LEITE, A. C. *Servovisao Adaptativa e Controle de Força para Robôs Manipuladores com Cinemática e Dinâmica Incertas interagindo com Ambientes Nao-Estruturados.* Tese de Doutorado, Universidade Federal do Rio de Janeiro, 2011.

[72] KHALIL, H. *Nonlinear Systems.* Pearson Education. Prentice Hall, 2002. ISBN: 9780130673893. Disponível em: <`https://books.google.com.br/books?id=t_d1QgAACAAJ`>.

[73] IOANNOU, P. A., SUN, J. *Robust Adaptive Control.* Upper Saddle River, NJ, USA, Prentice-Hall, Inc., 1995. ISBN: 0-13-439100-4.

[74] LIZARRALDE, F., LEITE, A. C., HSU, L., COSTA, R. R. "Adaptive visual servoing scheme free of image velocity measurement for uncertain robot manipulators", *Automatica*, v. 49, n. 5, pp. 1304 – 1309, 2013. ISSN: 0005-1098. doi: https://doi.org/10.1016/j.automatica.2013.01.047.

[75] HSU, L., COSTA, R. R., LIZARRALDE, F. "Lyapunov/Passivity-Based Adaptive Control of Relative Degree Two MIMO Systems With an Application to Visual Servoing", *IEEE Transactions on Automatic Control*, v. 52, n. 2, pp. 364–371, Feb 2007. ISSN: 0018-9286. doi: 10.1109/TAC.2006.890381.

[76] ZACHI, A. R. L., LIU, H., LIZARRALDE, F., LEITE, A. C. "Adaptive control of nonlinear visual servoing systems for 3D cartesian tracking", *Sociedade Brasileira de Automatica*, v. 17, pp. 381 – 390, 12 2006. ISSN: 0103-1759.

[77] HSU, L., COSTA, R., IMAI, A. K., KOKOTOVIC, P. "Lyapunov-based adaptive control of MIMO systems". In: *Proceedings of the 2001 American Control Conference. (Cat. No.01CH37148)*, v. 6, pp. 4808–4813 vol.6, June 2001. doi: 10.1109/ACC.2001.945743.

[78] HSU, L., COSTA, R. "B-MRAC: A New Model Reference Adaptive Controller Based on Binary Control Theory", *IFAC Proceedings Volumes*, v. 24, pp. 269–274, 09 1991. doi: 10.1016/S1474-6670(17)54181-6.